A Multivariable Controller for an Electromagnetic Bearing / Shaft System

by

Peter La Rocca
B.S. University of Connecticut (1984)

Submitted in partial fulfillment of
the requirements for the
degree of

Master of Science in
Aeronautics and Astronautics

at the

Massachusetts Institute of Technology
May 1988

Signature of Author
Peter La Rocca
Department of Aeronautics and Astronautics, May 19, 1988

Approved by
Mr. Edward M. Cusson
Technical Advisor, C.S. Draper Laboratory

Certified by
Professor Lena Valavani
Boeing Assistant Professor of Aeronautics and Astronautics
Thesis Advisor

Accepted by
Professor Harold Wachman
Chairman, Department Graduate Committee

I hereby grant permission to the Massachusetts Institute of Technology and the Charles Stark Draper Laboratory Inc. to reproduce and to distribute copies of this thesis document in whole or in part.

Peter LaRocca

A Multivariable Controller for an Electromagnetic Bearing / Shaft System

by

Peter La Rocca

Submitted in partial fulfillment of the requirements for the degree of Masters of Science in Aeronautics and Astronautics

ABSTRACT

A Multivariable Control System is designed for an Electromagnetic Bearing and Rotating Shaft System. The Linear Quadratic Gaussian with Loop Transfer Recovery (LQG/LTR) methodology is used to design a robust Model Based Compensator (MBC). The electromagnetic bearing consists of an electromagnetic actuator, operated in magnetic "attractive" force mode, with permanent magnet biased coils. The permanent magnet bias serves to linearize the actuator force application. The magnetic bearing operated in the attractive mode produces unstable system poles. The rotating member consists of a flexible shaft with an off center rotor. A simplified, scaled, infinitely stiff shaft model is used for the control system design. However robustness testing is done with a flexible shaft / rotor model. The thesis is concerned with the radial control of the combined system which is represented by a 4-input, 4-output plant model. A pair of magnetic bearings, each with orthogonal force capability, comprise the plant inputs, while shaft position within the bearings X-Y plane comprise the four outputs. Integral action is required to meet disturbance rejection specifications and is accomplished using state augmentation techniques. Nonlinear simulations are performed to complete the documentation of the design. Limitations of the compensator designed using the simplified model are discussed. A Model Based Compensator is also designed using the full order model of the flexible shaft. This compensator is combined with a flexible shaft model and system performance is compared to the baseline design.

Thesis Advisor : Professor Lena Valavani
Boeing Assistant Professor of Aeronautics and Astronautics

I would like to thank Professor Lena Valavani for her advice, guidance and encouragement, all of which contributed significantly to the completion of this thesis. Her confidence in my ability throughout my graduate career at M.I.T. is greatly appreciated.

I would also like to thank my 'Draper Connection': my immediate supervisor, Mr. Edward Cusson, who has shared his twenty... years of control system engineering experience in an enjoyable and stimulating environment; Mr Louis Martinage and Mr. Sanford Cohen who supported this research effort fully; and finally Professor Denis Fermental for his insights and suggestions. His methodical genius will always remind me of the correct way to approach a problem.

I'd also like to thank a fellow student, Mr. Duncan McCallum with whom I exchanged ideas and discussed theories. The many hours spent working with him also contributed to the completion of this thesis.

Most importantly, I'd like to thank my parents for their years of endless support and inspiration. They have been dedicated to my educational effort and I can only partially reciprocate by dedicating this thesis to them.

This research was conducted at the Charles Stark Draper Laboratory Inc. under IR&D contract number 18954.

Publication of this report does not constitute approval by Draper Lab of the findings or conclusions contained herein. It is published for the exchange and stimulation of ideas

Table of Contents

List of Figures

Chapter 5

Chapter 6

Appendix A

Chapter 1

1. Introduction and Thesis Approach

1.1 Introduction

Recent developments in high technology areas such as materials, computers and design techniques have allowed scientists and engineers to reconsider system designs in many well established fields. This thesis for example, deals with an alternative to standard mechanical journal bearings in the form of an electromagnetic bearing. The stabilization of a rotating shaft through the use of mechanical bearings has been studied extensively and, more importantly, has been used in countless applications for many years. More recent history suggests that the restorative forces provided by the mechanical bearings can be reproduced through the use of an electromagnetic bearing. While the scientific fields of rotor dynamics and electromagnetics are themselves mature, the combination of the two has proven a difficult and challenging system stabilization problem. This thesis combines the use of magnetic bearings for the stabilization of a rotating shaft and rotor system with the recent advances in the field of multivariable control system design to develop a stable, robust closed loop system.

1.2 Background

The advantages in use of magnetic bearings to stabilize a rotating shaft / rotor system are numerous. Magnetic bearings are virtually frictionless and, therefore, are not subject to wear; they require no form of lubrication; they can increase the accuracy of precision instruments; and, with the use of redundant electronics, they can be more reliable than their mechanical counterparts. It is for these as well as other reasons that magnetic

bearings have been the subject of extensive research for the past few decades. Johnson [4,5] provides an excellent narrative of the history, development and current state of the art of electromagnetics as applied to the levitation and stabilization of rotating bodies.

The focus of the thesis is on the application of advanced multivariable control theory to the control and stabilization of an electromagnetic bearing and rotating shaft system. The multivariable control theory specifically applied is the Linear Quadratic Gaussian with Loop Transfer Recovery (LQG/LTR) design. This procedure has been successfully applied to many multiple-input, multiple-output (MIMO) systems. The application of multivariable control theory to magnetic bearing and shaft systems is not new. Many papers have dealt with the issue, examining different models and controllers applying various simplification schemes. However, the multivariable controllers addressed are usually the full state feedback, constant gain type. The LQG/LTR methodology produces a dynamic multivariable compensator and use of such a dynamic controller has not been thoroughly documented. In fact, only one application of a dynamic multivariable compensator to the magnetic bearing problem was found in the literature [4].

Therefore, it is believed that an investigation into the combination of magnetic bearing technology with the LQG/LTR control system design methodology is necessary to determine the limitations of such a design with respect to a specific system configuration.

1.3 Thesis Approach

The thesis is concerned with an electromagnetic bearing / rotating shaft testbed to be constructed at Draper Lab. The configuration consists of a rotor mounted on a flexible shaft, sometimes called a Jeffcott rotor [5], which is supported by two permanent magnet biased electromagnetic bearings. The system is four input, four output, which makes it an excellent candidate for the application of multivariable control systems design. The complex dynamic modelling of the flexible shaft / rotor has been performed by McCallum [6] et al . The thesis approach, however, is to use a simplified stiff shaft model to design a

robust dynamic compensator, which, when combined with the actual flexible shaft / rotor, will meet all system specification. The goal is to determine the limits of the compensator designed with the simplified model. In addition, a compensator is designed using the full flexible model to determine its performance, relative to the simplified controller.

1.4 Thesis Organization

Chapter 2 contains a derivation of the simplified stiff shaft model. The magnetic bearings actuator is also presented. The actuator is a nonlinear device which uses a permanent magnet bias to linearize the force applied by the actuator. The resulting model is linear only in terms of flux density, and must be linearized around a nominal operating point, with respect to applied control current (voltage) and shaft position within the bearing. The linearization is performed and the combined simplified linear stiff shaft model is presented as the design plant model (DPM) for control system design .

Chapter 3 performs the analysis of the DPM to determine if the model is compatible with the control system design methodology. Model scaling is performed and controllability and observability issues are addressed. The resulting scaled design plant model (SDPM) is presented. Multivariable system modelling error analysis is introduced and applied.

Chapter 4 presents the LQG/LTR design methodology and applies it, thus producing the dynamic Model Based Compensator (MBC) for the aforementioned system. System performance specifications are defined and used to develop system design criteria. In order to meet certain specifications, integral control is required. State augmentation procedures are presented to introduce an integration into each control channel. Finally, a closed loop stability robustness test is performed employing the modelling error developed in Chapter3.

Chapter 5 evaluates the MBC designed in Chapter 4. A time domain simulation test plan is developed to verify compliance with performance specifications. Included in the

test procedure is a parameterization study to determine system robustness to changes in shaft rotational velocity. A configuration of linear stiff shaft model and compensator is tested to define the baseline system performance. A system configuration of nonlinear actuator and flexible shaft model is then tested using the same regime and compared to the baseline data. Limitations of the compensator are stated. Finally, system parameters are modified to verify the limitations, and it is proposed that a compensator developed using the flexible model should be designed.

In Chapter 6, the design of a MBC for a flexible shaft using the full flexible model is performed. The procedure introduced in Chapter 4 is repeated, and the compensator designed is evaluated using the test procedures of Chapter 5.

Chapter 7 summarizes the conclusions drawn and discusses the possible area of future research.

Chapter 2

2. Electromagnetic Bearing and Shaft / Rotor Model

2.1 Introduction

This chapter will develop the models for the electromagnetic bearing and the shaft / rotor system. A permanent magnet linearized magnetic bearing force equation is developed. Since flux is a nonlinear function of gap size and current, the force equation can then be linearized in those two parameters around the null operation point. The linearization of the actuator is done first because the resulting linearized equation appears in the derivation of the shaft / rotor model. The term shaft / rotor refers to the actual flexible shaft with an uncentered rotor mounted on it. For the controller design, a simplified model is used. It is comprised of an infinitely stiff shaft (no flexible modes, no rotor), modelled with equivalent inertias and the bearing actuators. This combined model will be referred to as the design plant model (DPM).

2.2 Electromagnetic Bearing Model

The electromagnetic bearing consists of a four pole piece configuration (see Figure 2.1). The individual pole pieces contain a permanent magnet housed in a ferro-magnetic shell. The actuator force is controlled by current passing through the coils shown. The opposing coils are differentially connected so that the application of control current causes an increase in flux in one side and a decrease in the other, producing the desired net force. It is important to note that the bearing is operating in a magnetic attractive force mode,

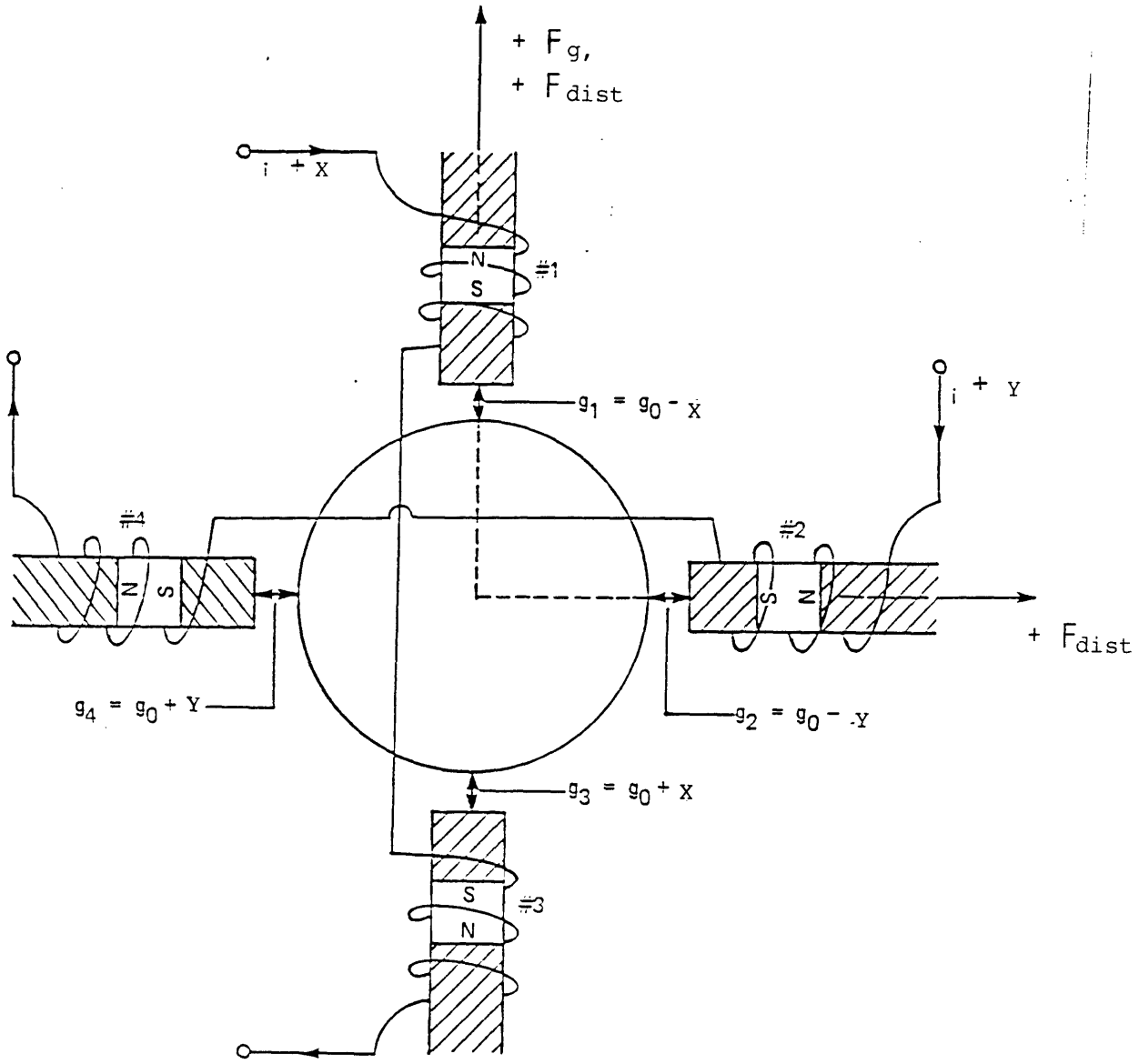

Figure 2.1 Four Pole Magnetic Bearing.

rather than a magnetic repulsive force mode. If a system operates under the forces of ferromagnetic attraction[1], then Earnshaw's Theorem [5,15,16] states that system will be will be inherently unstable.

The orthogonality of the pole pairs is representative. Actual construction procedures may vary [17,18], but the resulting orthogonal force vectors ensure application of force in any desired direction. The multivariable controller will maintain orthogonality, allowing the controller to be a four output controller with two control directions at the two bearings.

The linearization discussion starts with the shaft perfectly centered within the bearing with all initial gap distances equal to g_0 . This will be referred to as the null position throughout this thesis.

The attractive magnetic force between the gaps in one axis can be simply considered as

$$F \propto B^2 A$$

where F is the attractive force, B is the flux density in the gap and A is the area of the pole face. When the shaft is at null, this equation becomes

$$F_0 \propto B_0^2 A \quad ,$$

and the forces in the gaps, provided by the bias flux density B_0, are equal in magnitude and opposite in direction. When the shaft deviates from null, say downward (in the x direction), the bottom gap reduces, increasing its magnetic flux density to $B_0 + \Delta B$ while the upper gap widens, decreasing B to $B_0 - \Delta B$. The net force in that (x) direction is the sum of the top and bottom gap forces :

[1]The forces of magnetic attraction must vary with the inverse of the square of the distance between the magnetically attractive bodies. It will be seen that the system considered in this thesis is of this type.

$$F_{net} = F_{down} - F_{up} = (B_0 + \Delta B)^2 A - (B_0 - \Delta B)^2 A$$

This equation is expanded to

$$F_{net} = B_0^2 + 2B_0\Delta B + \Delta B^2 - B_0^2 + 2B_0\Delta B - \Delta B^2$$

Simplifying, the linear in flux force equation becomes

$$F_{net} = 4 A B_0 \Delta B$$

Since B_0 is a constant (the result of the permanent magnets), the net force is linear w.r.t B (i.e. ΔB). Also note that a significant gain increase is introduced. Further, since ΔB is a nonlinear function of gap size and current, it too can be linearized at null [6,7,17,20] resulting in the linearized net force equation

$$F = K_s x + K_i i \qquad (2.1)$$

where x is the shaft deviation from g_0 and i is the current applied[1]. It is important to note that this linearization is valid only around the null operating point. Equation (2.1) applies to each axis of both bearings.

Examination of (2.1) reveals the consequence of the attractive mode magnetic bearing. Using Newton's law, (2.1) can be rewritten as a second order differential equation (again using the x axis)

$$\ddot{x} = {}^1\!/_m \left(K_s x + K_i i \right) \qquad (2.2)$$

This systems solution consists of a pair of equally spaced poles (about the j ω axis) at $s = \pm\sqrt{K_s / M}$. The linearization has revealed an unstable system pole, one for each axis of each bearing. This system defined in (2.2) is known as an unstable spring, with K_s being the unstable spring constant. The spring natural frequency is $\sqrt{K_s / M}$.

[1]Complete expressions for K_s and K_i are given in Appendix A.1.

This linearized actuator model is used in the design plant model. For robustness testing, the complete nonlinear model is used. Appendix A.1 contains the nonlinear actuator equations.

2.3 Rotating Shaft Model

The purpose of the electromagnetic bearing is to maintain the stability of a flexible rotating shaft and rotor system. A dynamic model of a flexible rotating shaft and rotor which includes shaft damping and finite stiffness is quite complex (see Figure 2.2). The derivation of such a system can be found in McCallum [6]. Such a complex model, though complete, may not be necessary for a robust LQG/LTR design when a sufficiently stiff rotor spins below their critical (resonant) frequency. In this vein, a simplified model of the rotor and shaft will be derived. The simplified model assumes an infinitely stiff shaft with no rotor (Figure 2.3). Equivalent inertias can capture the effect of the rotor on the system. However, shaft flexing and damping are ignored. Robustness testing with the flexible model will determine the limitations of the controller designed with this simplified model.

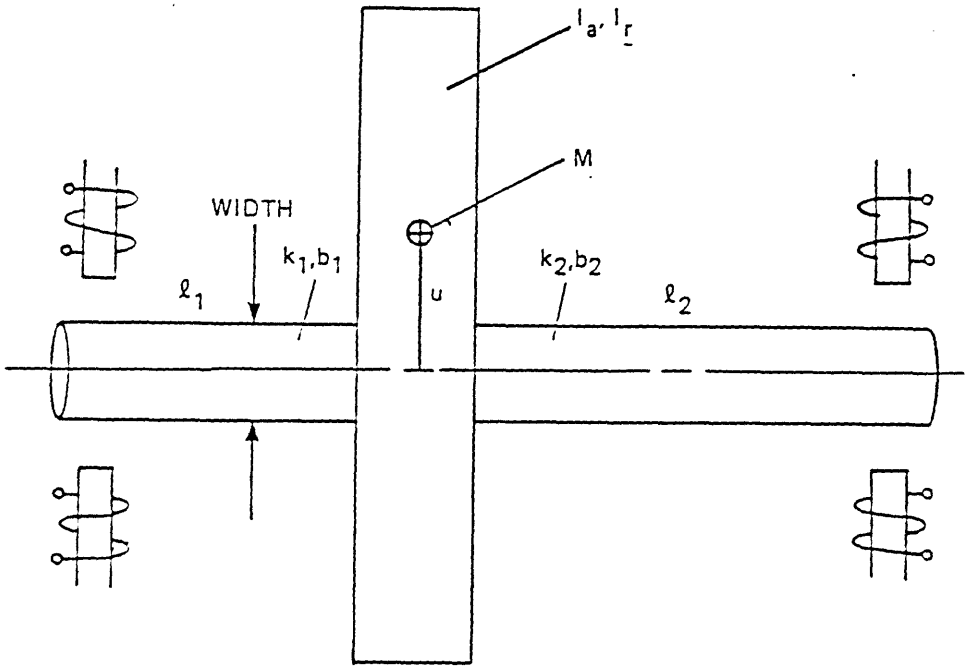

Figure 2.2 Flexible Shaft / Rotor System.

Before starting the derivation, it is necessary to define the state variables with which the system will be described. For this application, the system outputs are the shaft positions within the bearing X-Y plane (at both bearings). This creates four system outputs. It will be seen that the system can then be completely described with these outputs as system states, along with their time derivatives. Represented in vector form, the system states are

$$\mathbf{x} = \left[x_a,\ x_b,\ y_a,\ y_b,\ \dot{x}_a,\ \dot{x}_b,\ \dot{y}_a,\ \dot{y}_b \right]^T \tag{2.3}$$

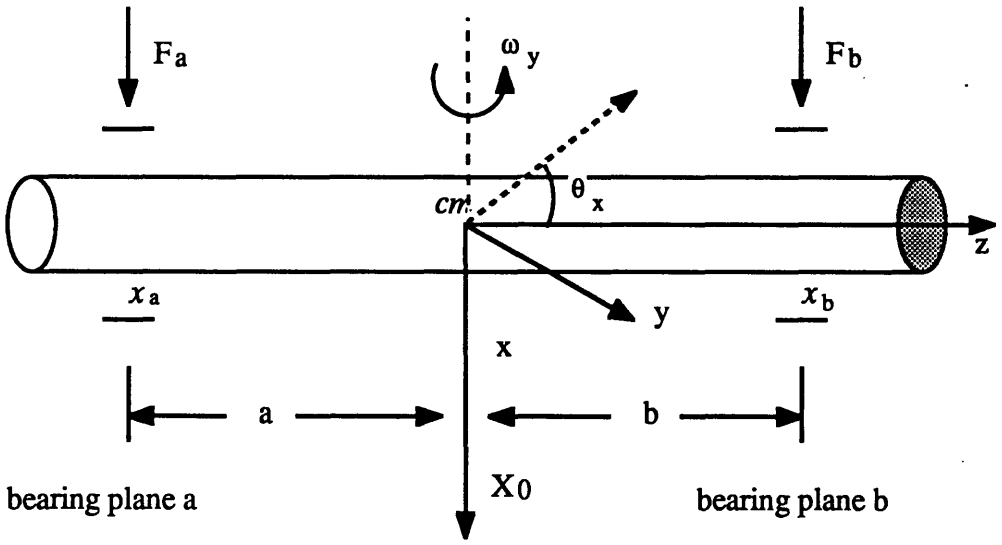

Figure 2.3 Simplified Stiff Shaft Model

Figure 2.3 depicts a shaft supported by two magnetic bearings. Only the x axis of the shaft is shown. The derivation will be carried out for this axis only, equations for the y axis are can be derived in a similar manner. The shaft is subject to both translational and rotational forces. The derivation starts by examining the translational forces.

The magnetic bearings cause translational motion via the force equation

$$F = K_s x + K_i i \qquad (2.1)$$

The translational force equation is

$$F_a + F_b = M \ddot{x}_0 - K_s (x_a + x_b) \qquad (2.4)$$

where $\ddot{x}_0$ is the acceleration of the center of mass, x_a and x_b are the shaft positions at the a and b bearings respectively, K_s is our now familiar spring constant, and F_a and F_b are the force inputs (again for the x axis only) provided by the current term, K_i, of equation (2.1).

The rotational forces are summed about the center of mass, *cm* in Figure 2.3. They satisfy

$$a F_a - b F_b = I_x \alpha_x - K_s (a x_a - b x_b) + \omega_y I_z \Omega_z \qquad (2.5)$$

where $I_x \alpha_x$ is the moment of inertia (radial inertia) and angular acceleration about the y-axis, ω_y it the angular velocity about the x-axis[1], I_z is the moment of inertia about the z-axis (axial inertia) and Ω_z is the angular velocity (i.e. spin rate) of the shaft. The entire term, $\omega_y I_z \Omega_z$ represents gyroscopic torquing effects on a spinning shaft. Continuing, under the assumption that both θ_x and θ_y remain small, so that

---

[1] Note that 1) $I_x = I_y$ and 2) there is a cross definition of axes and angles, meaning for example, θ_x is the angle of rotation about the y-axis so that α_x is the angular acceleration about the y-axis. This is done to allow θ_x to be defined in terms of displacements in the axis in question : x_a and x_b. Figure 2.4 illustrates this for the y-axis definitions.

$$a\theta_x \cong x_a - x_0 \qquad \text{and}$$
$$a\ddot{\theta}_x = a\alpha_x \cong \ddot{x}_a - \ddot{x}_0 \quad . \qquad (2.6)$$

Also, letting r equal the radius of gyration of the shaft, I_x can be written as $I_x = Mr^2$. The rotational force expression can now be rewritten as

$$\left(Mr^2/a\right)\left(\ddot{x}_a - \ddot{x}_0\right) = aF_a - bF_b + K_s\left(ax_a - bx_b\right) - \omega_y I_z \Omega_z \quad ,$$

and is easily rearranged to

$$\left(\ddot{x}_a - \ddot{x}_0\right) = \left(a/Mr^2\right)\left(aF_a - bF_b + K_s\left(ax_a - bx_b\right) - \omega_y I_z \Omega_z\right) \quad . (2.7)$$

The translation equation (2.4) can be written to solve for $\ddot{x}_0$ as

$$\ddot{x}_0 = \left(1/M\right)\left(F_a + F_b + K_s\left(x_a + x_b\right)\right) \quad . \qquad (2.8)$$

Inserting (2.8) into (2.7), the complete acceleration term for x_a becomes

$$\ddot{x}_a = 1/M\left[\left(1+\frac{a^2}{r^2}\right)F_a + \left(1-\frac{ab}{r^2}\right)F_b + K_s\left[\left(1+\frac{a^2}{r^2}\right)x_a + \left(1-\frac{ab}{r^2}\right)x_b\right] - \frac{a}{r^2}\omega_y I_z \Omega_z\right] \qquad (2.9)$$

The next problem is to find a simplified expression for ω_y. Again, with the assumption that θ_x and θ_y are small, approximations to ω_y can be made . Examining Figure 2.4,

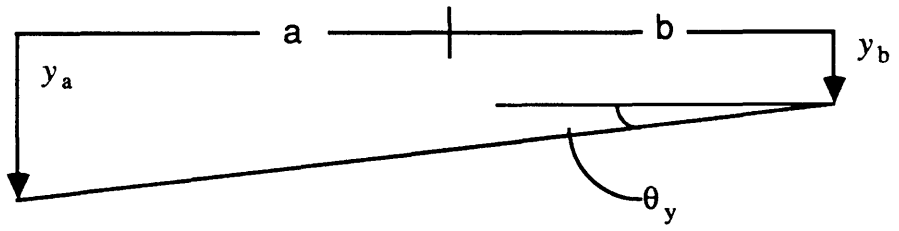

Figure 2.4 Small angle approximation diagram

for small θ_y, we find

$$(a+b)\theta_y = y_a - y_b \qquad \text{and, for velocity}$$

$$(a+b)\omega_y = \dot{y}_a - \dot{y}_b$$

Solving for ω_y and combining with that term in (2.9), we get

$$\frac{I_z \Omega_z}{M r^2}\,\omega_y = \frac{I_z \Omega_z}{M r^2}\left(\frac{a}{a+b}\right)\left(\dot{y}_a - \dot{y}_b\right) \tag{2.10}$$

Making the substitution into (2.9) produces

$$\ddot{x}_a = {}^1\!/_M\left[\left(1+\frac{a^2}{r^2}\right)F_a + \left(1-\frac{ab}{r^2}\right)F_b + K_s\left[\left(1+\frac{a^2}{r^2}\right)x_a + \left(1-\frac{ab}{r^2}\right)x_b\right]\right]$$

$$-\frac{I_z \Omega_z}{M r^2}\left(\frac{a}{(a+b)}\right)\left(\dot{y}_a - \dot{y}_b\right) \tag{2.11}$$

Equation (2.11) must now be redefined in term consistent with the development of a state space system. Using the following matrix entry assignments

$$K_{11} = {}^{K_s}\!/_M\left[1+\frac{a^2}{r^2}\right] \qquad K_{12} = {}^{K_s}\!/_M\left[1-\frac{ab}{r^2}\right]$$

$$G_{11} = {I_z \Omega_z}/{Mr^2}\left[\frac{a}{(a+b)}\right] \qquad G_{12} = {I_z \Omega_z}/{Mr^2}\left[\frac{-a}{(a+b)}\right]$$

(2.11) can be written as

$$\ddot{x}_a = \left({1}/{K_s}\right)\left[K_{11}F_a + K_{12}F_b\right] + \left(K_{11}x_a + K_{12}x_b\right) - \left(G_{11}\dot{y}_a - G_{12}\dot{y}_b\right) \qquad .(2.12a)$$

This is the final equation describing the acceleration of the shaft in the x direction at the 'a' bearing. A similar expression for the 'b' bearing can be derived as

$$\ddot{x}_b = \left({1}/{K_s}\right)\left[K_{21}F_a + K_{22}F_b\right] + \left(K_{21}x_a + K_{22}x_b\right) - \left(G_{21}\dot{y}_a + G_{22}\dot{y}_b\right) \qquad (2.12b)$$

where

$$K_{21} = {K_s}/{M}\left[1 - \frac{ab}{r^2}\right] \qquad K_{22} = {K_s}/{M}\left[1 + \frac{b^2}{r^2}\right]$$

$$G_{21} = {I_z \Omega_z}/{Mr^2}\left[\frac{-b}{(a+b)}\right] \qquad G_{22} = {I_z \Omega_z}/{Mr^2}\left[\frac{b}{(a+b)}\right]$$

With (2.12a) and (2.12b) the dynamics of the x-axis of the shaft are completely described in terms of system inputs, outputs, and desired states.

Equations for the y-axis follow the same derivation, the only difference being a sign reversal in the G matrix terms. They are :

$$\ddot{y}_a = \left({1}/{K_s}\right)\left[K_{11}F_{ya} + K_{12}F_{yb}\right] + \left(K_{11}y_a + K_{12}y_b\right) + \left(G_{11}\dot{x}_a - G_{12}\dot{x}_b\right) \qquad (2.13a)$$

$$\ddot{y}_b = \left({1}/{K_s}\right)\left[K_{21}F_{ya} + K_{22}F_{yb}\right] + \left(K_{21}y_a + K_{22}y_b\right) + \left(G_{21}\dot{x}_a + G_{22}\dot{x}_b\right) \qquad (2.13b)$$

The design plant model (DPM) is now complete. A summary of equations in matrix form is given below.

In a canonical state space representation form, the dynamics of a linear time invariant (LTI) system can be completely described by the familiar state space representation as

$$\dot{\mathbf{x}}(t) = \mathbf{A}\,\mathbf{x}(t) + \mathbf{B}\,\mathbf{u}(t)$$

$$\mathbf{y}(t) = \mathbf{C}\,\mathbf{x}(t) + \mathbf{D}\,\mathbf{u}(t) \qquad (2.14)$$

where **x** (t) is the system state vector that varies with time, **u** (t) is the system input vector, also a function of time and **y** (t) is the system output vector given as some linear combination of states and inputs. A, B, C and D are the system matrices, specific to the DPM in question. Recalling the definitions of the state variables

$$\mathbf{x} = \left[x_a,\ x_b,\ y_a,\ y_b,\ \dot{x}_a,\ \dot{x}_b,\ \dot{y}_a,\ \dot{y}_b \right]^T, \qquad (2.3)$$

the system A and B matrices can be assembled in block matrix form using (2.12) and (2.13) which contain the sub-matrix entries as defined above. They can now be represented in state space form as

$$\dot{\mathbf{x}}(t) = \begin{bmatrix} 0 & 0 & I & 0 \\ 0 & 0 & 0 & I \\ K & 0 & 0 & -G \\ 0 & K & G & 0 \end{bmatrix} \mathbf{x}(t) + \frac{K_i}{K_s} \begin{bmatrix} 0 & 0 \\ 0 & 0 \\ K & 0 \\ 0 & K \end{bmatrix} \mathbf{u}(t) \qquad (2.15)$$

where I is a 2 x 2 identity matrix, G and K are also 2 x 2 matrices which contain stiffness, mass, geometric and gyroscopic terms whose entries are defined above and K_i is an input force gain constant. The system of equations in (2.14) are consistent with the literature for a similarly characterized shaft and bearing system [7].

The system state vector, **x** is defined in (2.3); the control input vector, **u** is defined as the four control currents, two into each bearing :

$$\mathbf{u} = \left[u_{xa}, u_{xb}, u_{ya}, u_{yb} \right]^t$$

For completeness, the C matrix will be given as :

$$C = \left[I_{4\times4} \quad 0_{4\times4} \right] \qquad (2.16)$$

where the outputs are the shaft position states in meters. The D matrix is a 4 x 4 matrix of zeroes.

The DPM that will be used for the control system design is now completely defined by (2.15) and (2.16).

To reiterate, the DPM is a simplified version of a complex, nonlinear magnetic bearing and flexible shaft / rotor system. It is hoped that the DPM captures the dynamics of the actual system such that a controller designed for it will work equally well for the nonlinear, flexible shaft / rotor system. In order to verify that this is indeed true, nonlinear simulations with the complete flexible shaft / rotor model will be done. It is for this reason that the state equations for this system shown in Figure (2.2) is given in Appendix A.2.

2.4 Summary

In this chapter, the design plant model (DPM) for use in control system design was presented. The nonlinear magnetic bearing actuator was introduced. It was linearized around the null operating point through the superposition of opposing bias flux densities provided by permanent magnets. It was then shown how such an actuator, operated in attractive force mode, produces unstable system poles. The actuator is used to control a spinning shaft / rotor system. The actual system, a flexible shaft and rotor, was simplified by assuming infinite stiffness, and equivalent inertias. The simplified shaft was then combined with the linearized actuator, and the composite system dynamics were derived. The differential equations of motion, described in terms of the system states, were then put into a state space representation which can now be used for control system design. Finally,

the true shaft / rotor system and nonlinear actuator dynamics were documented in the form of Appendix A for use in robustness testing simulations and error analysis.

Chapter 3

3. Analysis of the Linear Model

3.1 Introduction

This chapter will analyze the linear model derived in Chapter 2. It will start with the introduction of system parameters into the design plant model (DPM). The eigenstructure of the DPM will then be analyzed, with emphasis on controllability and observability issues. Scaling is perhaps the most important problem in the design of this multivariable control system. It will be fully documented here and the scaled design plant model (SDPM) will be derived. It is this SDPM that will ultimately be used in the controller design. The final section of this chapter will derive the model error that will be used in checking the closed loop system robustness. The model error is developed as the error between the flexible shaft / rotor and the simplified stiff shaft model.

3.2 Design Plant Model

The DPM defined in equations (2.15) and (2.16) can now be applied to a system by the specific choice of system parameters. For this particular application, system parameter values are based on a magnetic bearing and rotating shaft / rotor testbed to be built at Draper Lab. Numerical values for the complete testbed system are given in Appendix B. The numerical form of the DPM system matrices are given in Appendix C. Two changes from equations (2.15) and (2.16) should be noted. The gain factor for the B matrix has been changed to reflect a voltage input.; thus, (2.15) becomes

$$\dot{x}(t)=\begin{bmatrix} 0 & 0 & 1 & 0 \\ 0 & 0 & 0 & 1 \\ K & 0 & 0 & -G \\ 0 & K & G & 0 \end{bmatrix} x(t)+\frac{K_v}{K_i}\frac{K_i}{K_s}\begin{bmatrix} 0 & 0 \\ 0 & 0 \\ K & 0 \\ 0 & K \end{bmatrix} u(t) \qquad (3.1)$$

where the units for K_v are Newtons / volt. Also, the output has been scaled to reflect the sensor gain. System outputs will now be in volts and (2.16) becomes

$$C = K_{sensor}\begin{bmatrix} I_{4\times4} & 0_{4\times4} \end{bmatrix} \quad . (3.2)$$

At this point, the tool available for multivariable frequency domain analysis is introduced. In single input single output (SISO) systems, frequency domain analysis is accomplished by examining the Bode plot of the system transfer function [10]. The multivariable extension of the Bode plot is the plot of the singular values[1] of the loop transfer function matrix (TFM) as a function of frequency. The TFM, analogous to the SISO transfer functions, defines the input / output relationship for a multiple input multiple output (MIMO) system. If a MIMO system is described by (2.14), it can be shown that the TFM is defined as

$$G(s) = C(sI-A)^{-1}B + D,$$

where s is the Laplace variable. The singular value plot for the DPM are shown in Figure 3.1. The units for the plot are volts / volt . This plot can be interpreted in a similar manner as one would do for a SISO system. The plot shows that the system has D.C. gain of less than one, that there are no (transmission) zeroes in the system, and that the plant has a -40 dB per decade roll off at high frequencies. Since the DPM is a 4-input 4-output system, G(s) will be a 4 by 4 matrix. It will have four singular values for each frequency point.

[1] A definition of singular values and a discussion of singular value plots can be found in [1,2,9].

Figure 3.1 shows that at low frequencies, these four values are nearly the same, while at the higher frequencies, the singular values of G (s) separate.

With the DPM matrices defined, the eigenstructure analysis of the system can be performed. The eight system poles are located at

$$-222.9 \pm .83j$$

$$222.9 \pm .83j$$

$$-287.9 \pm 16.9j$$

$$287.9 \pm 16.9j \quad .$$

These values correspond to the break frequency in Figure 3.1. The effect of the attractive mode magnetic actuators is clearly seen in the unstable system poles. This simplified system model contains NO transmission zeroes[1].

The complete eigenstructure includes the eigenvectors defined by

$$A v_i = \lambda_i v_i$$

where v_i is the *i* th eigenvector which corresponds to the *i* th eigenvalue (pole) λ_i . The eigenvectors for this DPM expose the numerical instability of the system A matrix. Figures 3.2 and 3.3 are bar graph representations of each eigenvalue. Inspection of the graph reveals that the eigenvectors are dominated by the velocity states (entries 5 through 8 in each eigenvector). In linear algebra terms, the A matrix does not span the n-dimensional space, where n = 8 in this case. This is because the system has not been properly scaled. In fact, A is a numerically ill conditioned and this can be observed by considering its condition number. The condition number of a matrix is defined as the ratio of the largest singular value to the smallest [1,4,11] and it is denoted as cond(M). A well conditioned matrix has a condition value near 1. The condition of our DPM A matrix was found to be

[1] However, the true flexible shaft / rotor system does contain transmission zeroes. This will become evident in the development of the system modelling errors. A definition of transmission zeroes can be found in [1].

8.33×10^{4} (hardly near 1 !!). This is indeed an ill-conditioned matrix. The numeric stability of A is important in the LQG/LTR design process because of the extensive use of the Riccati equation, whose numerical convergence heavily depends on the condition of the matrices used, among which is A. This is an additional reason that the scaling of this particular multivariable system is so important.

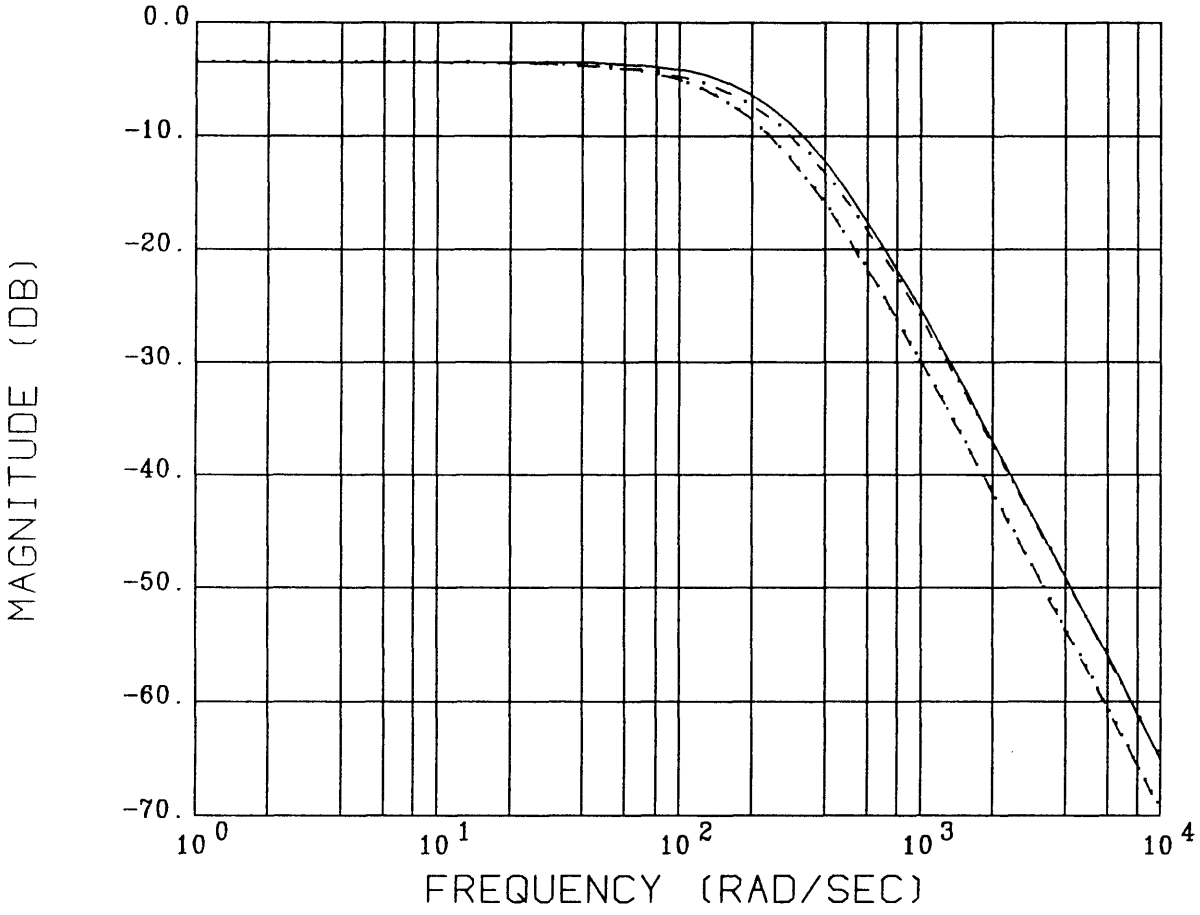

Figure 3.1 Singular Values of the Design Plant Model

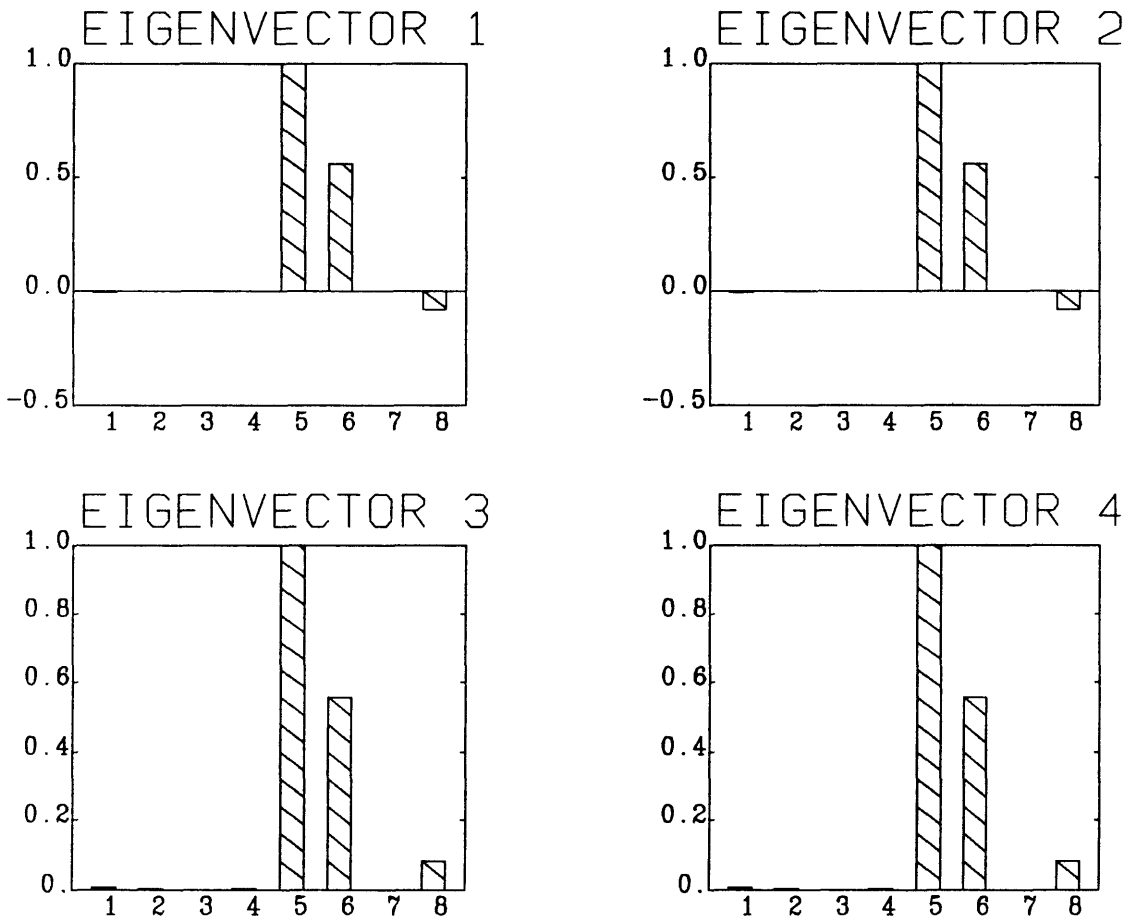

Figure 3.2 Design Plant Model Eigenvectors

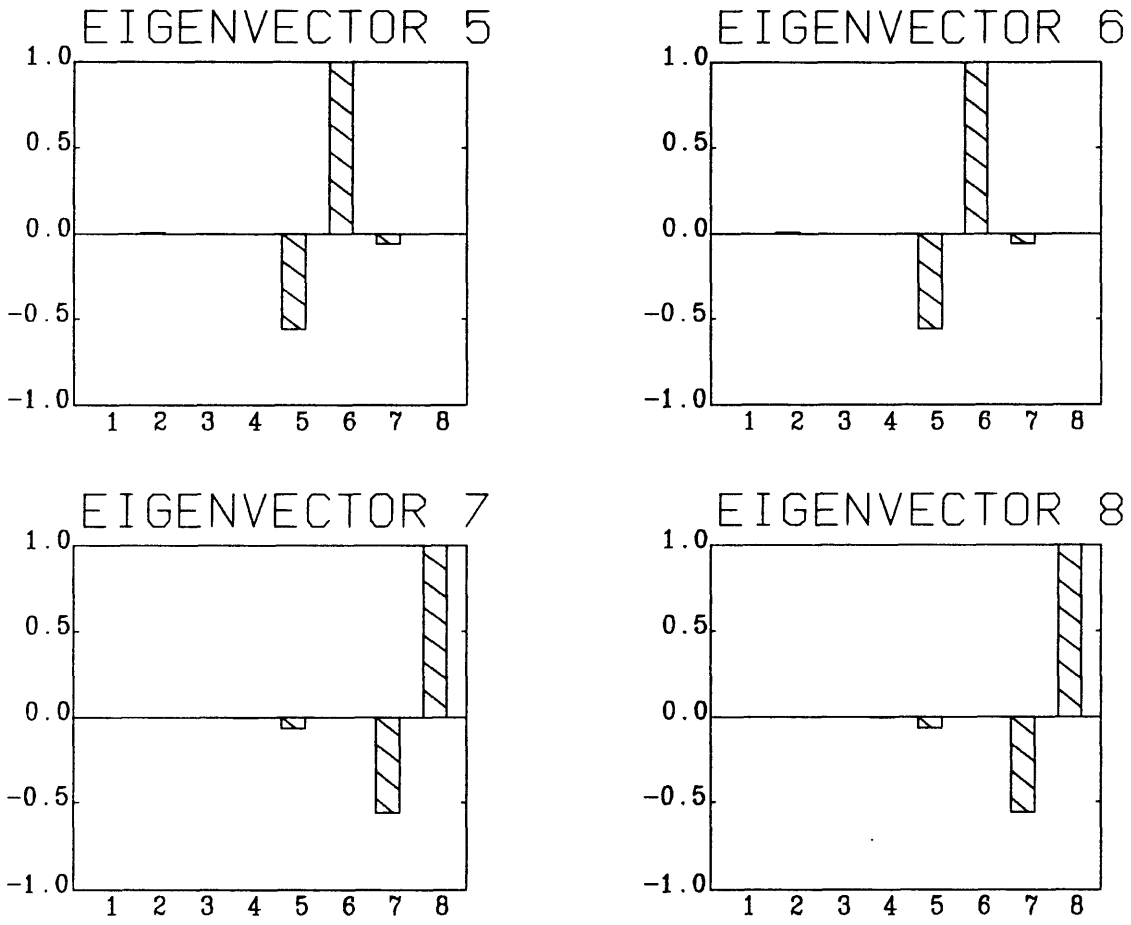

Figure 3.3 Design Plant Model Eigenvectors

3.3 Scaling of the Design Plant Model

As discussed earlier, scaling in a multivariable control system design is quite important. The LQG/LTR design methodology uses a model based compensator (MBC) which contains the A, B, C and D (if non-zero) of the DPM. If the system is not properly scaled, its ill-conditioned nature, as defined above, will then appear in the MBC. It is possible, among other considerations, that a MBC may not even be realizable; that is, solutions to the Control Algebraic Riccati Equation (CARE) and the (Kalman) Filter Algebraic Riccati Equation (FARE) may not even exist (the equations may not converge). In this case, an LQG/LTR compensator can not be found. The unscaled system of this thesis is a prime example.

A solution to this problem is to perform a complete system scaling. Complete scaling means state scaling via a state transformation, input matrix scaling and output matrix scaling. The specific combinations of scaling used is unique for each particular system. There are, however, a few guidelines to follow : One technique of state scaling is an attempt to weigh state deviations in a systematic manner that makes physical sense; input and output scaling is done to confine the system to a unit square (if 2-input, 2 output) or a unit pseudo-cube in this case; one final hint is to perform state scaling with concentration on producing a well conditioned system A matrix. It will be shown that a proper application of state scaling can produce a well conditioned system matrix. Also note that since scaling affects the input - output relationship of the DPM, it can be expected that the singular value plot of DPM (Figure 3.1) will change with the scaling also.

The state scaling is performed to normalize the state variables with respect to each other. That is, it provides a measure of relative importance of a state expressed in meters / second to one expressed in meters etc. This is the exact type of scaling necessary for our problem. Examination of the unscaled system eigenvectors reveals that for a given system

modal excitement, a unit response of velocity output will be seen, while only a fractional amount (.0045) of position response will be observed. In order to 'balance' the system, a state scaling should "balance out" the different state variables, with respect to their units so that the state space is spanned appropriately, i.e. the eigenstructure is not skewed because of a unit inconsistency. The following will document this procedure.

A state transformation can be defined as

$$\mathbf{x}_s(t) = T^{-1}\,\mathbf{x}(t) \qquad (3.3)$$

where $\mathbf{x}_s$ is the new state vector related to $\mathbf{x}$ by the state transformation matrix T^{-1}. If $\mathbf{x}_s$ is considered as the scaled system states, then the time evolution of the scaled states is completely described by

$$\dot{\mathbf{x}}_s(t) = S_x^{-1} A S_x\,\mathbf{x}_s(t) + S_x^{-1} B\,\mathbf{u}(t) \qquad (3.4)$$

where $S_x^{-1} = T^{-1}$ is the scaling transformation matrix. The output equation, as defined in (3.2) is also affected by this state transformation. It will be redefined following the input / output scaling found below.

The state scaling matrix S_x^{-1} is defined as

$$S_x^{-1} = \begin{bmatrix} (1/.0045)\,I_{4\times4} & 0_{4\times4} \\ 0_{4\times4} & I_{4\times4} \end{bmatrix}.$$

Recall that the first four system states are the position states and the second group of four are velocity. It can be seen in the S_x^{-1} matrix that the position states are being amplified by a factor of 1/.0045 (22.2) so that for the same modal excitation as mentioned above, the scaled system will respond relatively equally (in terms of velocity vs. position). The application of this state scaling matrix in (3.4) immediately produces the desired scaled system A matrix. It is important to note that a diagonal state transformation like this does

not affect the definitions of the states, that is, the states retain their physical meanings. Recall that the cond(A) = 8.33×10^4 and that the desired condition of a matrix is close to 1. After performing the defined state scaling, it was found that the condition of scaled system matrix A has been reduced to 1.729. Therefore, the state scaling applied in terms of normalization of relative states also improved the numeric condition of the system.

The the remaining scaling issue is concerned with the system inputs and outputs . Input (output) scaling is done to either emphasize/de-emphasize a control input (system output) or to normalize inputs (outputs) or any combination thereof [2]. Since the state scaling performed above resulted in a physically meaningful, numerically stable system, it was decided to just use input/output normalization scaling in order to 1) make the system transfer function matrix (TFM) independent of units and 2) to confine the TFM to the unit pseudocube. The scaling matrices in this case are related to the maximum values expected at the inputs and outputs (in this case both in volts). The input scaling matrix, S_u, can be defined as follows

$$\mathbf{u}_{unscaled}(t) = S_u \mathbf{u}_{scaled}(t) \quad , \qquad (3.5)$$

and the output scaling matrix, S_y, is defined as

$$\mathbf{y}_{unscaled}(t) = S_y \mathbf{y}_{scaled}(t) \qquad \text{or}$$

$$\mathbf{y}_{scaled}(t) = S_y^{-1} \mathbf{y}_{unscaled}(t) \qquad (3.6)$$

Where the scaling matrices are

$$S_u = \mathbf{u}_{max} \left[I_{4\times4} \right] \qquad \text{and}$$

$$S_y = y_{max}\left[I_{4\times4}\right] \Rightarrow S_y^{-1} = \frac{1}{y_{max}}\left[I_{4\times4}\right]$$

The maximum control command voltage for this system, u_{max}, is 30 Volts, and the maximum output voltage y_{max}, is 10 Volts.

Input and output scaling transformations can now be combined with the new state equations (3.4) to yield the scaled design plant model (SDPM)

$$\dot{x}_s(t) = S_x^{-1} A S_x x_s(t) + S_x^{-1} B S_u u_{scaled}(t) \qquad (3.6)$$

$$y_{scaled}(t) = S_y^{-1} C S_x x_s(t) \qquad (3.7)$$

Figure 3.4 contains a block diagram of the complete SDPM.

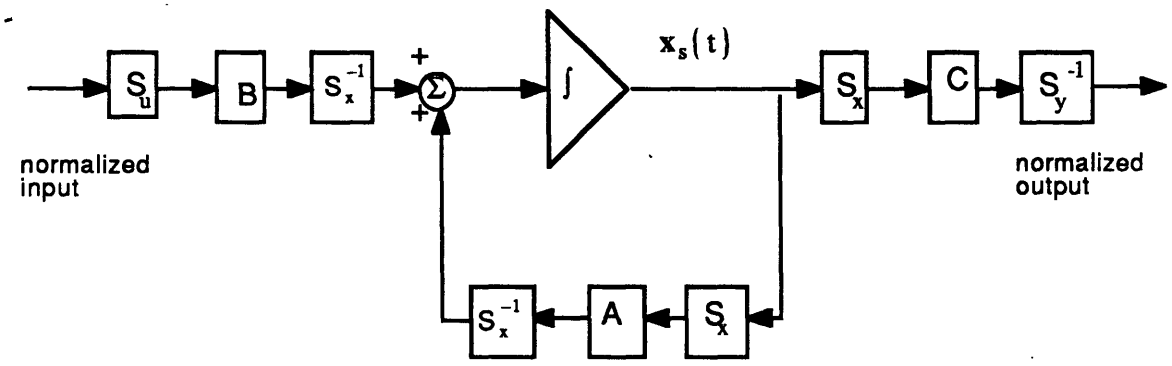

Figure 3.4 Scaled Design Plant Model

The SDPM can now be summarized by the following state equations

$$\dot{x}_s(t) = A_s\, x_s(t) + B_s\, u_{normalized}(t) \tag{3.8}$$

$$y_{normalized}(t) = C_s\, x_s(t) \tag{3.9}$$

where 'normalized' has replaced 'scaled' as a more appropriate term because the input / output scaling created a dimensionless system contained in the unit pseudocube. The scaled system matrices are defined as

$$\begin{aligned} A_s &= S_x^{-1} A S_x \\ B_s &= S_x^{-1} B S_u \\ C_s &= S_y^{-1} C S_x \end{aligned} \tag{3.10}$$

Eigenstructure analysis of the system state matrix reveals no change in the system eigenvalues as expected; they are preserved through any similarity transformation, while the system eigenvectors have changed dramatically. Figures 3.5 and 3.6 are bar graph representations of each eigenvector, similar to Figures 3.2 and 3.3. The effects of system scaling are seen clearly in a comparison of the two sets of figures. In Figures 3.5 and 3.6 it can be observed that the system now spans the 8-dimensional space. Figure 3.7 contains the singular value plot for the SDPM. Also note that the D.C. gain of the system changed with the scaling as expected, but the shape of the plot remained basically the same. Through scaling, the TFM has become dimensionless so the plot has no units associated with it. The open loop system has singular value crossover frequencies (defined as the 0 dB crossing) in the range of 200 to 400 r/s.

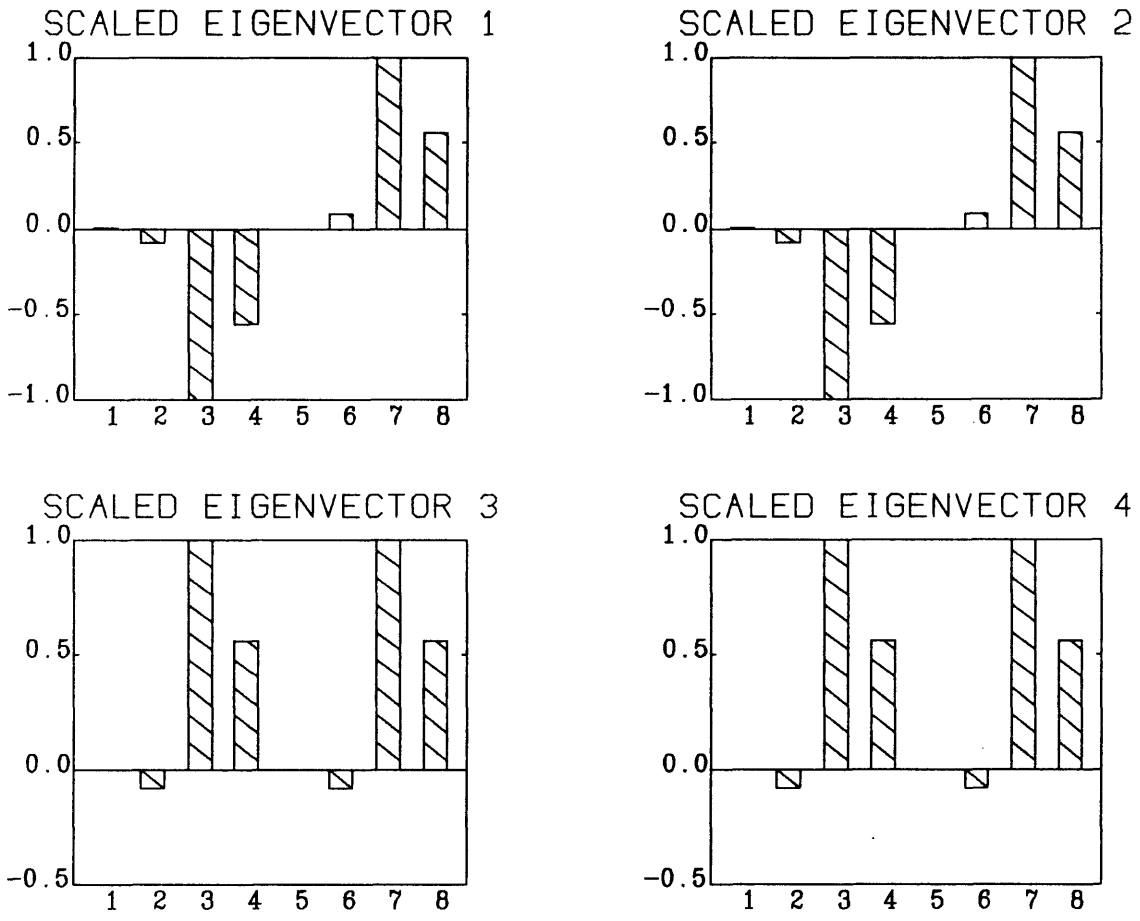

Figure 3.5 Scaled Design Plant Model Eigenvectors

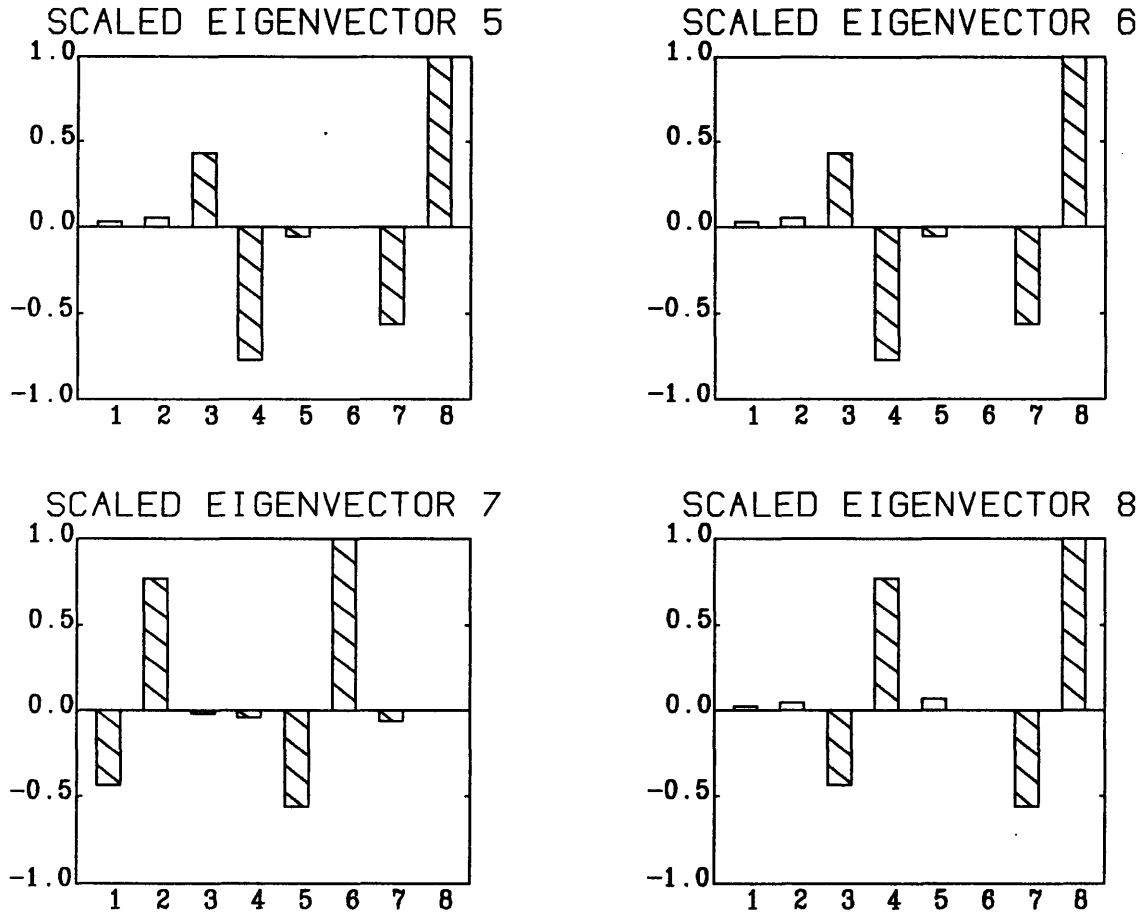

Figure 3.6 Scaled Design Plant Model Eigenvectors

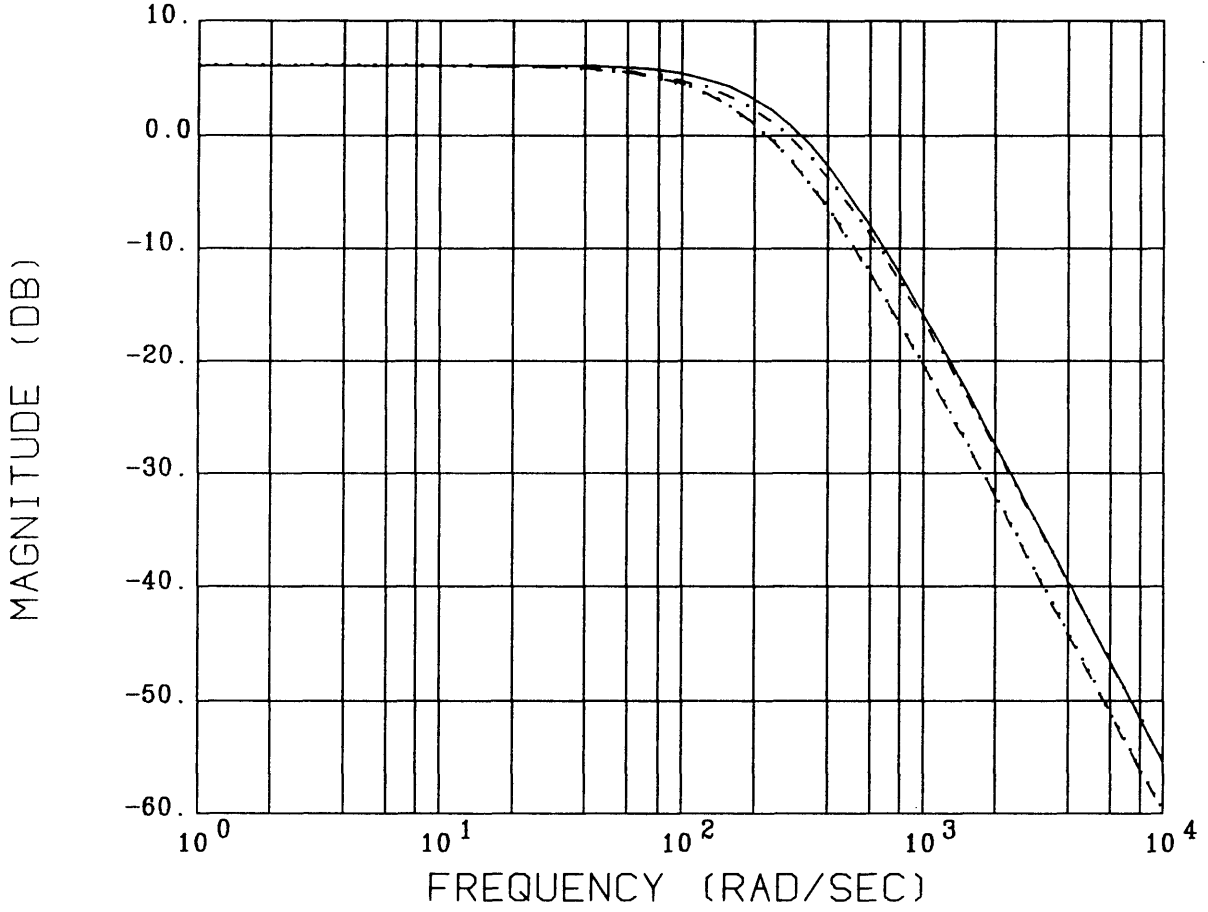

Figure 3.7 Singular Values of the Scaled Design Plant Model

3.4 Controllability and Observability

The issues of system controllability and observability are extremely important in any control system design and the use of the LQG/LTR methodology is no exception. The concepts of controllability and observability are introduced in an introductory systems analysis course [10]. These restrictive concepts can be relaxed to the respective concepts of stabilizability and detectibility [1]. These less restrictive constraints are necessary and sufficient to guarantee the existence and uniqueness of the optimal solution to both the Linear Quadratic Guassian (LQG) and Kalman Filter (KF) problems that are the significant parts of the LQG/LTR design process [1]. Without further delay, simply stated :

> The dynamic system described by (2.15) and (2.16), with numerical parameters as defined in Appendix B, and the resulting system state matrices of Appendix C is both completely controllable and completely observable.

These properties can be shown through use of the unscaled eigenvectors combined with the system B and C matrices. The i^{th} system mode is observable if $C v_i \neq 0$, where v_i is the i^{th} right eigenvector, and the j^{th} system mode is controllable if $w_j^T B \neq 0$, where w_j^T is the j^{th} left eigenvector. Application of these tests leads to the above conclusion.

3.5 Model Errors

In this section, we will develop the system model error. The only modelling error that will be considered is the known error between the DPM and the flexible shaft / rotor model whose state space representation is given in Appendix A.2. Modelling errors concerning sensor and actuator dynamics and the accuracy of the flexible model will not be addressed here.

There are several approaches to defining modelling errors [1,9]. The approach to be used here is to consider the model error as a multiplicative error where the modelling error is chosen to be reflected at the plant output.

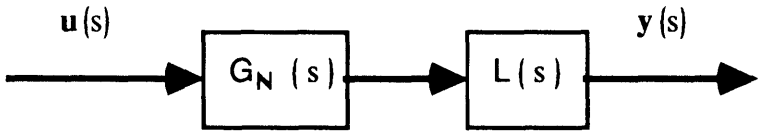

Figure 3.8 Model Error Reflected at Plant Output

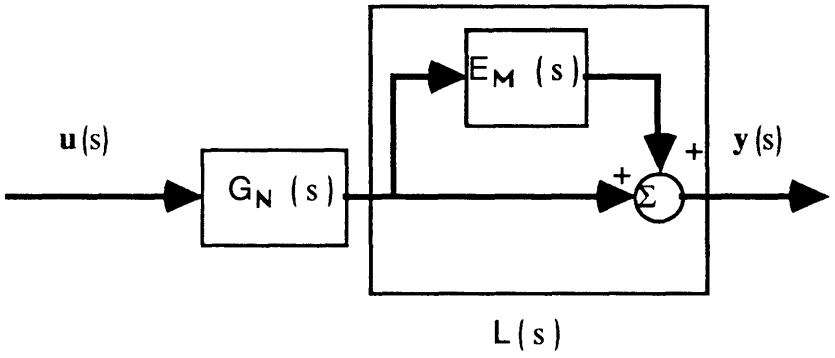

Figure 3.9 Multiplicative Error Block Diagram

Figure 3.8 implies that the actual plant, G_A, is a combination of the nominal plant (DPM), G_N, and a multiplicative error L(s). Equation (3.11) summarizes this statement

$$G_A(s) = L(s)G_N(s) \quad . \qquad (3.11)$$

The model error, L(s), can be visualized (see Figure 3.9) as

$$G_A(s) = [I + E_M(s)]\, G_N(s) \qquad (3.12)$$

and the multiplicative error TFM, $E_M(s)$, can be found in terms of G_N and G_A, which are both known. Solving (3.11), $E_M(s)$ becomes

$$E_M(s) = [G_A(s) - G_N(s)]\, G_N^{-1}(s) \quad . \qquad (3.13)$$

This TFM can easily be calculated using matrix algebra if the individual TFMs are known. Figure 3.10 contains the singular value plot[1] of $G_A(s)$. It is used in calculation of $E_M(s)$, shown in Figure 3.11. The multiplicative error singular values imply that the simplified model is accurate at low frequencies, but modelling errors become appreciable well within the system bandwidth. This plot will be used later in a check for guaranteed closed loop system robustness.

[1] The singular values of the flexible shaft reveal the effect of the transmission zeroes in that system. The zeroes exist beyond the system bandwidth, and are minimum phase.

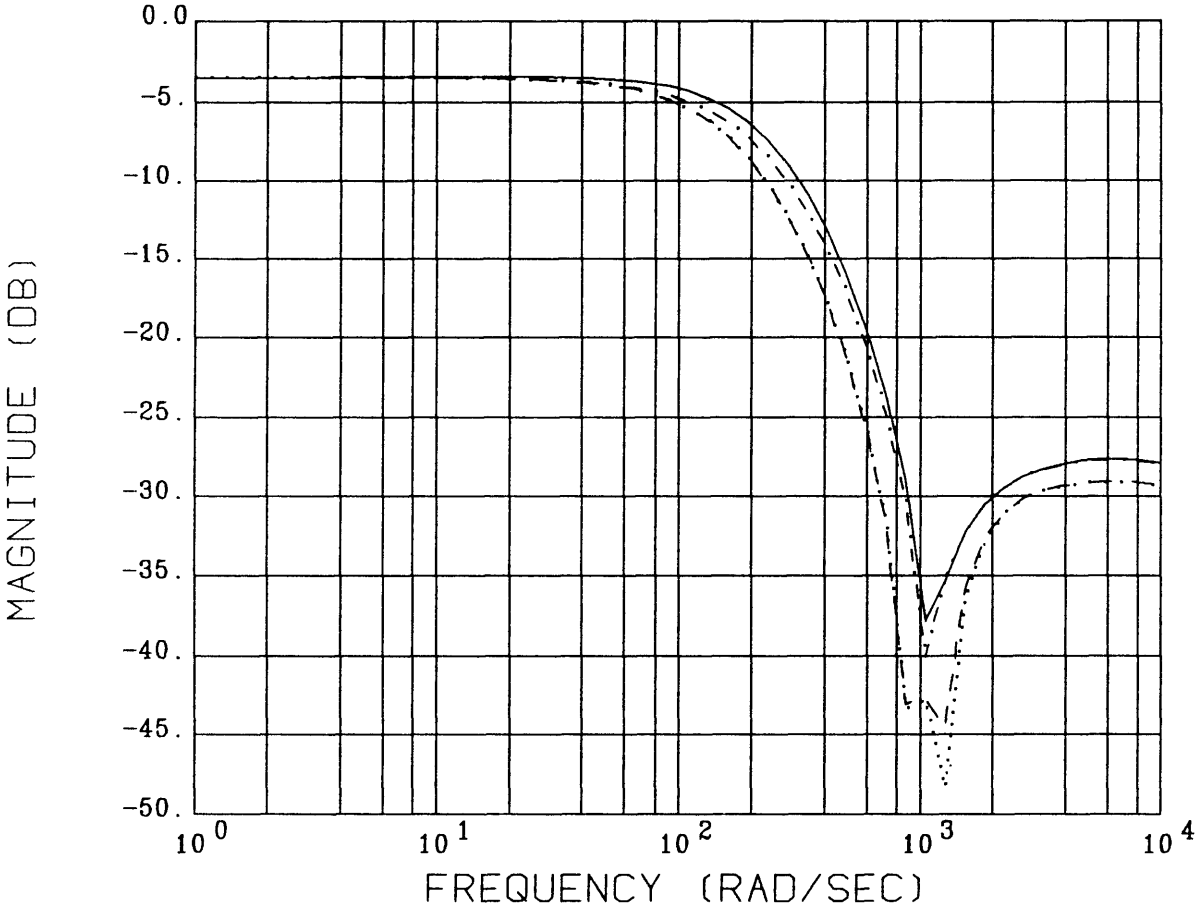

Figure 3.10 Singular Values of the Flexible Rotor Model

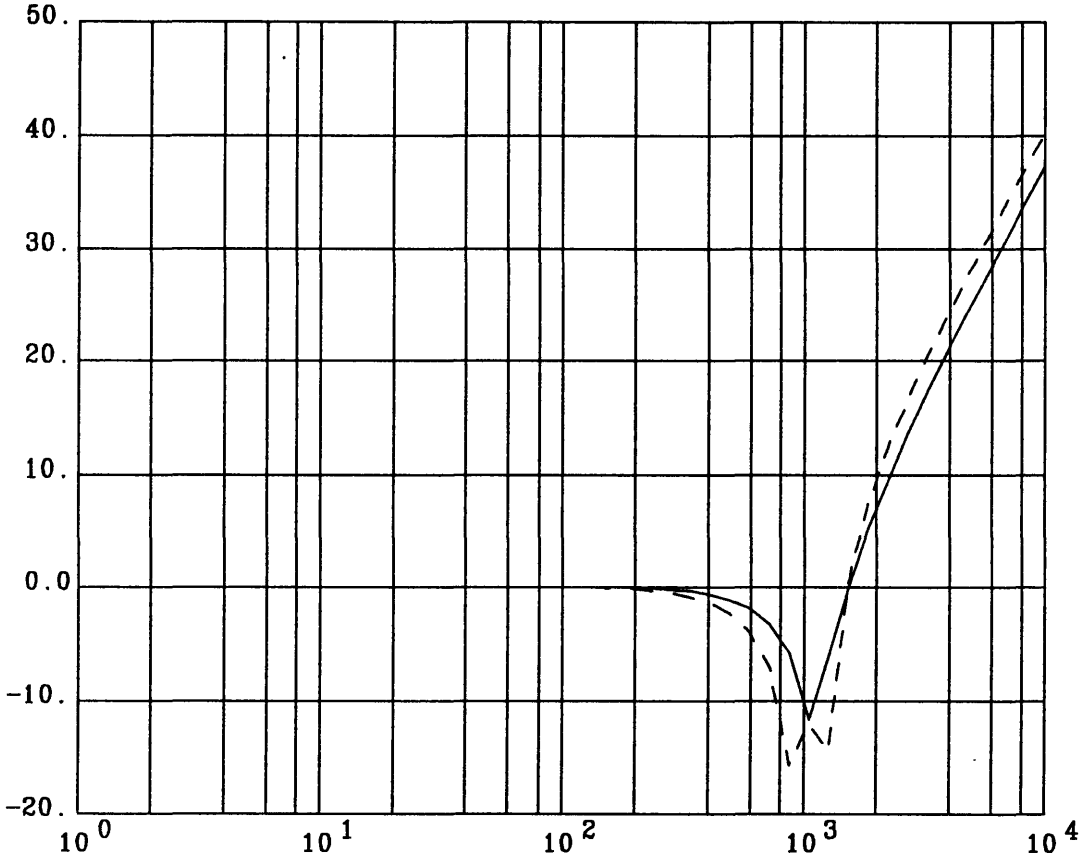

Figure 3.11 Singular Values of the Multiplicative Error

3.6 Summary

In this chapter, numerical values were introduced into the DPM derived in Chapter 2. Eigenstructure and matrix condition analysis was performed on the system state matrix and it was found that the system was ill-conditioned. Matrix condition implications were discussed and it was suggested that system scaling could be done to improve the system numerical properties. Several scaling approaches were presented and the chosen scaling procedure for this system was clearly documented. The selected scaling procedures were applied and the scaled design plant model (SDPM) which will be used for controller design was defined. It was stated that the system was completely controllable and observable. The concept of multivariable error analysis was introduced and system multiplicative error was defined in terms of the DPM and the actual flexible shaft system.

Chapter 4

4. Design of the Multivariable Control System

4.1 Introduction

In this chapter, the design of the multivariable control system will be performed. Specifications for the system performance will be stated. The Linear Quadratic Gaussian with Loop Transfer Recovery (LQG/LTR) methodology will be introduced and applied to the scaled design plant model (SDPM). The controller will be combined with the design plant model (DPM) and the closed loop system robustness properties will be evaluated with respect to the modelling errors derived in Chapter 3.

4.2 Performance Specifications

In any control system design, there must be some criterion which enables the designer to make decisions which affect the closed loop system performance. These criteria can be combined under the heading of performance specifications. For example, the specifications may include, physical limitations for the system, or they may be specified as a desired level of performance with respect to a state variable or both. Before the system controller can be designed, some system specifications must be imposed.

The specifications for the electromagnetic bearing / shaft system are not well defined. They are based on the design goals of the Draper Lab testbed, which, at the inception of this thesis, were set to be the following : It is desired that

1) the system have a high degree of disturbance rejection at all frequencies,

2) there are zero steady state errors to step command inputs,

3) the open loop crossover frequency[1], ω_c, be 100 Hz and

4) that the system behave equally well in all directions.

The crossover frequency specification is consistent with other magnetic bearing controller designs found in the literature [20]. There exists a minimum crossover for systems with unstable poles [14] because some system gain is required to simply stabilize the system. We assume the specification given in (3) is beyond the minimum crossover for this system. The first two requirements are standard in many control system designs. The use of an integral controller will insure zero steady state error to D.C. disturbances and step command inputs. The final desired characteristic is not necessarily unique to MIMO systems. For example, if a system had several similar SISO loops, it maybe desirable that each loop have the same performance characteristics, if physically possible. In the frequency domain, this would mean they have identical Bode plots. Interpreting this in a MIMO context, we would say that all singular values would be identical over the entire frequency range. This is referred to as singular value matching.

In order to meet these design goals, some assumptions concerning actuator and sensor dynamics must be made . A conservative assumption is requiring the frequency response of the actuator and sensors to be flat from D.C. to 1000 Hz (10 times ω_c). The linearized model of the actuator, defined in Chapter 2, contains no dynamics so this assumption is valid.

[1]Crossover frequency is defined as the 0 dB crossing (as in Chapter 3).

In summary, two constraints have been placed on the control system design : the controller must contain an integrator for each of the control channels and the loop (controller and DPM) TFM must crossover at 100 Hz.

4.3 The LQG/LTR Design Methodology

The Linear Quadratic Gaussian with Loop Transfer Recovery (LQG/LTR) control system design methodology is a relatively mature design procedure. It has been applied to many multivariable systems from jet engines [3] to automobile engines [12] to submarines [2]. The basis of the methodology is frequency domain shaping of the loop (combined compensator and DPM) singular values.

Several steps of the design procedure have already been completed : deriving the DPM (in this case the SDPM), defining system specifications and performing rudimentary error analysis. The remaining steps combine Kalman Filter (KF) and Optimal Linear Quadratic Guassian (LQG) theory to design a Model Based Compensator (MBC).

4.3.1 Kalman Filter Design and the Target Feedback Loop

In this section, the basic concepts needed to design a KF for the SDPM will be presented. The KF will not be used as the optimal state estimator it is devised as but, rather, as a design tool to perform frequency domain loop shaping to meet system specifications. The goal in using the KF design procedure is to develop a Target Feedback Loop (TFL) which captures the desired characteristics of the combined controller and DPM, the loop transfer function GK(s), for the loop broken at the plant output.

We will start with the definition of the KF design. Again, consider the state space system as defined in (2.14) :

$$\dot{x}(t) = A\,x(t) + B\,u(t)$$

$$y(t) = C\,x(t) \qquad (4.1)$$

This description is modified to allow KF theory application, and (4.1) becomes

$$\dot{x}(t) = A\,x(t) + B\,u(t) + L\,\xi(t)$$

$$y(t) = C\,x(t) + \theta(t) \qquad (4.2)$$

where $\xi(t)$ is white process noise with unit intensity which enters the system through the matrix L, and $\theta(t)$ is white sensor measurement noise with intensity $\Theta = \mu I$. At this point, some restrictions must be applied. They are that

1) [A, L] must be stabilizable and

2) [A, C] must be detectable.

It was stated in Chapter 3 that the DPM was completely observable. This satisfies constraint (2). Constraint 1) implies that the process noise must (at least) excite all the unstable system modes. This depends on the choice of L. Having the design freedom to choose L and μ is what differentiates the standard optimal KF from our version. In the standard KF problem, these parameters are determined by the noise statistical properties and the system structure in question. In this case, L and μ can be chosen to perform the desired frequency domain loop shaping. Loop shaping is performed on the KF TFM defined as [1,2]

$$G_{KF}(s) = C(sI - A)^{-1}H \qquad (4.3)$$

where H is defined as

$$H = \left(1/\sqrt{\mu}\right)\Sigma C^{T} \quad , \qquad (4.4)$$

with Σ being the solution to the Filter Algebraic Riccati Equation (FARE) :

$$0 = A\Sigma + \Sigma A^{T} + LL^{T} - \left(1/\sqrt{\mu}\right)\Sigma C C^{T}\Sigma \qquad (4.5)$$

The Kalman Frequency Domain Equality [8] as defined for the KF problem,

$$\left[I + G_{KF}(s)\right]\left[I + G_{KF}(-s)\right]^T = I + \left(1/\mu\right)\left[C\,\phi(s)\,L\right]\left[C\,\phi(-s)\,L\right]^T$$

where $\phi(s) = (sI - A)^{-1}$, can be used to show that [1]

$$G_{KF}(s) \approx \left(1/\sqrt{\mu}\right) C(sI - A)^{-1} L \qquad (4.6)$$

This approximation can be analyzed to aid in the choice of the design parameters L and μ. It can be shown [1] that low frequency matching of the singular values of $G_{KF}(s)$ can be achieved by the choice of

$$L = -C^T\left(CA^{-1}C^T\right)^{-1} , \qquad (4.7)$$

and for high frequency singular values matching, choose[1]

$$L = C^T\left(C\,C^T\right)^{-1} , \qquad (4.8)$$

and the design parameter, μ can be use to control the system bandwidth.

Completion of the above procedure will produce a $G_{KF}(s)$ (for the design plant model) that will have the following guaranteed properties [1,2]:

1) the closed loop system will be stable

2) infinite upward gain margin

3) downward gain margin of at least 6 dB

4) at least $\pm$ 60° of phase margin

5) the loop will be minimum phase.

It is because the above properties represent a well designed control system that $G_{KF}(s)$ will be used as a Target Feedback Loop (TFL) which represent the desired characteristics of GK(s). The TFL properties are to be recovered in the next step of the design.

[1]Other choices of L can be found [1,2].

4.3.2 The Loop Transfer Recovery

The frequency domain shapes of the TFL to be designed will meet the design specifications placed on the system. The next step of the design process is to recover those shapes with the controller and DPM TFM, GK(s). This is accomplished by applying Linear Quadratic Guassian (LQG) design techniques, using 'cheap' control.

The LQG design produces a controller gain matrix G_ρ which is derived from the solution to the Control Algebraic Riccati Equation (CARE), with ρ being the design parameter that represents the cost of the control. The concept of 'cheap' control is defined by the solution to the CARE as $\rho \rightarrow 0$. The CARE is defined for the system in (4.1) as [1,8]

$$0 = -K_\rho A - A^T K_\rho - C^T C + \left(1/\rho\right) K_\rho B B^T K_\rho \qquad (4.9)$$

and the LQG gain G_ρ is defined as

$$G_\rho = \left(1/\rho\right) B^T K_\rho \qquad (4.10)$$

As was the case for the KF design, some design prerequisites are imposed. They are that

1) [A, B] must be stabilizable,

2) [A, C] must be detectable and

3) the system must be minimum phase (no RHP zeroes).

It was stated in Chapter 3 that the DPM was completely controllable and observable. This satisfies constraints (1,2). Constraint (3), which is important for the recovery of the TFL properties, is met by the fact that the DPM has no zeroes[1].

As a design goal for this procedure, it is desirable that the recovery of the TFL is completed to approximately one decade beyond the crossover. This 'amount' of recovery

[1] The fully flexible model contains transmission zeroes. It depends on specific system parameters whether or not they are minimum phase or not. See McCallum [6]. For the system as specified in Appendix B, using the full rotor model, the transmission zeroes that exist are minimum phase.

(vs. frequency) is dependent on the choice of ρ, i.e. how cheap the control is made. As with all LQG designs, there are design trade-offs with respect to the degree of cheap control used. This means that too cheap control may produce extremely large gains that will cause the controller to request excessively large control commands.

The LQG/LTR design procedure is now complete. The procedure produced two gain matrices K and G. These matrices will be used with the matrices of the SDPM (important to note *scaled*) to form a compensator known as the Model Based Compensator (MBC). It is called model based because the DPM is used as part of the dynamic compensator. Figure 4.1 contains the block diagram of GK(s), where K(s), the MBC, with its designed gain matrices H and G, is in series with the DPM. The MBC can be described by system equations as

$$\begin{aligned} \dot{\mathbf{z}}(t) &= (A - BG - HC)\,\mathbf{z}(t) - H\,\mathbf{e}(t) \\ \mathbf{u}(t) &= -G\,\mathbf{z}(t) \end{aligned} \tag{4.11}$$

To reiterate, if there are no non-minimum phase zeroes, then the frequency domain shape of the singular values of GK(s) will approach those of the TFL as $\rho \rightarrow 0$.

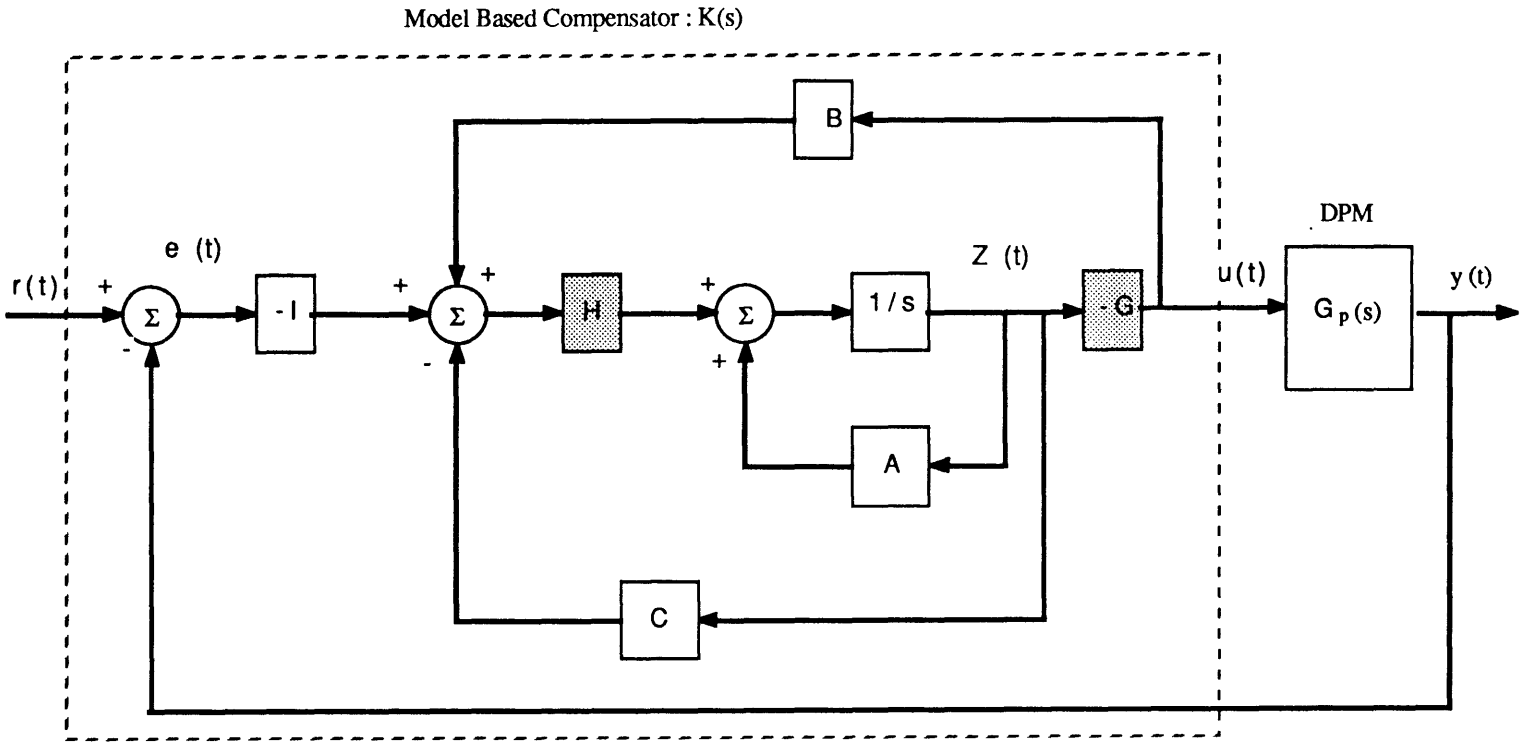

Figure 4.1 Model Based Compensator Block Diagram .

Shaded blocks represent Kalman Filter gain, H and LQG gain G

4.4 Control System Design

Now that the design procedure has been presented, the actual design process can begin. As stated above, the first step is the design of the target feedback loop (TFL) which meets all the system specifications. This is accomplished using Kalman Filter techniques. Before doing so, in order to meet the specification of having a type 1 TFL (i.e. integral control in loop), the scaled design plant model (SDPM) must be augmented with an integration in each control channel.

4.4.1 State Augmentation of the Design Plant Model

The desired performance characteristic of zero steady state error to step command inputs requires that a combined controller-plant system [GK(s)] be of type 1 (or greater). Since the SDPM is type 0, an integrator must be included in the compensator to increase the system type. Further, since the design process produces a TFL that is to have the desired response of GK(s), the integrator must be included in the TFL. Examining the TFL equation, defined in (4.3), it is clear that the only system dynamics are in the SDPM A matrix. Therefore, in order for GK(s) to be type 1 or more, the TFL must be type 1, which implies the SPDM must be augmented with an integrator in each control channel. Figure 4.2 illustrates this idea in block diagram form.

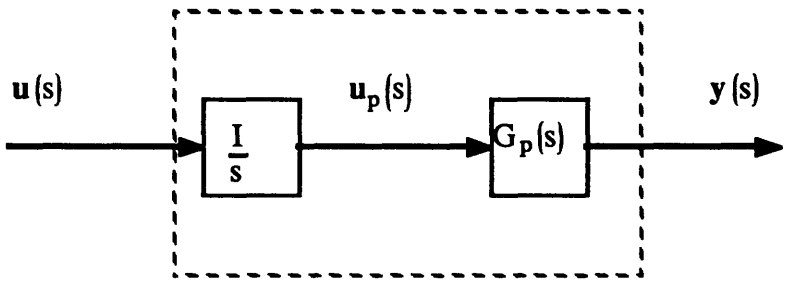

Figure 4.2 Augmented Design Plant Model

The augmentation starts with the SPDM defined in (3.8) and (3.9). The augmented system in state space form is

$$\begin{bmatrix} \dot{u}_n(t) \\ \dot{x}_p(t) \end{bmatrix} = \begin{bmatrix} 0_{m\times m} & 0_{m\times n} \\ B_s & A_s \end{bmatrix} \begin{bmatrix} u_n(t) \\ x_p(t) \end{bmatrix} + \begin{bmatrix} I_{m\times m} \\ 0_{n\times m} \end{bmatrix} u(t)$$

$$y(t) = \begin{bmatrix} 0_{m\times m} & C_s \end{bmatrix} \begin{bmatrix} u_n(t) \\ x_p(t) \end{bmatrix} \qquad (4.12)$$

where n = 8, m = 4, x_p , has been substituted for the SPDM state vector x_s , I is the 4 X 4 identity matrix, **u** is the controller output and u_p is the control input applied to the plant. The resulting augmented system is 12 th order (n + m). The KF frequency domain loop shaping procedure is to be applied to the system of (4.12). Figure 4.3 is a singular value plots of the augmented SDPM (compare to Figure 3.7).

4.4.2 Design of the Target Feedback Loop

The target feedback loop (TFL) is to be designed using the Kalman Filter design technique described above. Frequency domain loop shaping will be done to 1) match singular values at high and low frequencies and 2) to produce a TFL bandwidth of 100 Hz.

In order do both high and low frequency singular value (SV) matching, the SV matching concept introduced in section 4.3.1, must be modified to take advantage of the additional degrees of design freedom which were created via the state augmentation performed above. Equations (4.12) must be redefined as in (4.2). Recall that the state vector of (4.12) now has m+n states (12) and that the L matrix is now 12 by 4. L can be partitioned to

$$L^T = \begin{bmatrix} L_L^T & L_H^T \end{bmatrix} \qquad (4.13)$$

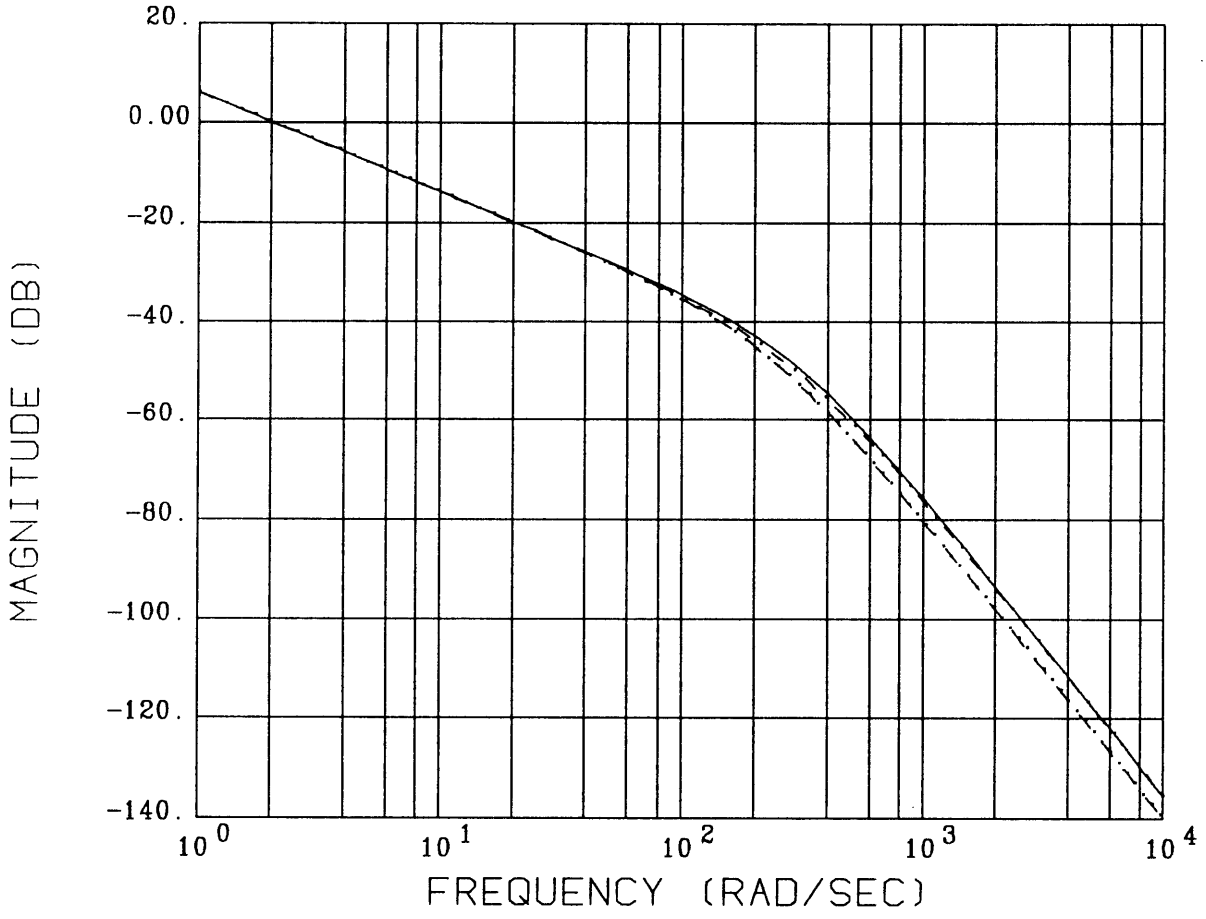

Figure 4.3 Singular Values of the Seated Augmented Design Plant Model

where L_L, a 4 by 4 matrix, can be used to shape the low frequency response of the TFL transfer function matrix (TFM), and L_H, 4 by 8 matrix, can be similarly used for the high frequency SV shaping. It can be shown through use of the Kalman Frequency Domain Equality that the following choices for L_L and L_H will produce the desired SV matching [1]:

$$L_L = -\left[C_s A_s^{-1} B_s \right]^{-1}$$

$$L_H = C_s^T \left[C_s C_s^T \right]^{-1} \qquad (4.14)$$

where the SDPM matrices of (3.10) are used. For this design, some scaling of these definitions of L were necessary, see Appendix D for the numerics. With the SV matching achieved, the remaining step of the TFL design is to force its TFM to have (approximately) the correct crossover frequency . This is accomplished through manipulation of the design parameter μ. To achieve the desired TFL, some fine tuning was required to arrive at the correct combination of L_L, L_H and μ. The μ used in the final design is $2\pi * 1500$.

The design parameters were defined and the solution to the Filter Algebraic Riccati Equation found. The resulting KF gain matrix H can be found in Appendix D. H will be used as part of the model based compensator K(s).

With H defined, the TFL can now be presented. Recalling the TFL TFM as defined by equation 4.3

$$G_{KF}(s) = C(sI - A)^{-1} H , \qquad (4.3)$$

the singular value plots of the TFL can be examined. Figure 4.4 reveals that the system design specifications are clearly met by this TFL, with the only noteworthy feature of Figure 4.4 being that the SV's may not be matched well enough at the crossover frequency.

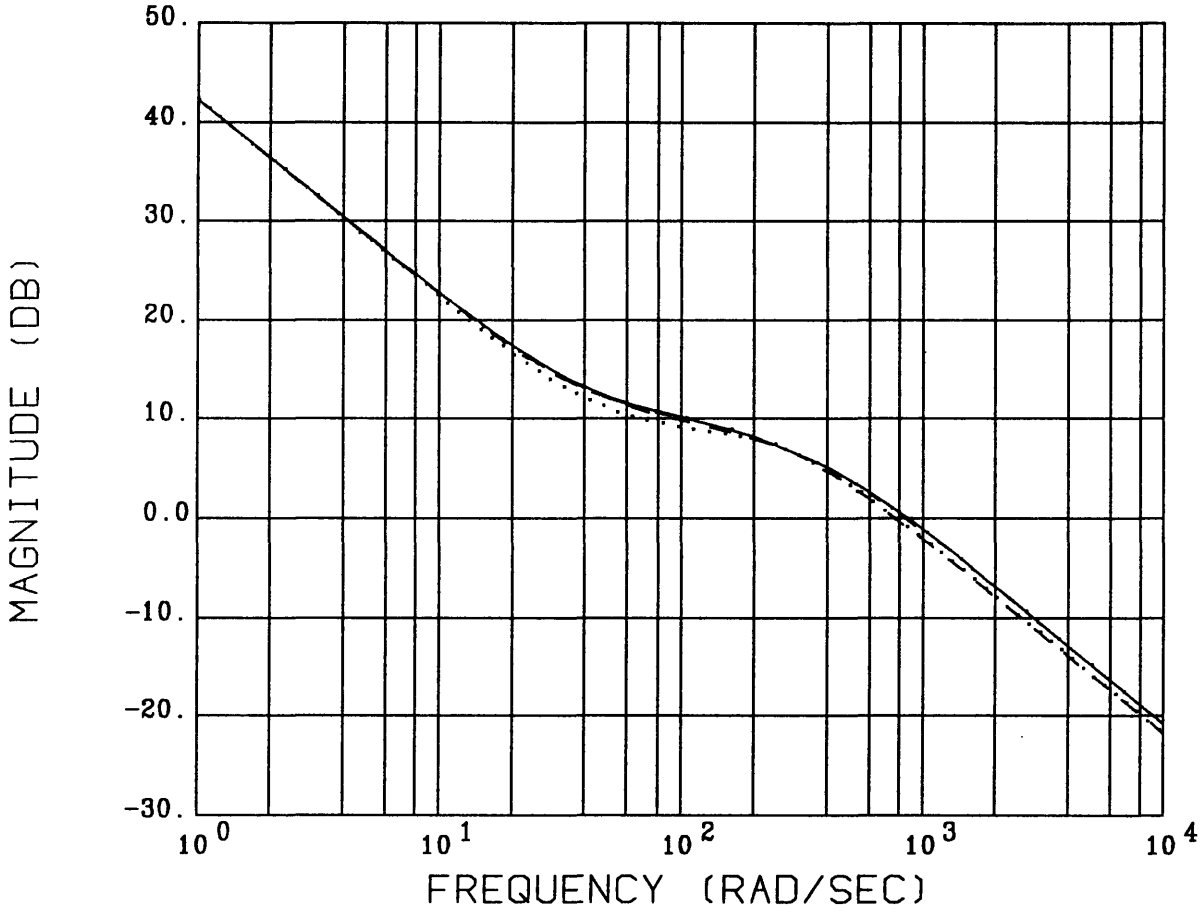

Figure 4.4 Singular Values of the Target Feedback Loop

4.4.3 Application of the Loop Transfer Recovery

With the TFL design complete, the remaining step in the controller design procedure is to recover the TFL by use of Linear Quadratic Gaussian (LQG) theory, solving the cheap control problem. As stated earlier, cheap control implies solving the Control Algebraic Riccati Equation (CARE), defined in equation (4.9), as $\rho \rightarrow 0$, using the system matrices defined in equation (3.8) and (3.9). As discussed above, the goal of this procedure is to recover the TFL to approximately one decade beyond crossover. The 'degree' of recovery depends on ρ. Choosing $\rho = 1 \times 10^{-11}$, satisfactory recovery is achieved without requiring excessively large control commands. The LQG gain matrix G produced by the LTR procedure can be found in Appendix D. Figure 4.5 is the SV plots of GK(s), which shows the recovery of the TFL to slightly less than a full decade beyond crossover, then the system rolls-off at -40 dB per decade[1].

4.4.4 The Augmented Model Based Compensator

With the LTR complete, the MBC can be assembled. There are some additional details that must be addressed. The A, B and C matrices of the MBC are from the augmented SDPM. Recall that the integral control requirement was produced by augmentation of the SDPM for the KF design procedure. In order to actually implement the integral controller, the compensator itself must be augmented to produce pure integral control. Figure 4.6 illustrates the process of moving the integration from the augmented plant to the controller.

[1] The K(s) used here has been augmented and scaled as in Figure 4.7.

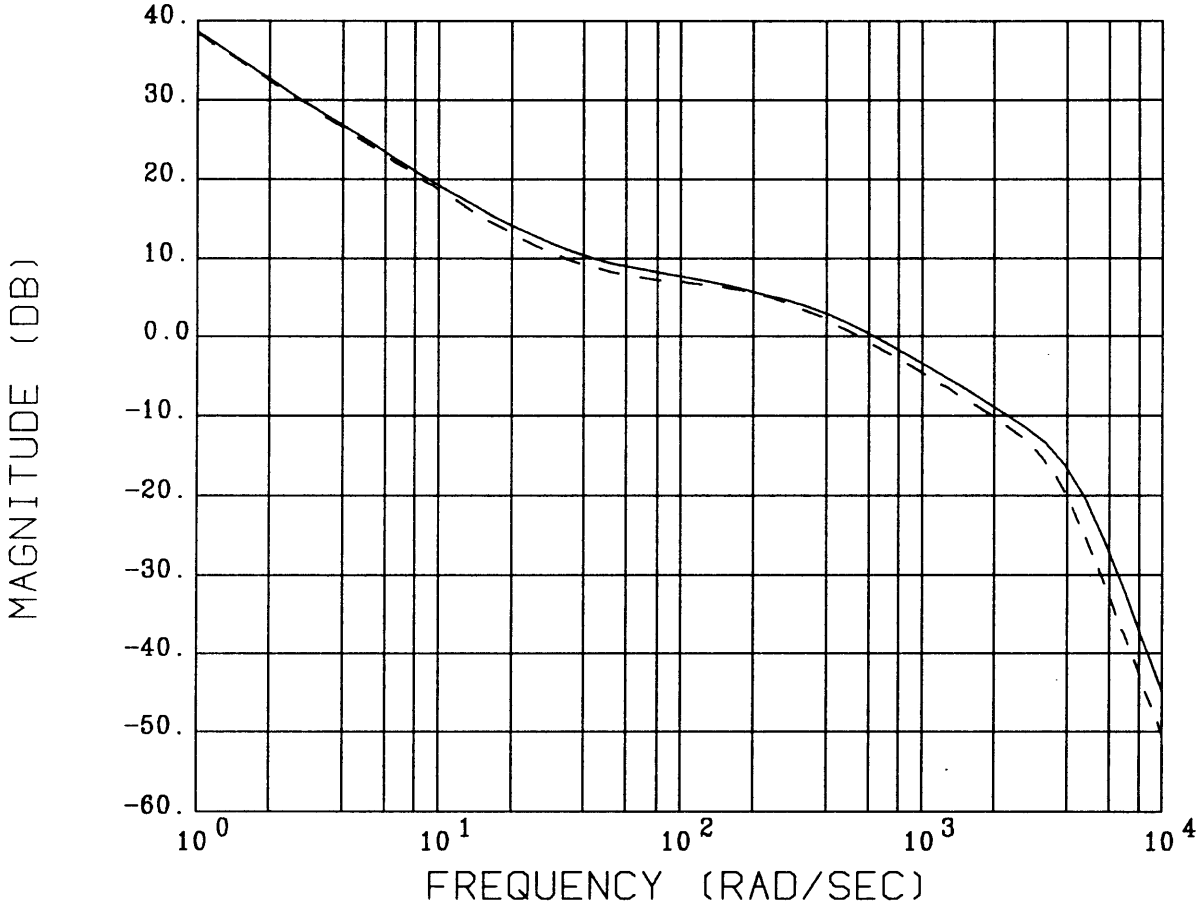

Figure 4.5 Singular Values of GK(s)

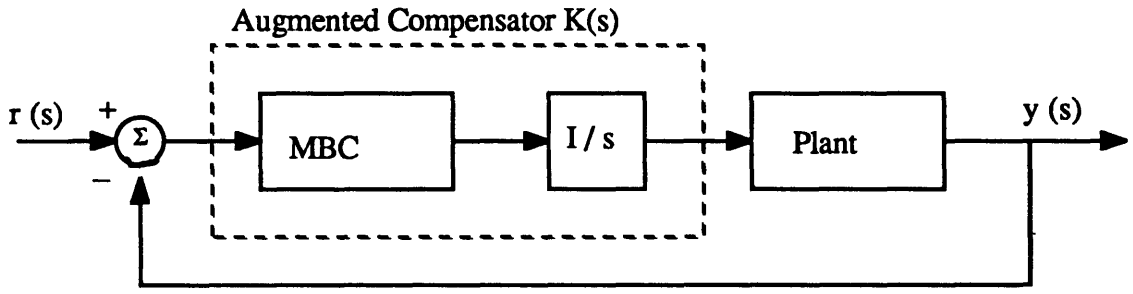

Figure 4.6 Integral Control by Compensator Augmentation

The augmented controller in state space form is

$$\begin{bmatrix} \dot{\mathbf{z}}(t) \\ \dot{\mathbf{u}}_p(t) \end{bmatrix} = \begin{bmatrix} A - BG - HC & 0_{m+n \times m} \\ G & 0_{m \times m} \end{bmatrix} \begin{bmatrix} \mathbf{z}(t) \\ \mathbf{u}_p(t) \end{bmatrix} + \begin{bmatrix} H \\ 0_{m \times m} \end{bmatrix} \mathbf{e}(t)$$

$$\mathbf{u}_p(t) = \begin{bmatrix} 0_{m \times m+n} & I_{m \times m+n} \end{bmatrix} \begin{bmatrix} \mathbf{z}(t) \\ \mathbf{u}_p(t) \end{bmatrix} . \qquad (4.15)$$

The MBC of equation (4.11) was 12^{th} order (eight order DPM, plus the original 4 integrators). The augmented MBC, K(s), is now 16^{th} (12 plus 4 pure integrators).

The compensator is not complete yet because it was designed with a normalized (scaled) DPM which is dimensionless. The compensator is expecting normalized input data and it produces normalized command outputs. In order to control the real DPM, not the scaled or normalized DPM, the compensator inputs and outputs must be scaled. The correct scaling matrices are the same ones used in the original DPM input and output scaling equations (3.5) and (3.6). This procedure is reflected in Figure (4.7).

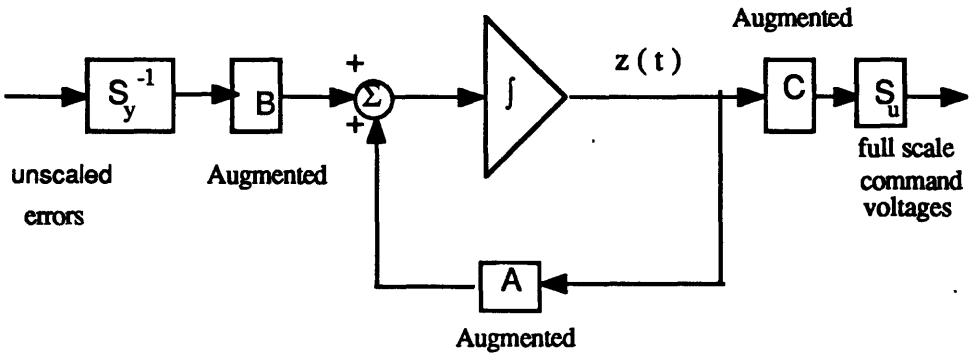

Figure 4.7 Scaled, Augmented Model Based Compensator

In summary, the scaled, augmented compensator matrices are

$$\begin{aligned} A_{comp} &= A_a \\ B_{comp} &= B_a S_y^{-1} \\ C_{comp} &= S_u C_a \end{aligned} \quad , \qquad (4.16)$$

where matrices with the subscript 'a' represent the augmented system matrices from (4.15) and the matrices, S_y^{-1} and S_u are the output / input scaling matrices defined in Chapter 3.

The augmented MBC completely described by (4.16) is ready for evaluation. The singular value plots of K(s) are shown in Figure 4.8. Examination of the plots reveals the integral-integral recovery, lead/lag form of the controller. This form is consistent with many SISO magnetic bearing/shaft compensator designs found in the literature [18], and with the lead/lag character of the LQG/LTR MIMO compensator. The numerical values of the MBC system matrices are given in Appendix E. Also included there is a listing of K(s) poles and transmission zeroes.

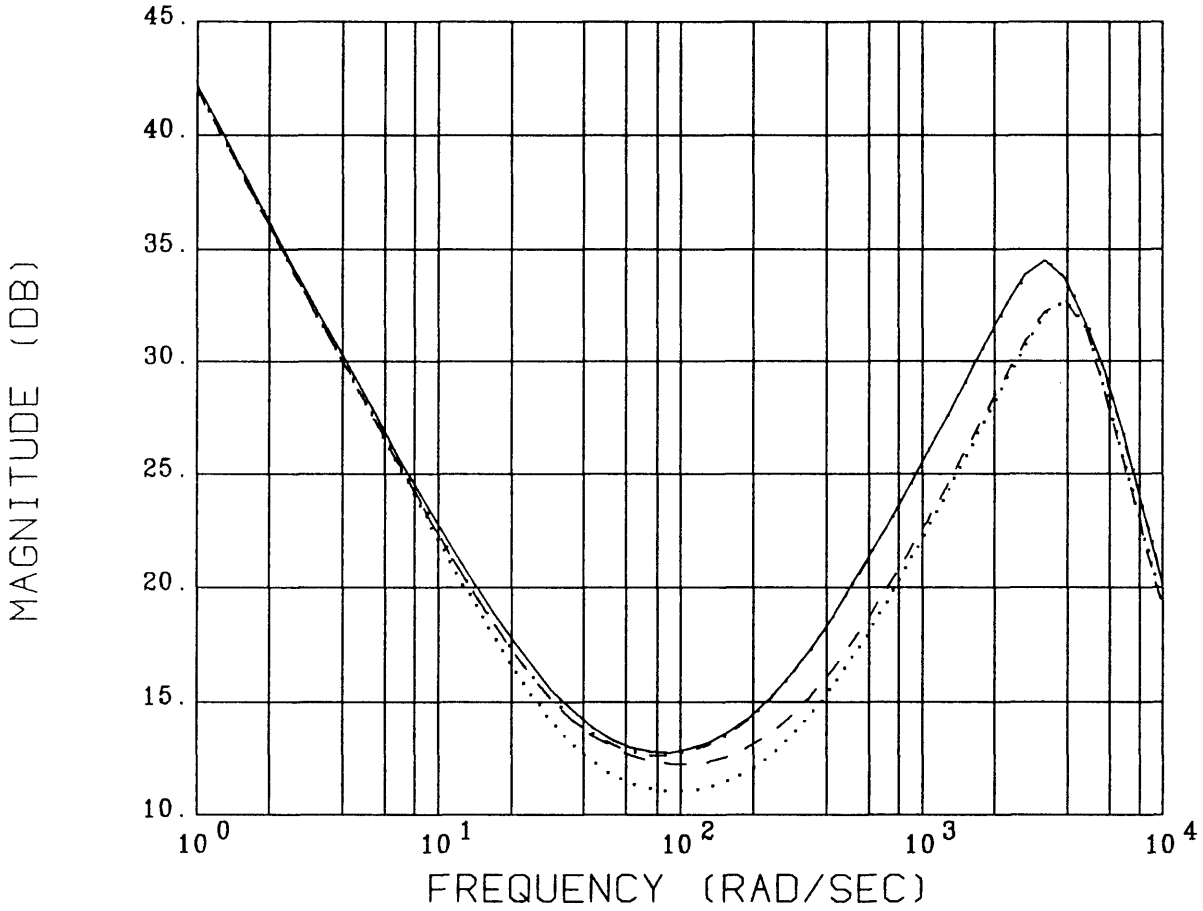

Figure 4.8 Singular Values of the Scaled Augmented Model Based Compensator

A comment must be made regarding the compensator poles. The poles are

$$0.0,\ 0.0,\ 0.0,\ 0.0,$$
$$-1630.8 \pm 3152.5\,j,$$
$$-1630.8 \pm 3153.6\,j,$$
$$-3864.6 \pm 0.6\,j,$$
$$-1934.6 \pm 3725.3\,j,$$
$$-1933.8 \pm 3747.5\,j,$$
$$-4569.0 \pm 11.6j\,.$$

These are all high frequency poles. This is because of the high bandwidth system specification. The recovery of the LTR process is required to be effective to well beyond the crossover. In fact, recovery is achieved to approximately 2000 r/s. The (relatively) small ρ needed for this amount of recovery produces the high frequency poles. It is known that if a compensator contains some high frequency poles, relative to the plant poles, then a reduced order compensator can (possibly) be found. This means that the high speed response of the compensator may not be necessary for satisfactory closed loop performance. An attempt was made reduce the K(s) designed here, using the residue method [1,3] for system reduction. It was found that the compensator could not be reduced. Any removal of compensator dynamics resulted in an unstable closed loop system. Therefore, because high system bandwidth specifications requires high frequency 'recovery' for the design to be effective, the compensator must retain all of high frequency dynamics.

The closed loop SV plots of GK(s), is shown in Figure 4.9. Some closed loop peaking occurs and the closed loop bandwidth is beyond the desired open loop bandwidth.

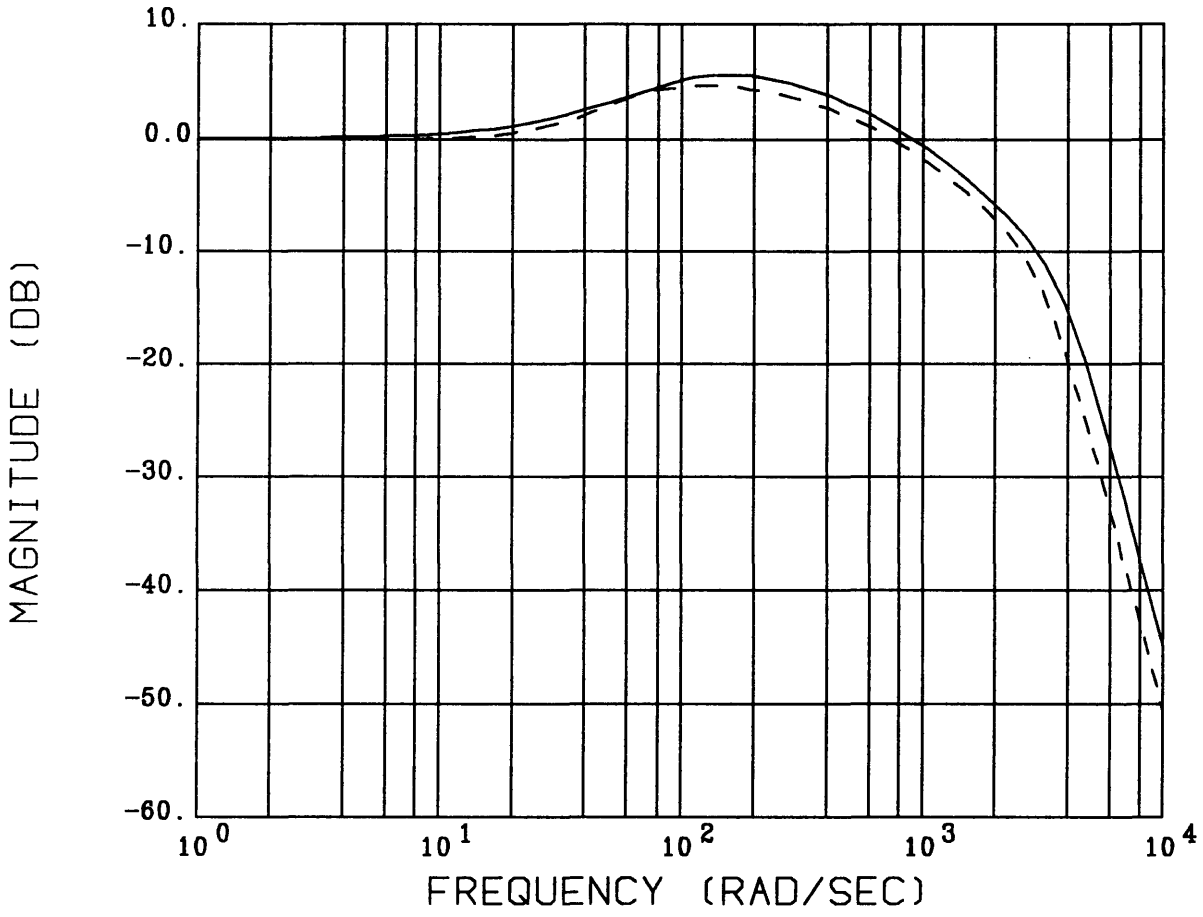

Figure 4.9 Closed Loop Singular Values of GK(s)

4.5 Closed Loop Robustness Test

The MBC, K(s) was completely designed using the simplified, stiff shaft model. Simulations will be run with that DPM to show that K(s) works, but the true test for the controller is having it work with the known plant : the flexible shaft rotor model[1] (of Appendix A.2). This testing will determine the robustness of the compensator design to modelling errors.

A conservative robustness test can be done on the basis of the known modelling errors. Multivariable error modelling was introduced in Chapter 3. Specifically, the multiplicative modelling error (MME) was defined and applied, producing the multiplicative error singular value plots of Figure 3.11. There exists a robustness criterion which relates the multiplicative modelling error SV to the closed loop SV plots of Figure 4.9 [1,3,9]. The criterion is that if the maximum singular value of closed loop system is strictly less than the inverse of the maximum singular of the MME, then the resulting closed loop system is guaranteed to be stable. In equation form, this is

$$\sigma_{max}[\, C(j\omega)\,] < {}^{1}\!/_{e_m(\omega)} \quad . \qquad (4.17)$$

Figure 4.10 contains the SV's of both the maximum 'sigma' of C (jω) (the closed loop system TFM) and the inverse of the maximum sigma of the MME. The intersection of the two plots violates the criterion of (4.17). This means that the closed loop stability of the flexible rotor and compensator is not guaranteed. But the criterion, being a very conservative and sufficient condition, does not preclude stable operation of the actual system, that is, violation does <u>not</u> guarantee instability, so there is a possibility that the closed loop system will be stable.

---

[1] Another important testing procedure is performing non-linear simulations with the non-linear bearing model (also of Appendix A). This will be discussed in Chapter 5.

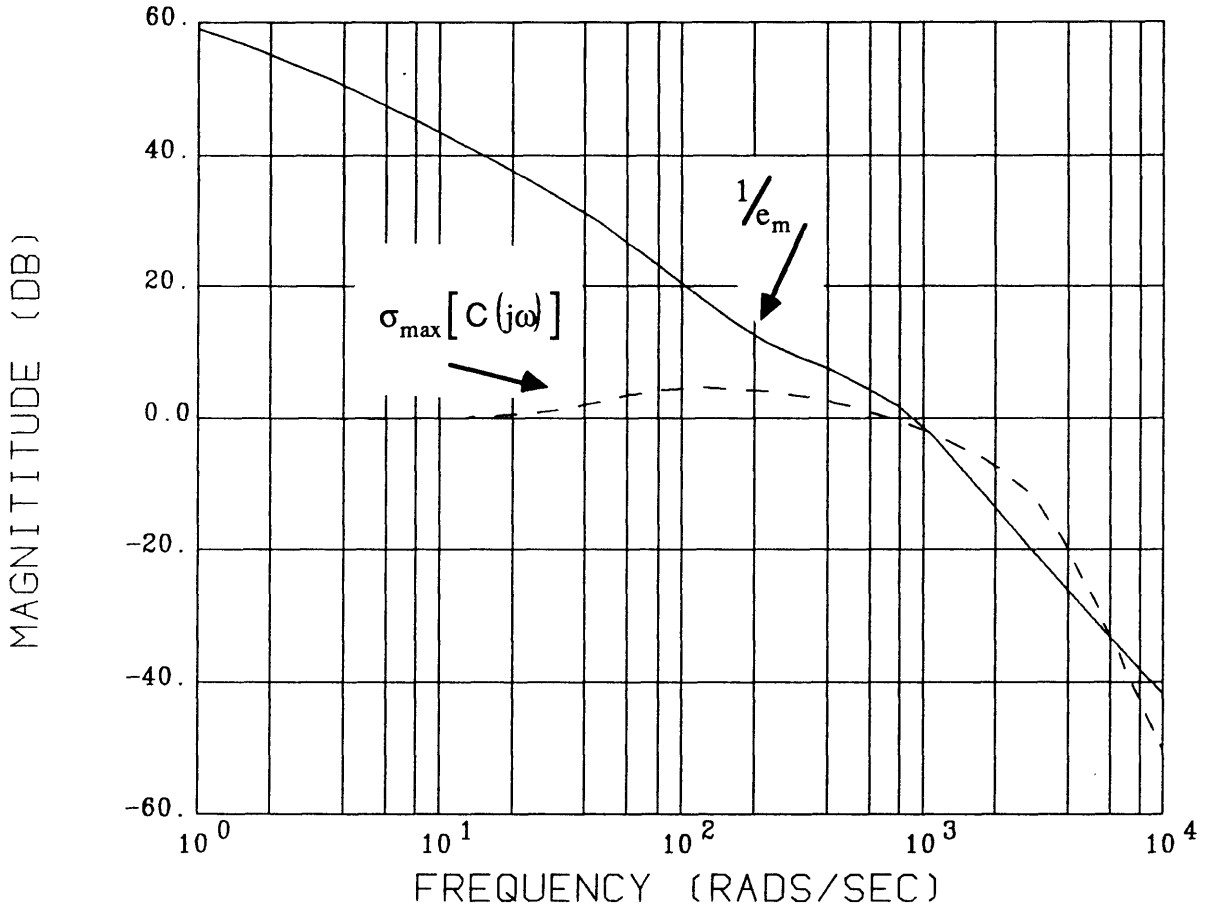

Figure 4.10 Closed Loop Stability Robustness Singular Values

4.6 Summary

In this chapter, the Linear Quadratic Guassian with Loop Transfer Recovery (LQG/LTR) multivariable control system design methodology was introduced, described and applied. A multivariable integral controller was designed for the simplified stiff shaft and linearized magnetic bearing actuator model derived in Chapter 2 and analyzed in Chapter 3. The design procedure included state augmentation to provide integral control. The resulting 16^{th} order Model Based Compensator (MBC) was scaled to be compatible with the Design Plant Model, and the closed loop system formed. Preliminary robustness analysis was performed using the Multiplicative Modelling Error derived in Chapter 3. This analysis showed that the control system as designed is not guaranteed to stabilize the flexible shaft / rotor.

Chapter 5

5. Model Based Compensator Testing

5.1 Introduction

This chapter will validate the Model Based Compensator (MBC) designed in Chapter 4. It was concluded in that chapter that the MBC did not satisfy the robustness test to the known modelling errors (see section 4.5). Hence, there is no guarantee that the closed loop system GK(s) will be stable. But, since the robustness test is only a sufficient condition, its violation does not necessarily mean that the overall system will be unstable either. Therefore, the MBC must be thoroughly tested in order to have confidence in its ability to stabilize the unstable, nonlinear plant under the operating conditions for which it was designed. Stability alone is not sufficient to deem this compensator successful, it must meet some performance criterion as well. Time domain simulations will be used to judge the controller performance with respect to command following, disturbance rejection and insensitivity to modelling errors.

Time domain simulation facilities[1] available at Draper Lab allow nonlinear and parameter dependent (such as variation of shaft rotational speed) simulations to be performed. Before proceeding, some performance specifications for a successful controller must be stated.

[1] Nonlinear simulation tools were designed and supported by Mr. Harold Bussey. The Systems Control Technology product MODEL_C was also used for nonlinear simulation [11].

5.2 Compensator Test Plan

This section outlines the desired performance of the closed loop system in terms of specific testing procedures to verify compliance with the performance specifications set in section 4.2. Reviewing those specifications, we can design a set of standardized tests to be used in time domain simulations of the controller combined with the following possible configurations of models :

1) Linear actuator, simplified stiff shaft

2) Nonlinear actuator, simplified stiff shaft

3) Liner actuator, flexible shaft / rotor model

4) Nonlinear actuator, flexible shaft / rotor model.

Before defining the test regime, a discussion about the operating conditions of the system will be helpful. The shaft / rotor system is representative of a testbed to be built at Draper Lab. The system will be affected by gravity (a d.c. disturbance) and in addition, the rotor is subject to other a.c. and d.c. loads. The shaft / rotor will be mechanically balanced but for testing purposes a mass unbalance will be introduced. The nominal rotating speed of the shaft / rotor is 3600 rpm (60 Hz.), although it is desired to be able to operate at rates up to 5000 rpm[1]. There are mechanical touch-down bearings at ±10 mils (half of the magnetic bearing air gap), which was reflected in the 10 Volt maximum position output, and the control supply voltage is limited to ± 30 Volts (see input and output scaling, §3.4). The nonlinear actuator simulations use the equations given in Appendix A which show the actuator force dependence on applied current (voltage) and shaft position within the bearing.

[1] Note that both the simplified shaft and the flexible shaft / rotor models are dependent on their rotating speed, ω. The system poles and therefore the closed loop poles change as a function of ω.

TEST 1 : Step Response

As specified, it is desirable to maintain a zero steady state error to step command inputs (for example, the position commanding of a milling machine). Therefore, step response simulations must be carried out. This test is conducted in a zero gravity field, at nominal operating speed, with no mass unbalance. To illustrate system performance in all directions (design specification 4), simultaneous step commands on both axes of both bearings will be issued.

TEST 2 : D.C. Load Disturbance Rejection

A static load specification has been set as d.c. force disturbance. This test is performed at nominal rotational frequency, in the presence of gravity (1333 Newtons, 300 lbs). The maximum static force is set at 888 Newtons (200 lbs).

TEST 3 : Mass Unbalance Simulation

This test addresses the effects of mass unbalance caused by imperfections in the construction of the shaft / rotor. The representation of this is seen in Figure 2.2 as the variable 'u' and McCallum's derivation [6] includes this parameter in the state equations. As a system specification, mass unbalance is specified at 666 Newtons (150 lbs) dynamic force applied to the center of mass, which sinusoidaly varies with the rotating speed of the shaft.

TEST 4 : Rotational Frequency Dependence (Simulation)

Both plant models[1] (simplified and full) are dependent on the rotational velocity of the shaft, Ω_z . The location of the closed loop poles is therefore dependent on the current rotational velocity. The compensator was designed to stabilize the shaft at the nominal

[1]Their open loop poles and zeroes are rotational frequency dependent.

operating speed of 60 Hz. It is desirable to have the compensator be robust enough to maintain stability throughout the spin-up operation, to a maximum rotational velocity of 5000 rpm. If this proves true, then a gain scheduled compensator, as a function of Ω_z, will not be required. This test will be addressed by an analysis which determines the closed loop pole locations as a function of rotational frequency.

5.3 Compensator Testing

In this section the results of the compensator performance testing are presented. The section is divided into two parts: baseline system testing (configuration (1) above) and nonlinear actuator, flexible shaft / rotor model testing (configuration (4) above). Since the two interim combinations were used only for the development of the actual system configuration of (4), documentation will be limited to a comparison of the actual system performance to the baseline system performance.

5.3.1 Compensator Testing : Baseline Configuration

To determine the performance levels of any controller, a test procedure should be applied initially to the design plant model (DPM) the controller was designed with. Since this compensator was designed using linear control theory, the simplified stiff shaft and nonlinear actuator model were linearized around a nominal operating point. Testing of the compensator with the nominal linear DPM will provide a baseline of performance which will be used as the performance criteria for the actual system.

Before proceeding, let's take a moment to define the sign convention. Examine Figure 2.1. Observe that a positive disturbance force in the x-axis is defined as 'up' in the figure. The same can be said for positive gravity. Also note that positive displacement is in the same direction. So positive gravity and positive force disturbance would produce positive displacement. Next note that positive current (volts) increases the attractive force

in the 'up' (top) pole. Therefore, to reject positive gravity and disturbance, we would expect negative current (voltage) commands. The same reasoning can be applied to the y-axis, with positive disturbance force defined as to the 'right' in Figure 2.1.

Test 1. is the system response to step command inputs. As prescribed above, the test is conducted in zero g gravity, at nominal 60 Hz shaft rotation speed assuming a perfectly balanced shaft (no mass unbalance). It is required to have zero state steady error to these command inputs. To test the directional behavior of the controller, simultaneous commands will be issued in every command input channel. The selected test command vector is : [5, 3, –4, 1]', where the vector entries correspond to the following desired outputs

x_a = 5 Volts (mils) : 1/2 hard stop

x_b = 3 Volts

y_a = – 4 Volts

y_b = 1 Volt.

Table 5.1 : Plot Legend

————	x_a , V_{x_a}
– – – – – – – –	x_b , V_{x_b}
– • – • – • – • –	y_a , V_{y_a}
.....	y_b , V_{y_b}

The plot legend gives in Table 5.1 is valid for all time based simulation plots in Chapters 5 and 6. Figure 5.1 contains the baseline step response of the system. Positions and control commands are both shown in volts. The observables are : there is a 60 % overshoot in the response of the x_a channel, slightly less than that in the y_a channel, peaking at –6.25 volts;

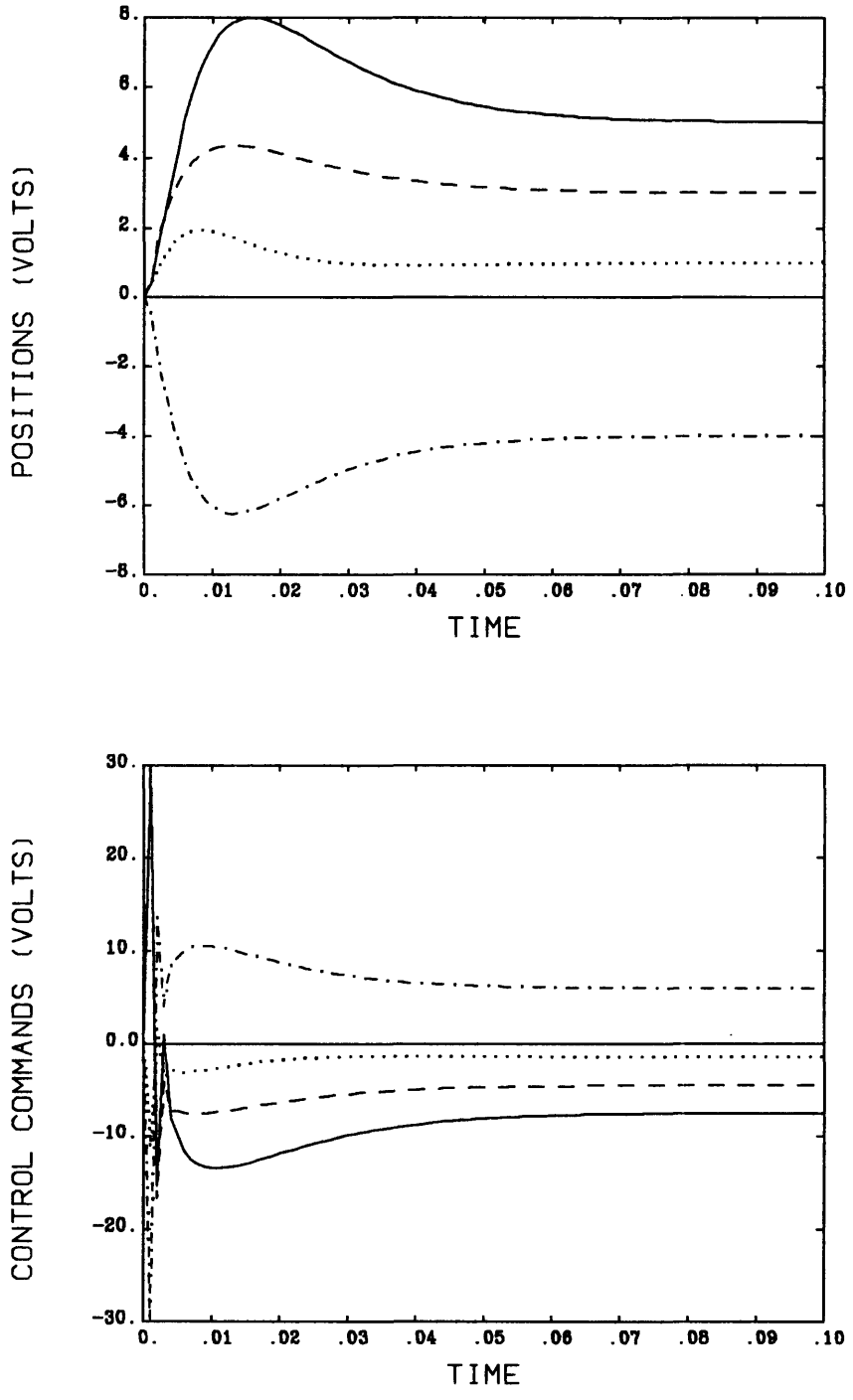

Figure 5.1 Baseline Step Response

the compensator commands the maximum of 30 volts in several channels, but only for a very short time period; the system has zero steady state error and the response time of 100 milliseconds is acceptable. During the design procedure, it was found that the large control commands were a result of the high speed compensator poles and that the plant, acting as a low pass filter, does not significantly respond to those commands. It was also found that as ρ was increased to yield more loop transfer recovery (LTR), the magnitude (unlimited control commands) and duration of those initial commands grew larger because compensator poles became faster as a function of the amount of LTR (i.e. $\rho \rightarrow 0$). This was a significant factor in deciding on the final choice of ρ. Reducing the order of the compensator by removing its high frequency poles would reduce the high speed, high gain response of the compensator. However, it was found that the compensator as designed could not be reduced and maintain stability (see §4.4.4). Finally, note that the integral control action provides the d.c. voltage necessary to maintain zero steady state command following error. The d.c. voltages are necessary because the plant has been displaced from the static equilibrium of the nominal operating point. The observed responses are consistent with the sign convention defined above.

Figure 5.2 is the system response to d.c. loading. First, the system is subject to a one g gravity field, an equivalent force disturbance of 1333 Newtons (300 lbs), on the x-axis only, then a static d.c. disturbance of 888 Newtons (200 lbs) is applied at t =.01 seconds on both system axis. For simplicity, these disturbances were equally distributed to both bearings; that is the gravity force for example, was applied as 666 Newtons to each of the 'a' and 'b' bearings.

Analyzing the figure, we see that the application of gravity caused a maximum shaft displacement of 1.8 mils (volts) on the x_a axis. The integral controller reacts to the d.c. disturbance as required, driving the steady state error to zero in finite time, requesting finite maximum d.c. voltage command of nearly –8 volts. The controller never saturates due to the application of gravitational force..

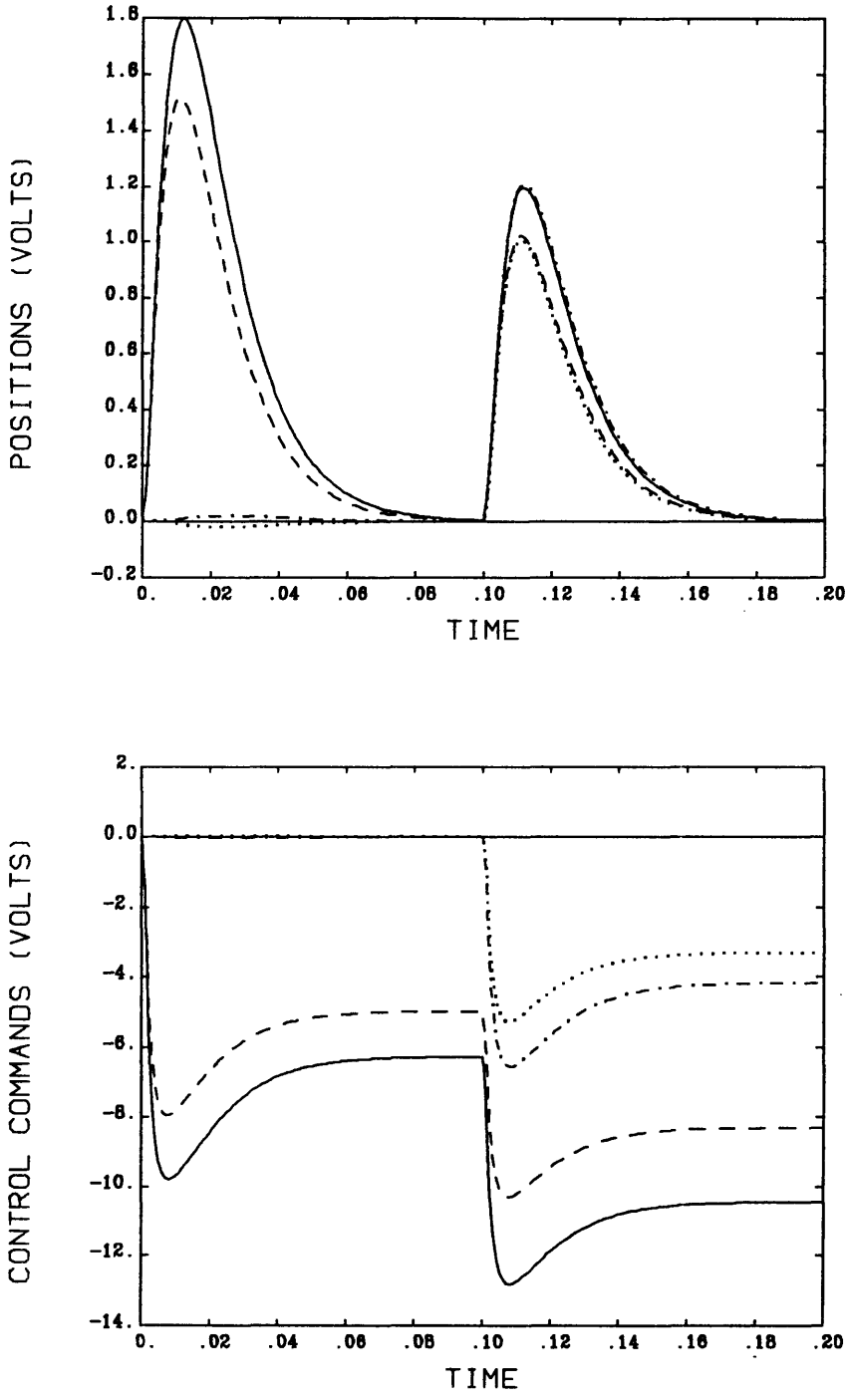

Figure 5.2 Baseline Gravity / D.C. Disturbance Response

In part two of the test, a static load of 888 Newtons is applied after the gravity application has reached steady state. A simultaneous displacement of all shaft positions is observed. Identical excursions are seen in the x- and y-axis of each bearing. Maximum deviation from nominal for this static load is 1.2 mils (volts). Again the integral control action returns the system to equilibrium displacements by applying the necessary d.c. voltage levels. Note that the x-axis voltages, previously at a nonzero level due to gravity, have increased by –10.5 volts due to the additional load.

Test 3 deals with the effects of an imperfectly constructed shaft represented as a single speed force disturbance. Single speed implies that the force sinusoidally varies with the rotational velocity of the shaft. In this test case, the shaft is at its nominal operating speed of 60 Hz, in the presence of gravity. The maximum mass unbalance force has been specified at 666 Newtons (150 lbs).

Figure 5.3 reveals the effect of mass unbalance on the baseline system. Steady state oscillation at the spin frequency is observed. Maximum excursions from null are relatively small. They are .5 mils (volts) peak. Control commands are 4 volts peak superimposed on any d.c. voltage required for gravity rejection. Because the system bandwidth (100 Hz) is beyond the nominal operation frequency, the open loop system gain is approximately 6 dB at 60 Hz. This implies a slight rejection of the mass unbalance disturbance. One other note : the .5 mils peak error gets amplified by the compensator to 4 volt peak control commands. This is consistent with the compensator gain at 60 Hz of 15 to 18 dB (see Figure 4.8).

Test 4 is concerned with the robustness of the compensator with respect to plant variation as a function of rotational velocity. McCallum [6] has done extensive research on the location of plant poles and transmission zeroes with respect to the following parameter variations : rotational velocity, internal shaft damping and shaft stiffness. Since this simplified design plant model assumed infinite stiffness and no internal shaft damping, examining the effects of variations of rotational speed is in order.

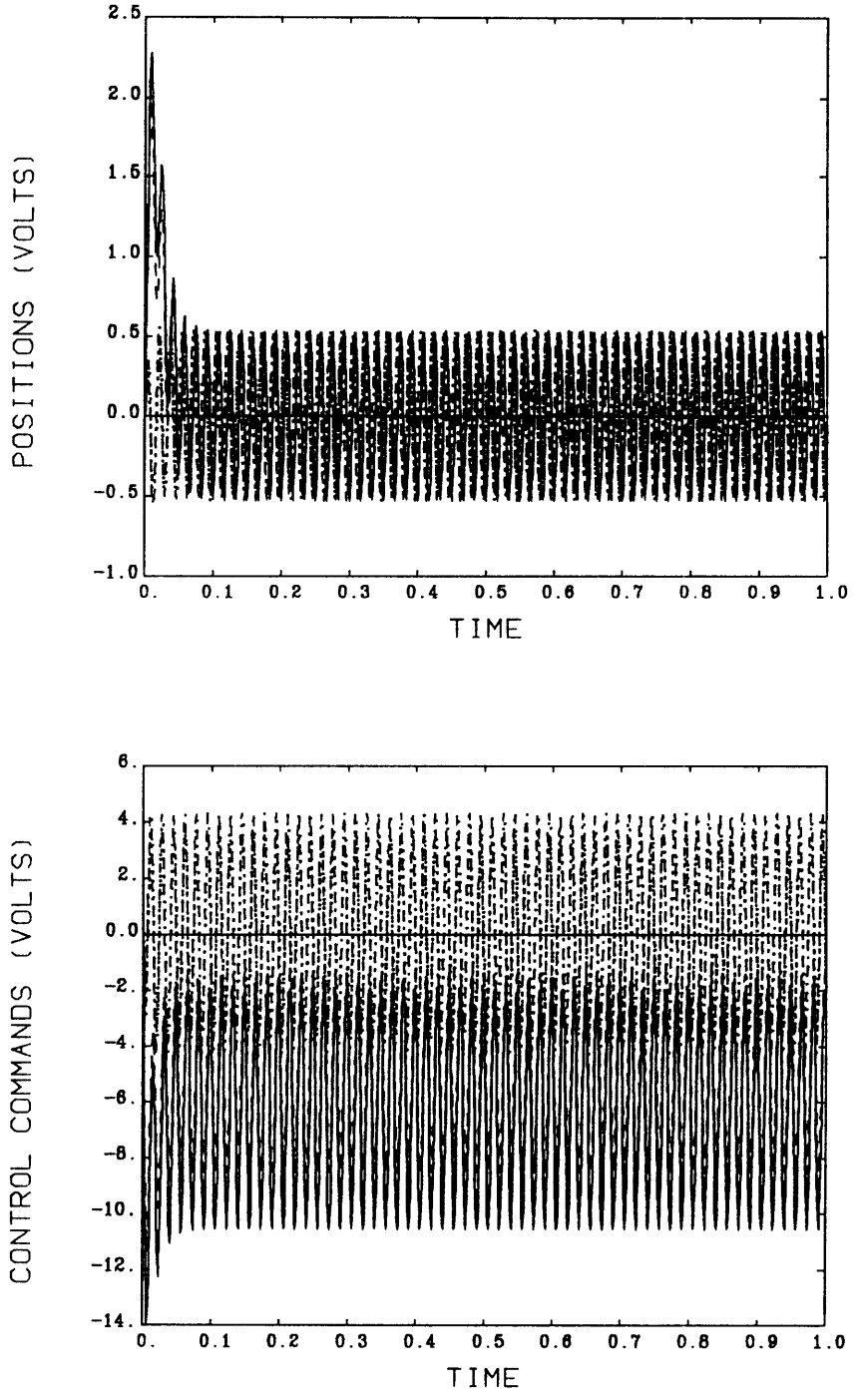

Figure 5.3 Baseline Mass Unbalance Response

An analysis of the closed loop pole locations as a function of rotational velocity revealed that the baseline configuration was stable over the entire defined operating range of d.c. to 5000 rpm (83 Hz). This implies that no gain scheduled or otherwise nonlinear compensator is required for this configuration.

5.3.2 Compensator Testing : Actual System Configuration

The term 'actual' system configuration means that all known system parameters are modelled. The nonlinear actuator equations of Appendix A.1 are combined with the flexible shaft / rotor model of Appendix A.2 to produce what has been termed the actual system. The plan is to apply the test procedure as defined above to the actual system and to compare the results to the baseline. In addition, the effect of parameter variations such as shaft stiffness and damping can be examined.

Test 1 is the step response test with the same conditions and commanded offsets as for the baseline test. The step response of the flexible shaft, nonlinear actuator system is shown in Figure5.4 (compare to Figure 5.1). In Figure 5.4, the step response overshoot is slightly less than the baseline in bearing 'a', but greater than baseline in bearing 'b'. The response times are nearly identical. The desired zero steady state error is achieved. The most noticeable difference (in the positions plot) is in the flexible shaft's response to the initial high speed, high gain controller commands. The energy introduced by this impulse has a measurable effect on the flexible shaft. A better illustration of the differences between the responses can be seen by examination of the control commands[1] . The actual system control commands, while having a similar form as the baseline response, are slower in time.

It is easier to observe differences in system performance by examining the results of the d.c. load testing. First, note that the state variables of the shaft / rotor model facilitate

[1]This is not to say that the compensators are different, but that a comparison of control commands is more revealing (with respect to the change of system dynamics) than a comparison of position responses.

application of disturbances directly onto the rotor (the baseline system could not do this). This produces a different system response within itself. Figure 5.5 contains the test results; compare to Figure 5.2. The initial application of gravity has much more of an effect on the system. The maximum position deviation is over 4 mils (compared to 1.8 mils baseline), and the y-axis deviations are significant. The maximum voltage command for gravity rejection is 24 volts, more than twice the baseline. The effects of the nonlinear actuator are clearly reflected in this test. The attractive force of the unstable spring increases nonlinearly as the shaft deviates form null. These nonlinear forces will require larger control voltages to counteract this effect than in the baseline linear system. Next, observe that the application of the static force load also produces larger deviations from null than for the baseline system. Position errors of greater than 3 mils are induced, as opposed to a maximum of 1.2 seen in Figure 5.2. The fact that the x_a axis command voltage almost saturates is very important. The steady state levels of control commands are much larger for this system than for the baseline also. The x_a axis command voltage in over –21 volts in the steady state. This allows less than 30% of control voltage for incremental dynamic disturbance rejection or command following. The system may not perform satisfactorily under all operating conditions. Note that during system testing, it was found that the system saturated and the shaft hit the hard stop when a d.c. load of 1111 Newtons (250 lbs) was applied.

Figure 5.6 shows the dynamic mass unbalance test applied to the actual system. The steady state oscillation error is approximately 1.2 mils peak, which results in steady state control commands of 10 volts peak (again compensator gain at 60 Hz is about 4). This is more than twice as large as the baseline test. Because the deviations from null are small compared to air gap size (1 mil vs. 20 mils), it could be implied that the difference in system response is solely due to the difference in the plant dynamics. This may be because of this models ability to apply the mass unbalance directly to the center of mass at the rotor. The x-axis control voltage, which was preloaded with gravity is peaking at –22.5 volts. A combination of mass unbalance with a d.c. loading as above, could staurate this system and drive the shaft into the hard stop. As stated above, this system as design may not be able to meet a simultaneous application of all design criterion. Further, this is not a reflection on the control system designed, but more a reflection of the system specification and hardware limitations. System level engineering concerns need to be addressed.

System robustness with respect to the change in rotational velocity is addressed in Test 4. For the baseline system, closed loop pole location analysis showed that the compensator was robust for all operational velocities. For the actual system, a similar closed loop pole analysis was performed and the system was found to be completely stable for all operating speeds also. In addition, a spin-up simulation was performed to observe the system response. Figure 5.7 contains the position errors and control commands for the x_a axis only as a function of rotational velocity in Hz. The system is subjected to gravity, and spun from d.c., through the nominal operating speed of 60 Hz, up to 110 Hz. This is done to observe the system response as it passes through the system bandwidth. As seen in Figure 5.7, the system maintains stability throughout the spin-up process. In fact, performance improves as a function of spin rate. There is some concern at low frequencies, that control saturation could induce system failure. At approximately 9 Hz, in the presence of gravity, the control commands are greater than –25 volts. Again, a d.c. disturbance at the time of crossing that frequency could cause system failure.

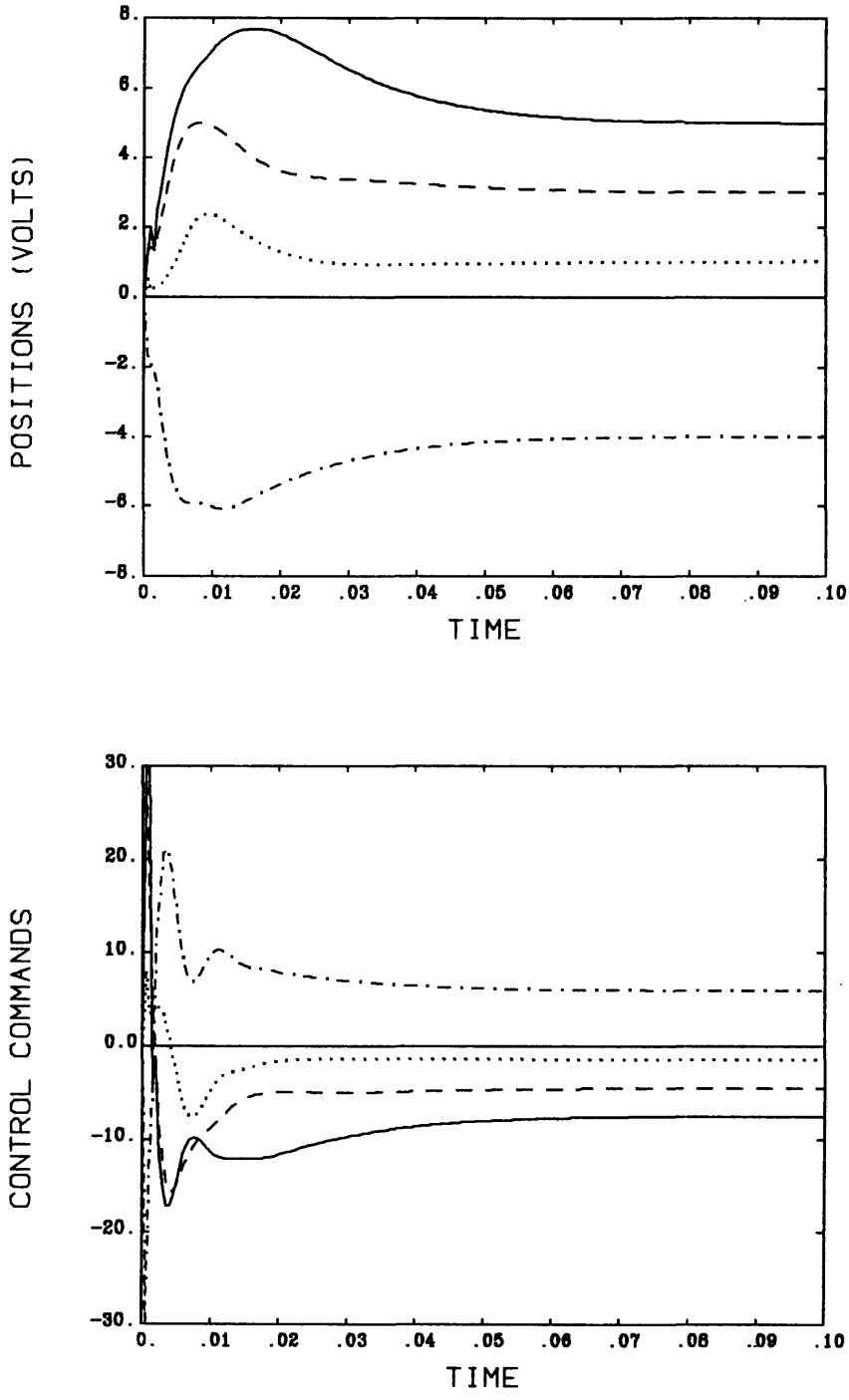

Figure 5.4 Flexible Shaft - Nonlinear Actuator Step Response

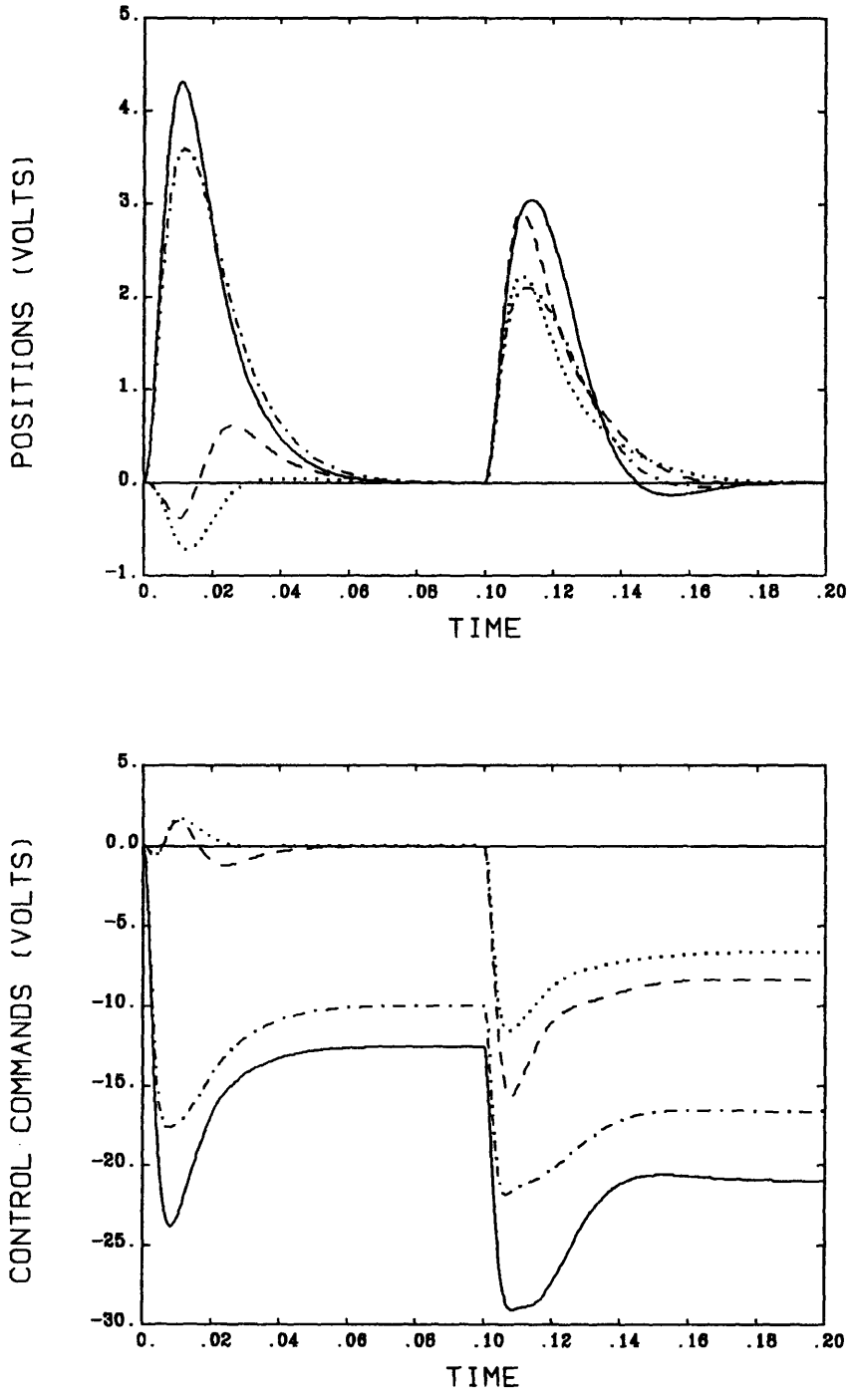

Figure 5.5 Flexible Shaft - Nonlinear Actuator D.C. Disturbance Response

Figure 5.8, which shows the system response ar rotational velocity is swept from 130 Hz to 160 Hz, is included to demonstrate shaft stability as it passes through its first critical speed of 150 Hz. We can see that both peak position error and control commands decrease with an increase of rotational velocity as in Firgure 5.7. But the compensator successfully meets an initial design goal of maintaining stability as the shaft passes through its critical speed. The crirtical speed for this shaft however, is well above nominal operating speed.

To substantiate the claim that additional control voltage may be necessary to maintain stability through the application of simultaneous operating environments, a test was designed which combined the d.c disturbances of gravity and static load, with shaft mass unbalance. When this combination of tests was applied to the ±30 volt limited system, it failed. An additional test , run with unlimited control voltage, revealed that more than –40 volts of control were commanded to reject the superposition of the additional static load. Figure 5.9 shows the system response.

In addition to performing stability analysis as a function of rotational speed, the flexible shaft / rotor can be parameterized with respect to stiffness and damping. Since the shaft critical speed (resonant frequency) is approximately the square root of shaft stiffness divided by the mass, the location of the closed loop poles as a function of stiffness will determine the limitations of this compensator. The result of this analysis revealed that the compensator will stabilize a shaft of similar design with stiffness reduced from the specified 12.2×10^7 down to approximately 4.6×10^7 . This corresponds to a critical speed of 93 Hz. In other words, if the critical speed of the flexible rotor / shaft system is less than this, the compensator designed using the stiff shaft approximation as the design plant model will not effectively stabilize the system and a new compensator will have to be designed based on the more complicated plant model. This is a major conclusion of this thesis.

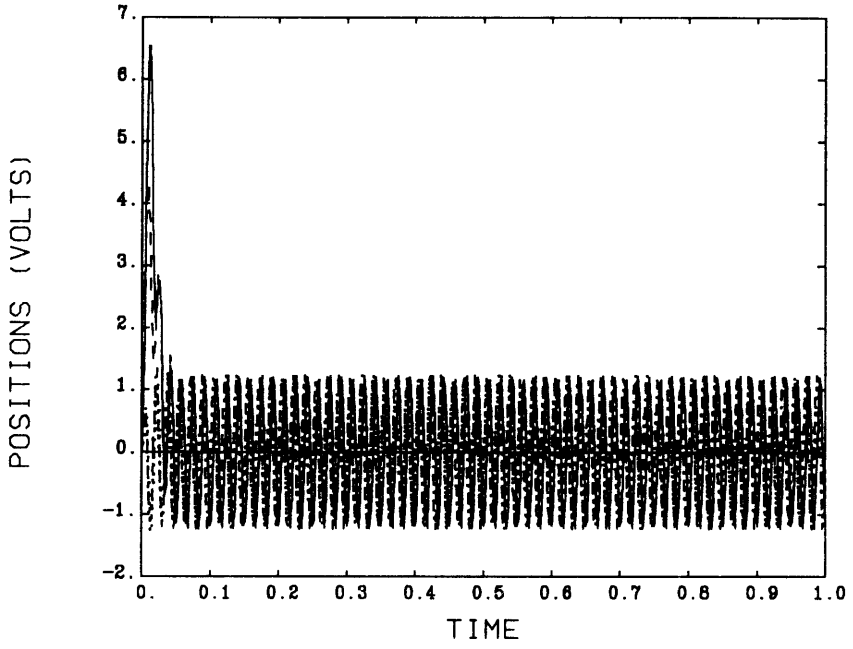

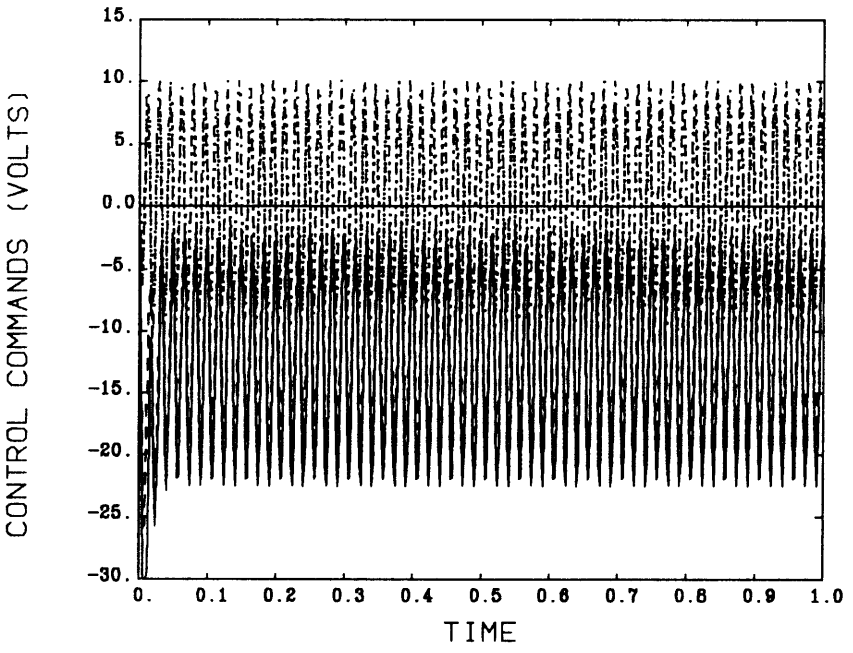

Figure 5.6 Flexible Shaft - Nonlinear Actuator Mass Unbalance Response

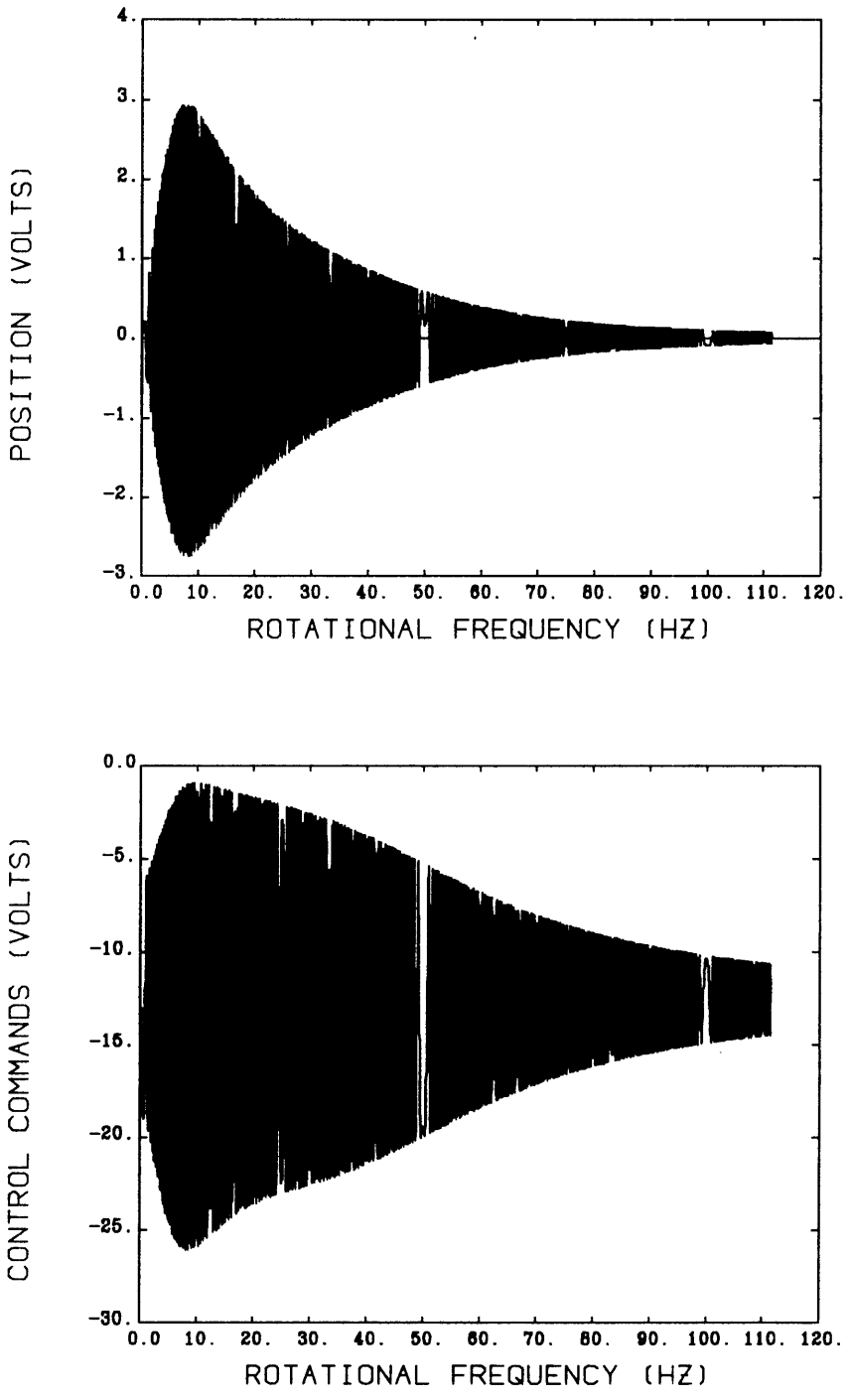

Figure 5.7 Flexible Shaft - Nonlinear Actuator Spin Up Response

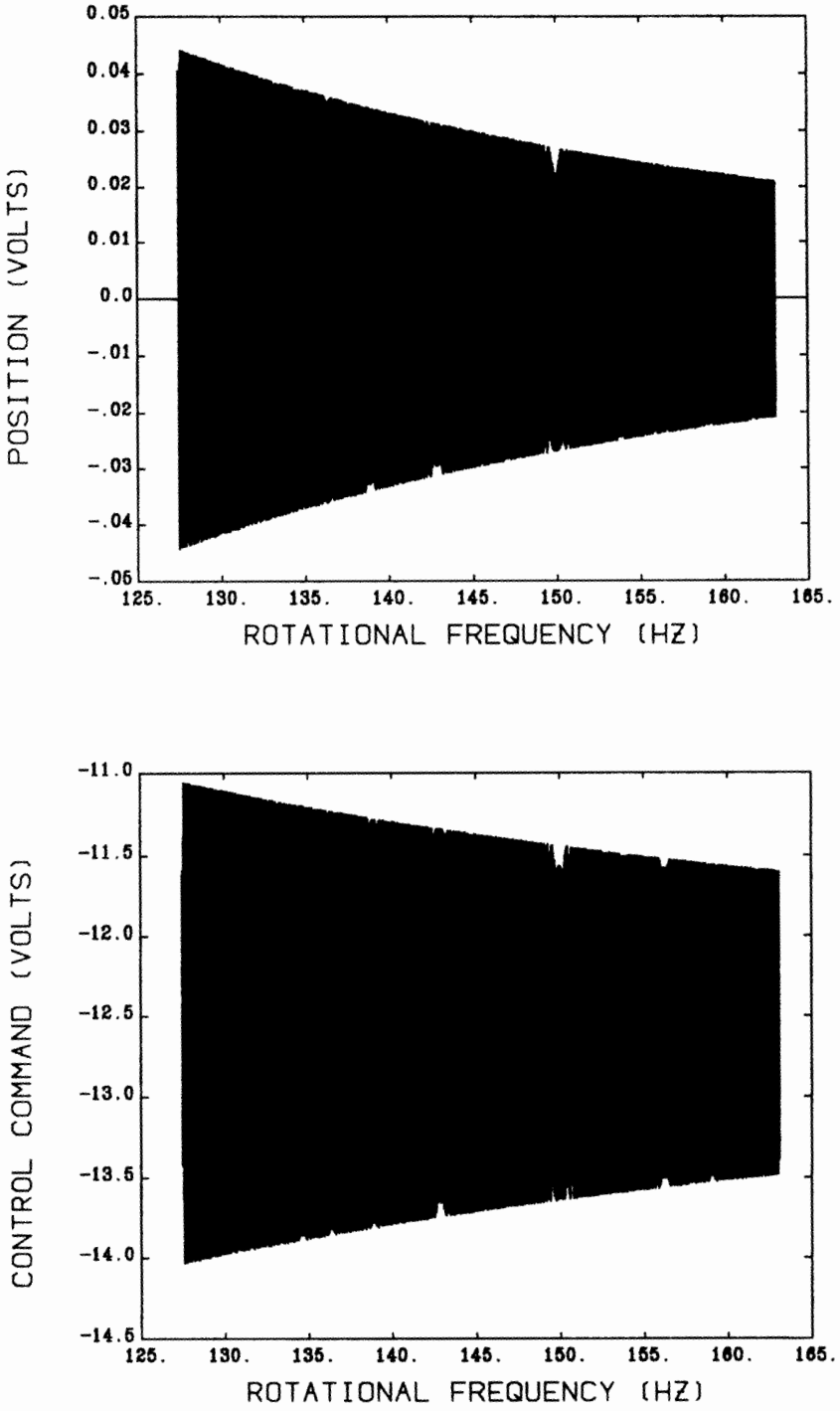

Figure 5.8 Flexible Shaft - Nonlinear Actuator;Spin Through Critical Speed

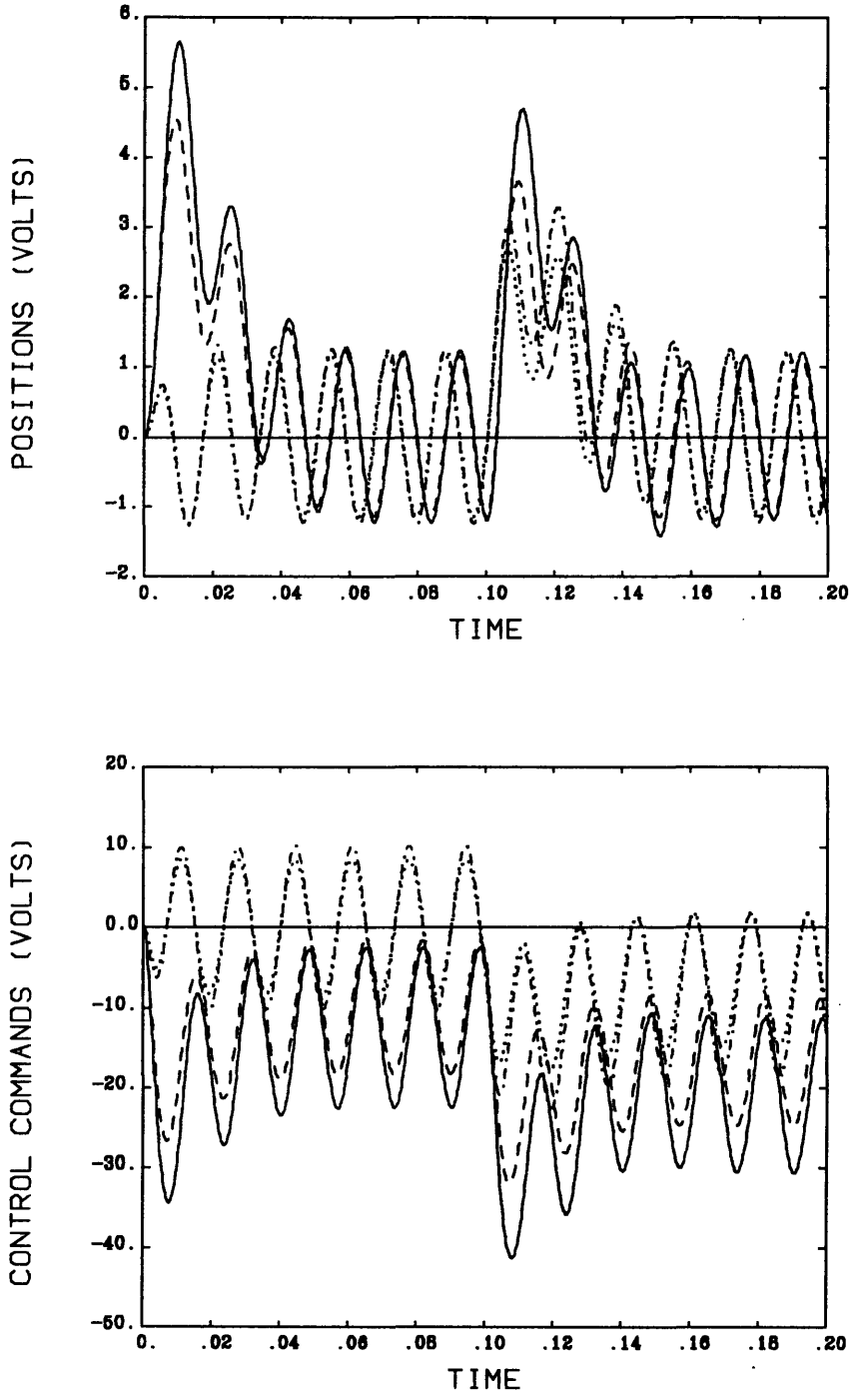

Figure 5.9 Flexible Shaft - Nonlinear Actuator Mass Unbalance and D.C. Disturbance Response

One of the original design goals of the Draper testbed was to operate a rotating flexible shaft beyond its first critical speed. However, the initial shaft design (used in this thesis) resulted in a critical speed of approximately 150 Hz which is well beyond the 60 Hz operating speed. As an academic exercise, the physical shaft parameters, namely shaft stiffness, will be redefined to produce a critical speed of less than 60 Hz (see Chapter 6). The shaft stiffness was set at 1.56×10^7 which has a corresponding critical speed of approximately 54 Hz. This system, when operated at 60 Hz has non-minimum phase zeroes, which are a non-trivial problem. As was stated above, a shaft with stiffness less than 4.6×10^7 could not be controlled by the compensator designed using the simplified stiff shaft model. A closed loop test of the new flexible model confirmed that fact. Therefore, in order to control the redefined model, a new compensator must be designed and tested. This is the subject of Chapter 6.

5.4 Summary

This chapter evaluated the Model Based Compensator (MBC) designed in Chapter 4. A testing procedure was defined to confirm compliance with the performance specifications defined in Chapter 4. This procedure consisted of time domain simulations which included step response, d.c. disturbance rejection, mass unbalance and shaft rotational frequency dependence simulations. A baseline of system performance was defined by applying the defined test procedure to the nominal linear design plant model and MBC configuration. The baseline results were presented and discussed. It was found that the baseline system met all system specifications.

Intermediate simulation development steps were not documented and the flexible shaft / rotor with nonlinear actuator system, termed the 'actual' system, was subjected to the defined test procedure. Testing results were presented and compared to the baseline. It was found that the actual system performance met all requirements. The actual shaft was spun-up from d.c. through its first critical speed of 150 Hz. The designed compensator

maintained shaft stability throughout the spin-up procedure, implying no need for a non-linear or gain scheduled compensator. The conclusion that the compensator designed for a simplified, linear model of a stiff shaft and nonlinear magnetic bearing system was adequate for actual system control was drawn. The conclusion, however, was made with conditions that the test procedures did not combine all system performance specifications in one test[1]. The limitations of control command voltages place limitations on the system performance. When a test that combined performance specifications was performed, the system failed. The same test, run with an increase in control command voltage limits, was shown to be successful.

The use of simplified stiff shaft modelling to design compensators for flexible shaft systems also has limitations. Through closed loop pole location analysis, it was determined that the controller designed in Chapter 4 will maintain the stability of a flexible shaft whose critical (resonant) frequency is greater than 95 Hz (the actual systems critical frequency as defined by system parameters is 150 Hz). A hypothetical system with critical speed of 54 Hz was developed. The stability analysis performed suggests that this system will not be stabilized by the compensator as designed. In fact, it was combined with the designed compensator and the resulting system was indeed closed loop unstable. A compensator designed using the flexible shaft / rotor model with critical speed less than nominal operating speed will be designed and tested in the next chapter. Results will again be compared to the baseline system of this chapter.

[1]The system performance specifications used in this thesis preliminary. They may be redefined (at Draper Lab) after further study.

Chapter 6

6. Control of a Flexible Shaft / Rotor

6.1 Introduction

In Chapter 5, it was found that the compensator designed for a flexible shaft / rotor and nonlinear magnetic bearing system by using a simplified stiff shaft as the design plant model was effective for controlling a flexible shaft / rotor whose stiffness was such that its critical speed (resonant frequency) was greater than 95 Hz. The stiffness of the actual system resulted in a critical speed of 150 Hz, and it was shown that the compensator met all system specifications when used with this model. However, the stiffness defined for the system is preliminary and since a goal of the Draper Lab testbed is to operate a flexible shaft / rotor beyond its first critical speed, it was taken as an academic exercise to redefine shaft stiffness to meet this goal while maintaining the nominal operating speed of 60 Hz. The stiffness was set such that the first critical speed was placed at 54 Hz. From the main thesis conclusion drawn in Chapter 5, we know that the compensator designed using the simplified stiff shaft model will not stabilize this newly defined system. Therefore, in this chapter, a new model based compensator (MBC) will be designed, again using the LQG/LTR methodology.

The procedures used in earlier chapters to apply the LQG/LTR methodology, will have to be repeated. The development of a linearized, scaled design plant model (SDPM) is essential for successful compensator design. The chapter will present the linear DPM of Appendix A.2 and discuss the scaling procedure applied. The LQG/LTR methodology, as outlined in Chapter 4, will be applied without the painstaking development found there.

The MBC designed will be tested in accordance with the procedures defined in Chapter 5 and the results will be compared to the baseline standard found there whenever possible.

The chapter is not intended to be the focus of the thesis. It is included merely to gain additional insight to the problem as a whole.

6.2 The Design Plant Model

The flexible shaft / rotor model developed by McCallum [6], shown in Appendix A.2, was combined with the linearized magnetic bearing actuator, and the resulting state space representation is given in Figure A.2.2. The system parameters are given in Appendix B, with the exception being that the shaft stiffness has been defined such that the shaft critical speed is at 54 Hz :

$$K_{s1} = .8462 \times 10^7$$
$$K_{s2} = .7238 \times 10^7 ,$$

with shaft critical speed in radians per second found by

$$\sqrt{K_{s1} + K_{s2}/M} .$$

After insertion of these parameters into the the model, we can analyze the system eigenstructure. The new system open loop poles are :

$$283.4 \pm 10.7\,j$$
$$-301.2 \pm 15.1\,j$$
$$376.7 \pm 29.1\,j$$
$$-415.3 \pm 15.9\,j$$
$$-1672.3 \pm 395.8\,j$$
$$-1898.5 \pm 384.9\,j .$$

The general configuration of pole pairs is not unlike the original system, the major difference being that the high frequency poles (produced by damping and stiffness) have become an order of magnitude slower.

Examination of the system transmission zeroes reveals the real impact of the change in shaft stiffness. The new transmission zeroes are :

$$-4.39 \pm 444.4\,j$$

$$-51.2 \pm 409.1\,j$$

$$-37.0 \pm 338.7\,\mathrm{j}$$

$$1.97 \pm 338.9\,j\ .$$

Again the structure of the zeroes is similar to the original system, but this system now has non-minimum phase (right half plane) transmission zeroes and the zeroes are an order of magnitude slower. They are now in the system bandwidth[1]. Recalling one of the criteria for guaranteed successful application of the loop transfer recovery (LTR) procedure from section 4.3.2, that the system must not contain any non-minimum phase zeroes, we see that this system violates that constraint and, therefore, complete recovery of the target feedback loop (TFL) is not guaranteed. Figure 6.1 contains the singular value plots for this system. It is clear that the zeroes have moved to within the system bandwidth, below the 60 Hz operating frequency.

Since the basic structure of the model did not change (only a relatively small parameter change), it is expected that this system will be numerically ill conditioned as the original. This can be observed by eigenvector examination and/or calculation of the system matrix condition (see § 3.3). For expediency, system scaling will be dealt with on purely numerical condition terms. Recall that the condition of a well conditioned matrix is near 1. For this system, cond(A) is 1.29×10^5. Therefore, the system must be scaled to improve

[1]Since the zeroes reflect the shaft critical speed, we effectively 'placed' the zeroes within the system bandwidth when we redesigned the system to force the shaft critical speed below nominal operating speed.

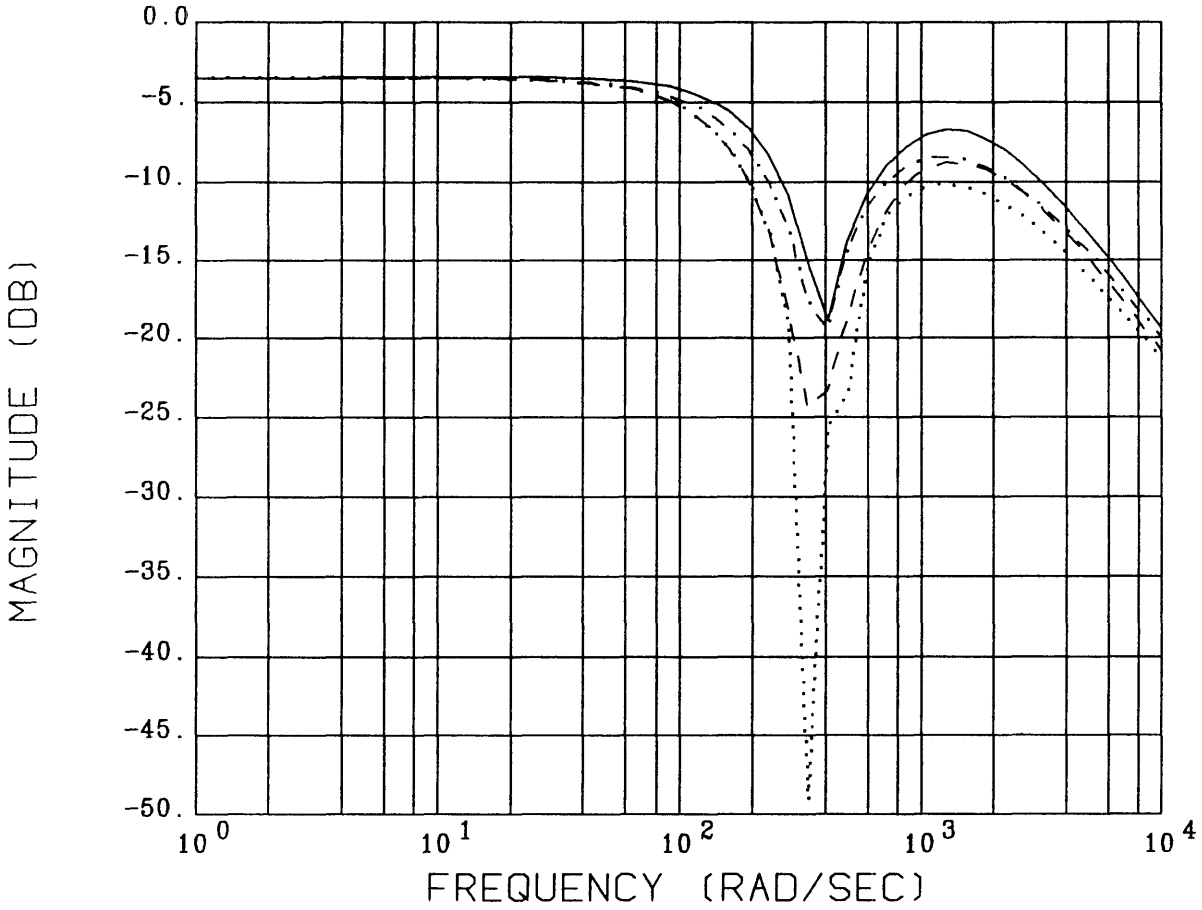

Figure 6.1 Singular Values of the Design Plant Model

its condition. Since scaling of the simplified stiff shaft system was thoroughly documented in Chapter 3, we will merely apply the conclusions drawn there to this system.

This system is scaled by a state transformation which produces a 'balanced' realization of the system. The balancing of a system has the effect of normalizing state variables with respect to each other and producing a numerically stable representation of that system. This is accomplished through use of available computer software [11]. Application of this procedure to the problem at hand resulted in a system matrix whose condition is now 18.3. The system eigenstructure was examined and the eigenvectors were found to span the 12 dimensional space.

In addition to numerical scaling, input / output scaling was applied to the DPM to normalize the system with respect to units. Since the sensor and actuator gains and limits did not change, the same I/O scaling matrices as used in section 3.3 can be applied here.

The resulting scaled design plant model (SDPM) singular value plots can be seen in Figure 6.2. The system poles and zeroes have not changed in frequency. The d.c. gain has changed with the I/O scaling (as before). There are multiple zero dB crossings.

6.3 Control System Design

In this section the LQG/LTR design methodology will be applied to the SDPM derived above. The process will parallel that in section 4.4, though not as much detail will be given. It is assumed that the same system specifications and modelling assumptions defined in section 4.3 will apply here.

The first step of the design procedure is to augment the SDPM to introduce integral control in each control channel (see § 4.4.1 for details). This increases the order of the SDPM from 12^{th} to 16^{th} and the augmented, scaled design plant model that will be used in the design of the target feedback loop (TFL) is defined.

The TFL is designed to meet system specifications. The most imposing, for now, are that the desired crossover frequency be near 100 Hz and that the system reacts equally

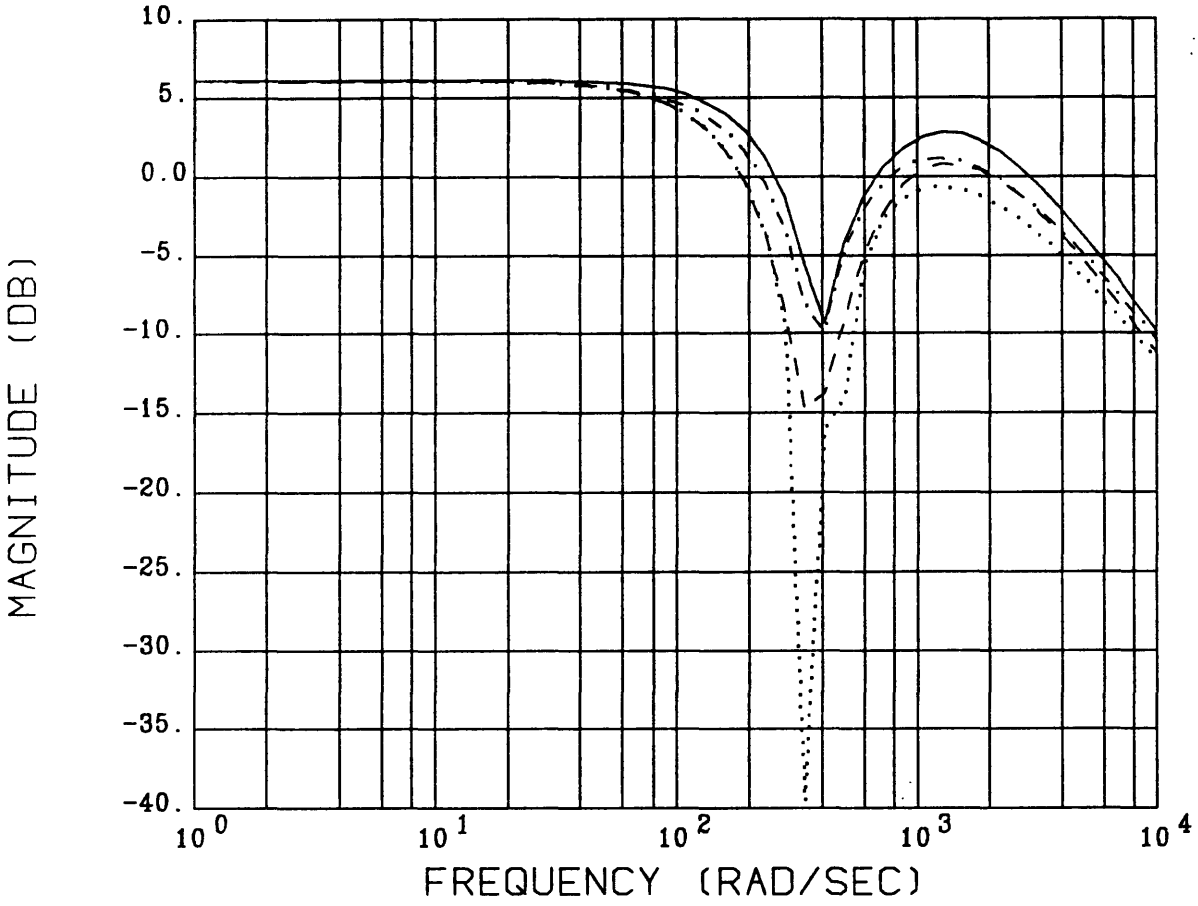

Figure 6.2 Singular Values of the Scaled Design Plant Model

well in all control directions. These specifications facilitate the choice of available design parameters. This step of the methodology involves solving a specialized Kalman Filter (KF) problem to perform system loop shaping in the frequency domain. The design freedom that exist is derived from the definition of the KF problem, in equation (4.2). Correct choice of these parameters will produce singular value matching and loop shaping as desired. The TFL to be shaped is the KF transfer function matrix (TFM) defined as

$$G_{KF}(s) = C(sI - A)^{-1}H \qquad (4.3)$$

where H is defined as

$$H = \left(1/\sqrt{\mu}\right) \Sigma C^{T} \quad , \qquad (4.4)$$

with Σ being the solution to the Filter Algebraic Riccati Equation (FARE) :

$$0 = A\Sigma + \Sigma A^{T} + LL^{T} - \left(1/\sqrt{\mu}\right)\Sigma C C^{T}\Sigma$$

where L and u are the design parameters discussed above (see § 4.3.1 and § 4.4.2). The singular value plots of the TFL can be seen in Figure 6.3 (compare with Figure 4.4). Ths figure shows that the frequency domain imposed system specifications are met. The TFL is ready for the application of the loop transfer recovery step.

The Loop Transfer Recovery (LTR) involves applying Linear Quadratic Gaussian (LQG) theory to solve the cheap control problem (see § 4.3.2 and § 4.4.3). There are design prerequisites imposed (in § 4.3.2) which will guarantee successful recovery of the TFL. One of the preconditions is that the DPM contains no non-minimum phase transmission zeroes. This condition is violated by the DPM as defined. This means that complete recovery of the TFL is not guaranteed. This is another conservative design condition. Complete TFL recovery may not be necessary for stable closed loop system operation. So, we proceed with the recovery process under the assumption that complete TFL recovery is not guaranteed. The range of recovery in the frequency domain is

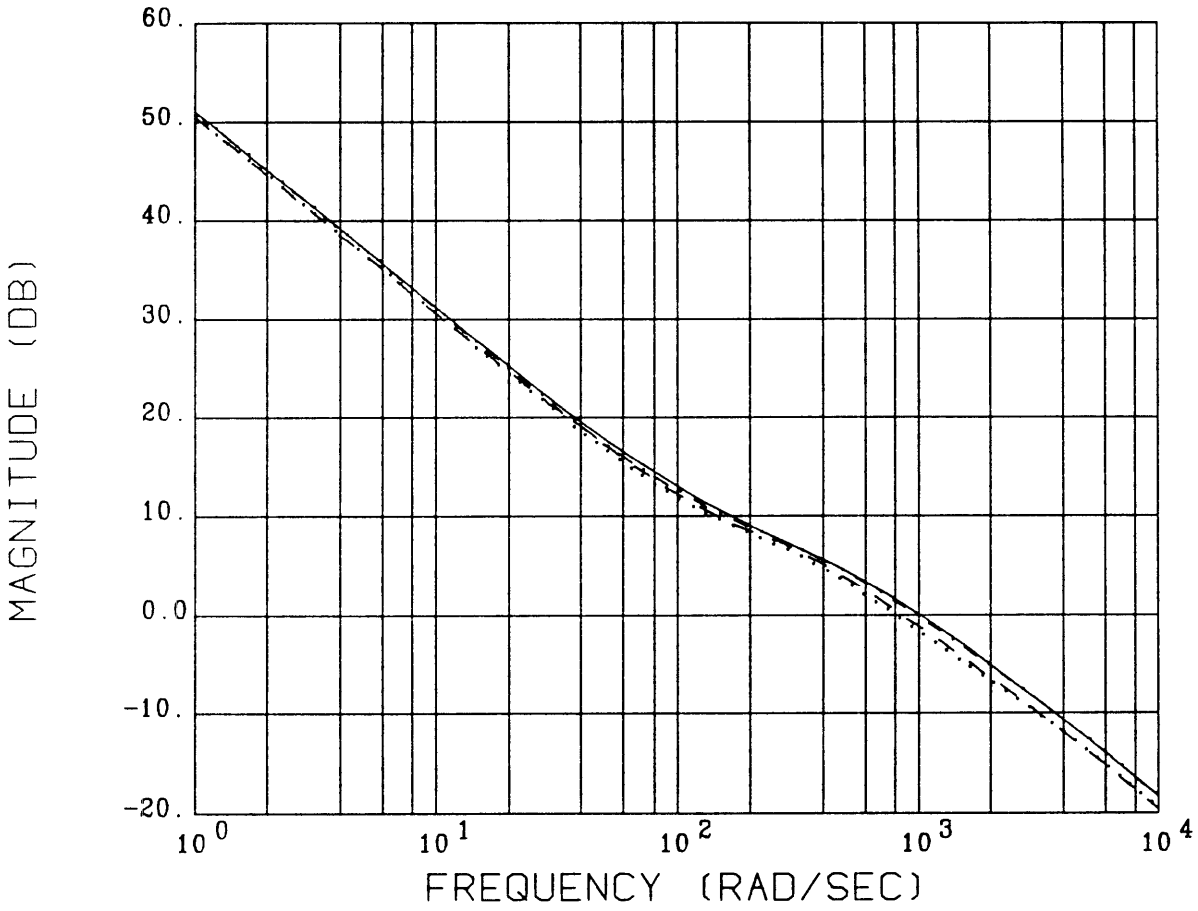

Figure 6.3 Singular Values of the Target Feedback Loop

dependent on the choice of the control cost parameter, ρ. The cheap control problem is defined as solving the Control Algebraic Riccati Equation (CARE) as $\rho \rightarrow 0$ (see equation 4.9). It is desired to recover the TFL to approximately one decade beyond the crossover frequency. In the previous design, it was found that a choice of $\rho = 1 \times 10^{-11}$ provided satisfactory recovery without requiring excessive control commands. This choice of ρ is also adequate for the design of this compensator.

The singular value (SV) plots of the system TFM, GK(s)[1], are shown in Figure 6.4. We can see that the recovery process is not completely successful. The minimum SV fails to remain consistent with the others at the frequency of the non-minimum phase zeroes, and in doing so, several crossover frequencies are created. The loop recovery is otherwise sufficient.

The model based compensator is now completely designed. It must be augmented to move the integrators from the augmented plant model to the compensator. It must be scaled to account for the input / output scaling performed on the DPM (see § 4.4.4). After these steps, the compensator is ready for implementation and testing.

Before testing, an examination of the compensator pole / zero structure is necessary. Calculation of the compensator poles reveals that the compensator designed is unstable. It contains right half plane poles which (effectively) cancel the plant non-minimum phase transmission zeroes. But, when the unstable compensator is combined with the unstable DPM, the closed loop system is stable, as expected.

6.4 Model Based Compensator Testing

In this section, the augmented, scaled model based compensator designed above is combined with the nonlinear actuator and flexible shaft / rotor model for system level testing. The test procedure defined in section 5.2 will be applied. The results of each test will be compared to the baseline responses developed in section 5.3.

[1]The K(s) used here has been scaled and augmented as in § 4.4.4.

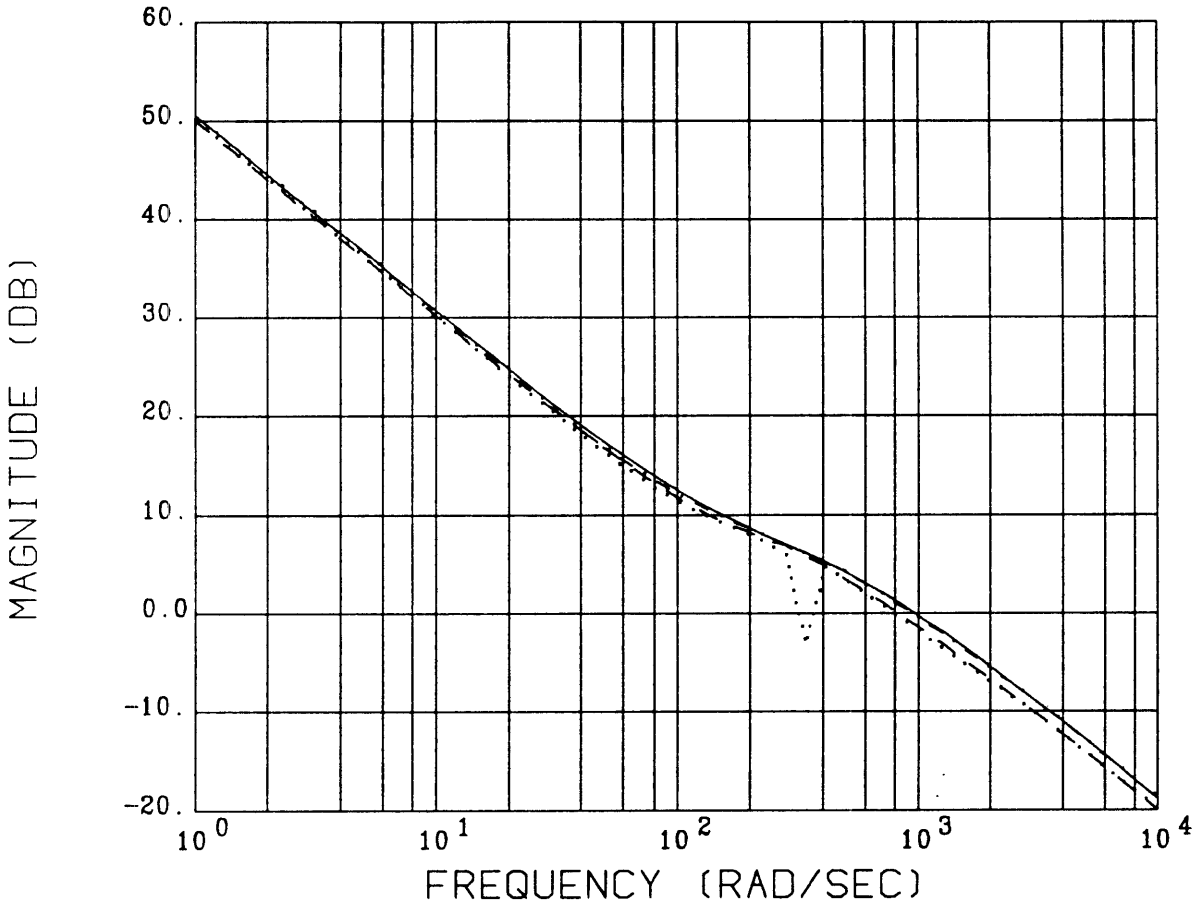

Figure 6.4 Singular Values of GK(s)

Test 1 is the step response to positions commanded simultaneously in all channels. Figures 6.5 through 6.7 contain the system response. Figure 6.5 shows that the step responses are successful, but the system requires a significant amount of time to reach steady state, much longer than the baseline system. We can see in the control commands that the unstable compensator rings substantially. The baseline response plots are .1 seconds in duration, so Figure 6.6 is shown to put this step response in that time frame. The maximum displacement of the x_a channel in over 9 mils, almost 90% overshoot and even worse, almost to the hard stop at 10 mils. The compensator saturates the actuator while trying to correct for the large overshoot and continues to ring at a frequency near 70 Hz (frequency of unstable compensator poles). The response is poor compared to the baseline (Figure 5.1). Figure 6.7 is included to illustrate the dramatic effect the nonlinear actuator has on system response. Compare Figures 6.6 and 6.7. They are the same test except 6.7 is with the linear actuator model. Although the compensator still exhibits ringing, the plant response, while slower than the baseline, has less overshoot in the x_a channel.

Test 2 is concerned with the system rejection of d.c loading. D.c. load testing consists of subjecting the rotor to a one g gravity field (a force of 1333 Newtons) and after the system reaches steady state, an additional d.c. load of 888 Newtons (200 lbs) is applied. Simply stated, the closed loop system limited to control commands of ±30 volts could not support the gravity load. The control command window was opened to ±50 volts and the test was repeated. Figure 6.8 contains the results of this test. The controller requested over –38 volts to stabilize the system after application of gravity. Further, when additional d.c. loading was introduced, the compensator requested almost –35 volts of control. Clearly, the original system specifications were not set with the premonition of possible variation of shaft parameters. No comparison to baseline can be made with a change in system parameters.

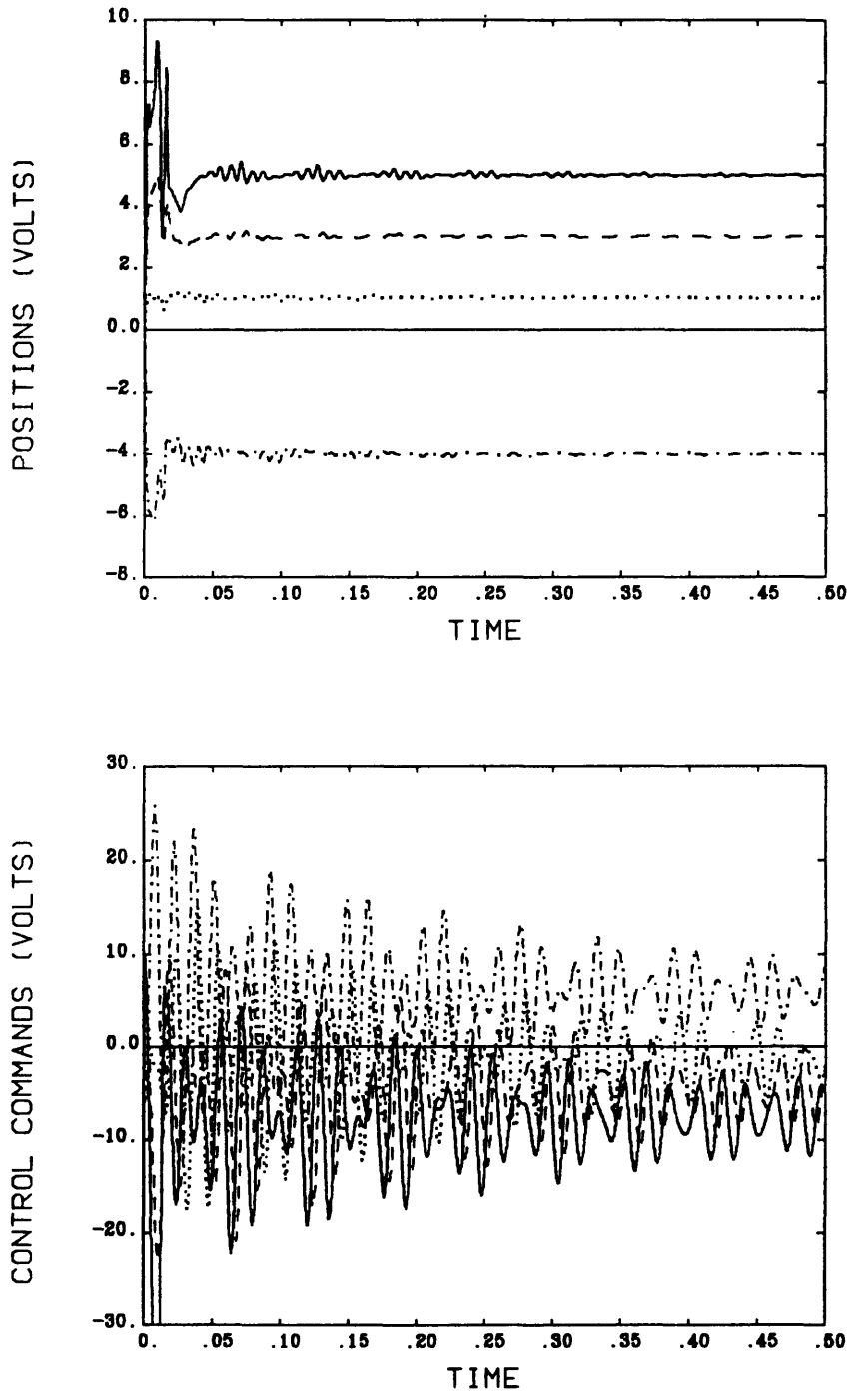

Figure 6.5 Very Flexible Shaft - Nonlinear Actuator Step Response

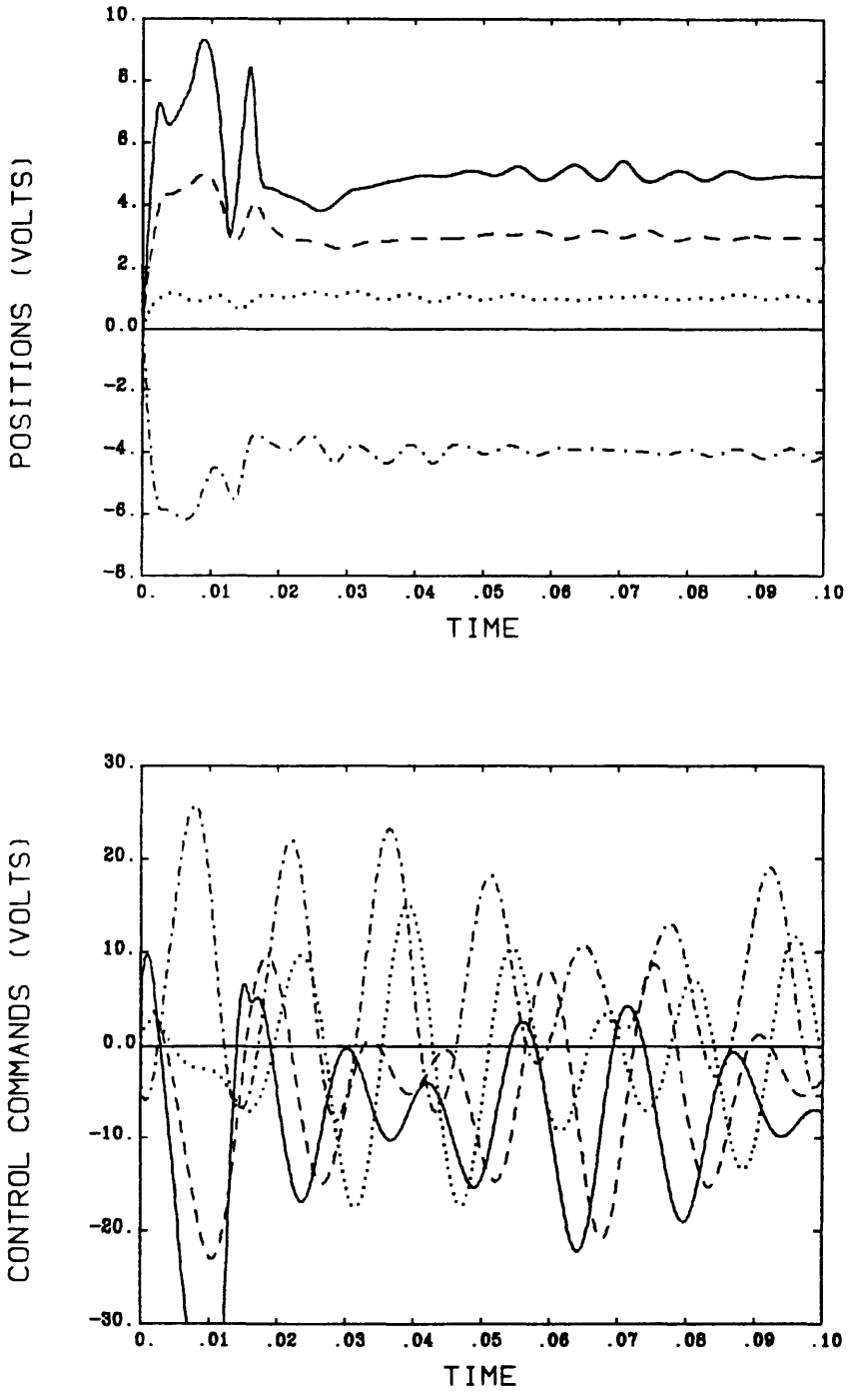

Figure 6.6 Very Flexible Shaft - Nonlinear Actuator Step Response

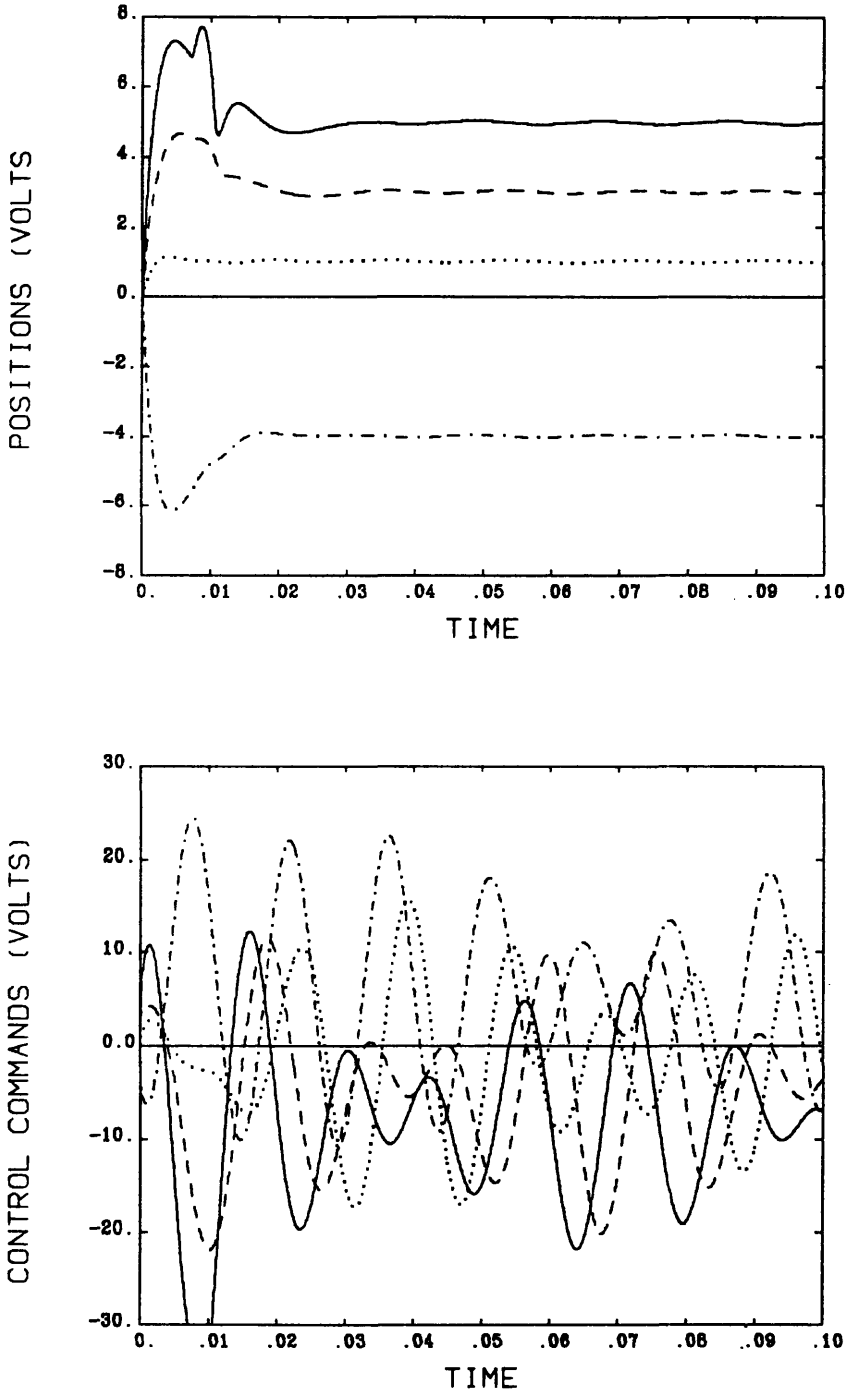

Figure 6.7 Very Flexible Shaft - Linear Actuator Step Response

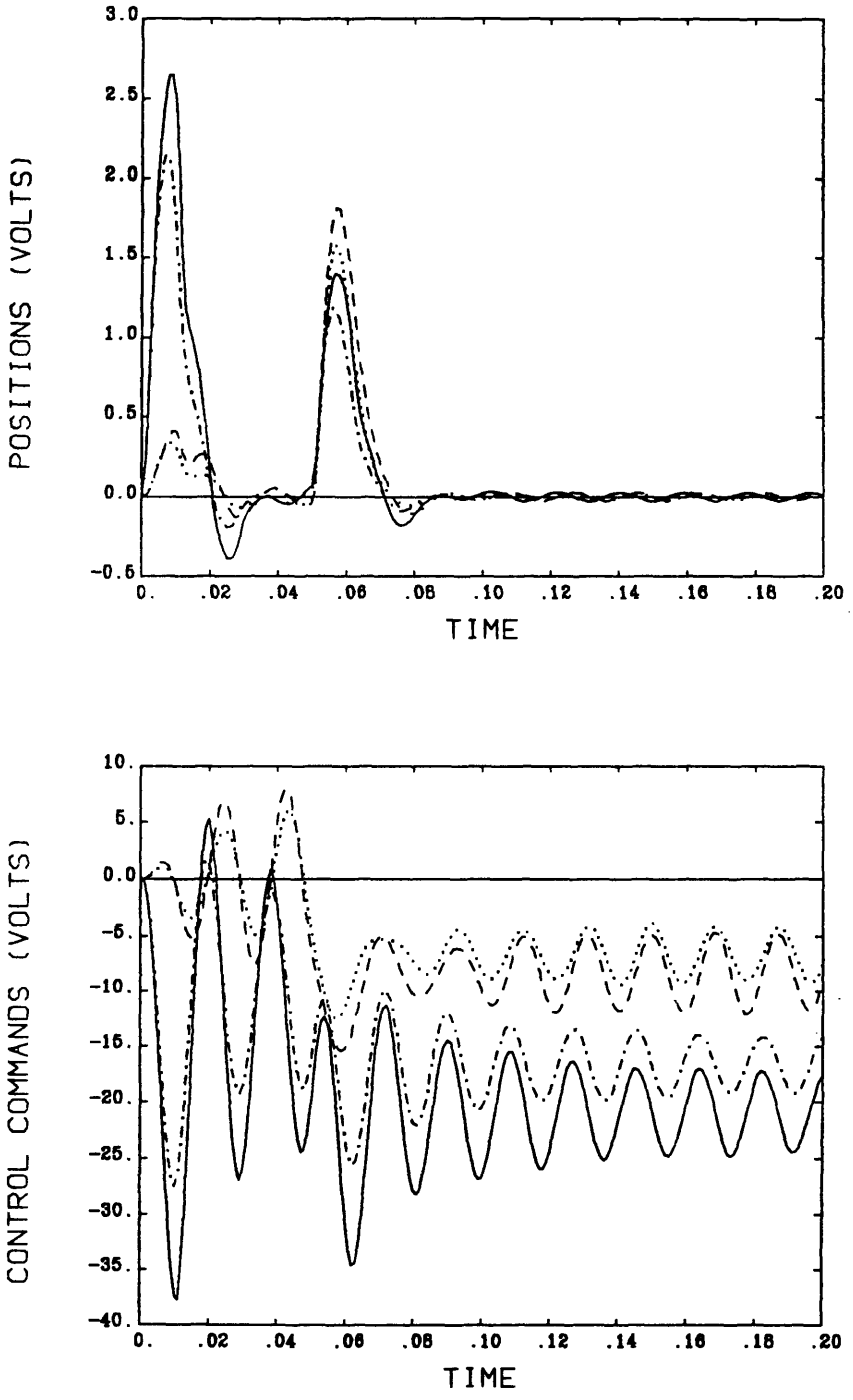

Figure 6.8 Flexible Shaft Nonlinear Actuator D.C. Disturbance Response

Test 3 considers the effects that mass unbalance has on system performance. The test simulates mass unbalance as a disturbance force which sinusoidally varies with shaft rotational frequency. The force is applied in combination with gravity. The magnitude of force used in baseline testing, 666 Newtons (150 lbs) immediately produced system failure (in its original configuration of ± 30 volt limit). Test specifications were modified by again increasing the available control voltage to ± 50 volts, also note this test was performed using the linear actuator. The test results are presented in Figure 6.9. The position excursions from null are a maximum at approximately 1.2 mils peak. The control commands are in the range of 35 to 40 volts peak, and when combined with the d.c. offset (from gravity), peak commands are at approximately –45 volts. As with the d.c disturbance test, changes in simulation parameters invalidate comparison to the baseline simulations.

To test the system robustness to change in rotational velocity, a closed loop pole analysis as a function of this parameter was performed. It showed that this system configuration remains stable over the entire operating region from d.c, through the critical speed, to the maximum operating speed of 5000 rpm.

6.5 Summary

This chapter was intended to document a trial control system design using the flexible model with its stiffness specification modified such that the shafts critical speed was below nominal operating speed. It was determined that the newly defined shaft has non-minimum phase transmission zeroes which affect the loop transfer recovery guarantees. The procedure was applied and an unstable compensator was designed. The unstable compensator, when combined with the unstable, non-minimum phase, nonlinear plant, produced a stable closed loop system. When this system was subjected to the test regime developed in Chapter 5, it failed two out of four of the tests. The d.c. disturbance test required an increase of control command voltage to at least ± 40 volts, and then it was

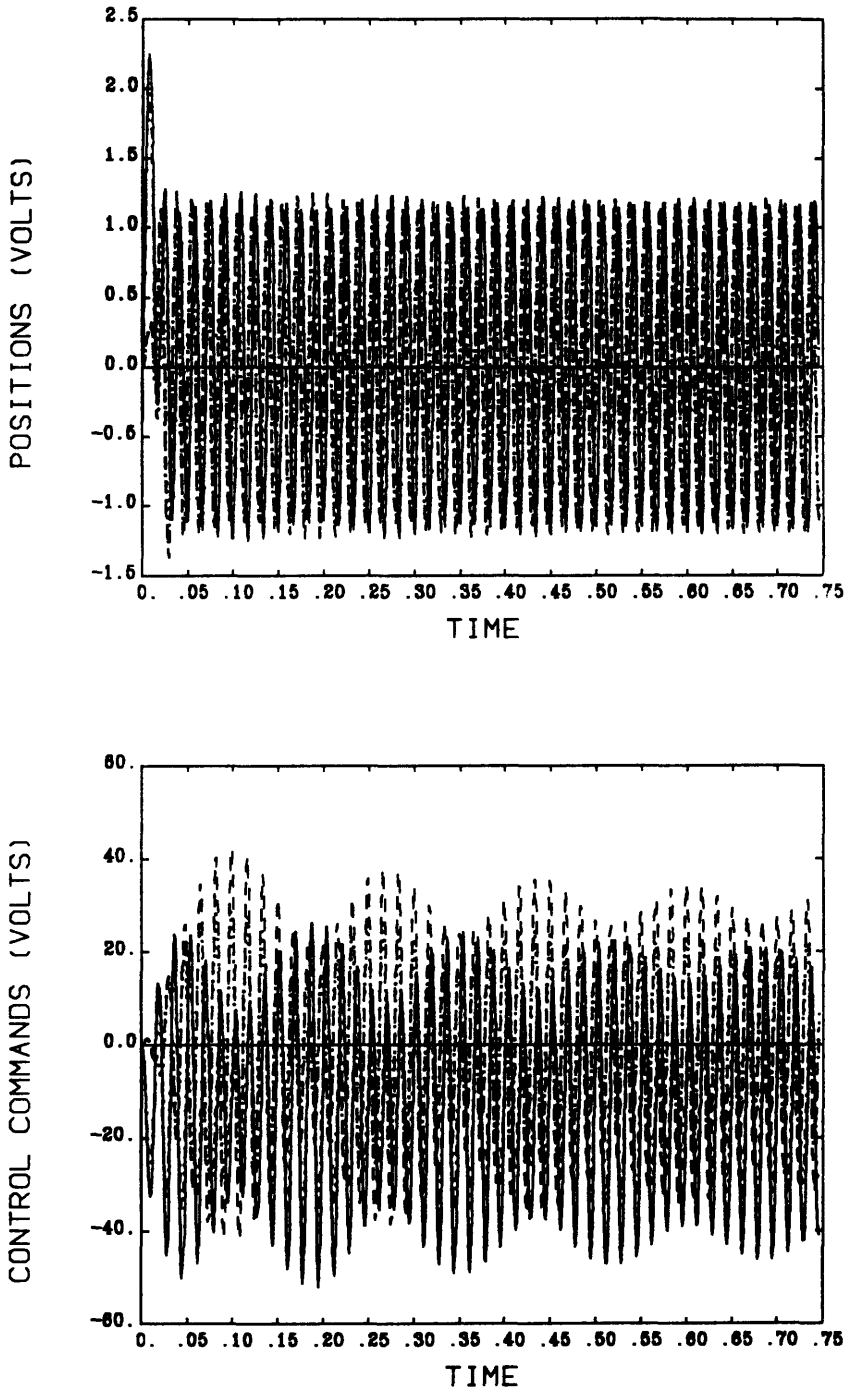

Figure 6.9 Flexible Shaft - Linear Actuator Mass Unbalance Response

determined that the application of the specified amount of mass unbalance force immediately caused system failure, even with the additional available voltage. The test conditions were redefined to 50% of specified unbalance force, and the results were acceptable.

It was determined, through the use of parametric closed loop pole location analysis, that the compensator, when combined with the linear version of the actual system, will be stable throughout the entire spin-up operation (as was the original compensator and its model). This implies that no gain scheduling will be necessary to allow the shaft to pass through its first critical speed.

An advantage of design using the simplified model is that the compensator order is minimized (unless compensator reduction can be successfully applied). The (augmented) compensator designed in Chapter 4 is 16^{th} order. The compensator designed using the flexible shaft model is 20^{th} order. The additional complexity of the flexible model compensator is another cost in having to control such a complex system.

This chapter provided much additional insight to the control of a flexible shaft / rotor system with an attractive force magnetic bearing actuator. We can see from the test results that the entire system must be re-evaluated before proceeding. Mainly, control command voltage supply limitations were cited as the limiting factor in the control problem.

Chapter 7

7. Summary and Conclusions

7.1 Summary

This thesis presented an application of the Linear Quadratic Gaussian with Loop Transfer Recovery (LQG/LTR) multivariable control system design methodology. A compensator was designed for a flexible rotating shaft / rotor system stabilized by a nonlinear electromagnetic bearing actuator. The design methodology produced a dynamic Model Based Compensator (MBC) which was designed using a simplified stiff shaft model of the flexible shaft system. The model was derived and presented in Chapter 2.

The design plant model (DPM) was analyzed and appropriate model scaling was performed and completely documented. The scaled design plant model was found to be both controllable and observable. The concept of multivariable modelling errors was introduced and applied to the simplified system model.

The LQG/LTR design methodology was presented with the necessary design prerequisites stated. The system specifications were defined in order to provide design guidelines. Application of the methodology produced a 16^{th} order dynamic compensator which included an integrator in each control channel. A preliminary closed loop robustness test was performed and it was found that the combined compensator and the actual flexible shaft / rotor were not guaranteed to be stable. The test as applied is very conservative and it was shown through nonlinear simulation that the combined system was, in fact, stable.

The necessary MBC evaluation was performed in Chapter 5. A simulation test plan was developed in congruence with the system specifications. A baseline system of linear actuator, simplified stiff shaft and MBC was defined and subjected to the test plan. The

actual nonlinear flexible configuration was also tested accordingly. A comparison of results was made. Closed loop stability as a function of system parameters was performed and significant conclusions were drawn. An academic exercise of system parameter change was suggested and it was found that a new compensator was needed to be designed to stabilize the new system. The LQG/LTR methodology was again applied using the full flexible shaft / rotor model. A 20^{th} order, unstable dynamic model based compensator was designed. The (unstable) flexible shaft plant was combined with the (unstable) compensator and the entire system was found to be closed loop stable. This system was then evaluated using the test procedure previously defined.

7.2 Conclusions

This thesis showed that a multivariable dynamic model based compensator (MBC) could be used successfully to stabilize a flexible rotating shaft and rotor through the use of nonlinear electromagnetic bearing actuators. The dynamic compensator was designed using the Linear Quadratic Gaussian with Loop Transfer Recovery methodology. A simplified stiff shaft and linearized magnetic bearing model was developed and used as the design plant model (DPM) for compensator design. The advantage to this approach is that the resulting dynamic compensator is of lower order when compared to the compensator designed using the full flexible model. This occurs because the compensator structure is 'model based,' meaning that the DPM itself is contained within the compensator and since the simplified stiff shaft model is an eighth order system while the full flexible is twelfth order, its respective compensator is of lower order.

The use of the simplified stiff shaft compensator was found to to be limited to specific applications. A closed loop pole parameterization study showed that this compensator will stabilize a similarly configured and specified system when the shaft stiffness is such that the shafts first critical speed (resonant frequency) is beyond 95 Hz. This defined the limitations of the use of the simplified stiff shaft compensator. The Draper

Lab testbed, whose current system parameters place its first critical speed near 150 Hz, will be adequately controlled by this compensator. A complete test procedure was applied to this flexible shaft and nonlinear actuator system (through the use of nonlinear simulation facilities). It was found that the system remained stable over the entire operating range of shaft rotational velocities, d.c through the nominal rate of 60 Hz and up to the specified goal of 100 Hz. This implies that the compensator is adequate for all operating conditions. No gain scheduled or nonlinear compensator is required. It was cautioned, however, that system performance limitations may be imposed by the limit of control command voltage. System level engineering studies must be conducted to determine the necessary voltage levels for specification compliance.

The flexible shaft parameters were then modified. Shaft stiffness was reduced to create a shaft whose first critical speed (54 Hz) was less than the nominal operating speed (60 Hz). This was done for two reasons : 1) to validate the conclusion made above and 2) to test a compensator designed using the full flexible model. The closed loop system formed using the new more flexible shaft and the stiff shaft designed compensator was found to be unstable. Therefore, to emphasize the flexibility of the compensator design methodology, a new compensator was designed for this flexible shaft. Again, this new compensator is of larger dimension than the simplified version, but that is unavoidable (at this time). The dynamic model based compensator designed is itself unstable, but when combined with the unstable plant, the system was found to be closed loop stable. This system was tested using the same procedure as before. It was found that for the system specifications as stated, this combination of plant and compensator failed to perform adequately due to actuator voltage saturation. It was shown, however, that if the limits imposed by control voltage hardware were relaxed, the system performed adequately. Further, the compensator was shown to successfully stabilize the system throughout its entire rotational velocity operating range (d.c. to 100 Hz), which includes passing through the shafts critical speed.

Also note that an attempt was made to reduce the order of both compensators by application of the residue expansion technique, but any compensator reduction was found to destabilize the system.

7.3 Topics for Future Study

Chapter 6 of this thesis is by no means the final word on the application of the LQG/LTR methodology to this magnetic bearing / flexible shaft system. While the simplified stiff shaft model used in this thesis is adequate for some systems, the flexible model may have been be too simplified for others. Therefore, other flexible model simplification techniques should be addressed with respect to applying the LQG/LTR methodology for specific purposes. If a simplified model can capture 'flexible' mode performance, then a reduced order dynamic model based compensator can be designed to operate with shafts of specified stiffness.

Investigation into the use of rotor position sensors must be done in conjunction with this design methodology also. The use of such sensors may eliminate system transmission zeroes which have a major effect on the compensator design.

Other magnetic bearing designs must be investigated also. The permanent magnet biased design, while used in many studies, may not be the best for this application.

References

[1] Athans, M. **Multivariable Control Systems I and II,** MIT courses 6.23, 6.232 class notes, Fall 1986, Spring 1987 (revised 1987 and 1988 respectively).

[2] Martin, J.M. **Multivariable Control System Design for a Submarine Using Active Roll Control,** MIT Engineers Thesis, May 1985.

[3] Kappos, E. **Robust Multivariable Control for the F100 Engine,** MIT Engineers Thesis, August 1983.

[4] Johnson, B.G. **Active Control of a Flexible, Two-Mass Rotor: the Use of Complex Notation,** MIT Sc. D. Thesis, September 1986.

[5] Johnson, B.G. **Active Control of a Flexible Rotor,** MIT S.M. Thesis, January 1985.

[6] McCallum, D.C. **Dynamic Modelling and Control of a Magnetic Bearing / Suspended Rotor System,** MIT S.M. Thesis, May 1988.

[7] Bleuler, H. and G. Schweitzer. **Dynamics of a Magnetically Suspended Rotor with Decentralized Control.** Proceedings of the IASTED Symposium on Applied Control and Indetification. Copenhagen : June 28-July 1, 1983.

[8] Kwakermaak, H. and R. Sivan. Linear Optimal Control Systems. New York : Wiley, 1972.

[9] Lehtimaki, N.A. **Practical Robustness Measures in Multivariable Control Systems Analysis.** MIT Ph. D. Thesis, 1981.

[10] Kuo, B.C. Automatic Control Systems. Englewood Cliffs, N.J., Prentice Hall, 1982

[11] Systems Control Technology Inc., **CTRL-C Manual,** Pato Alto CA, 1987

[12] Lewis, J.B. **Automotice Engine Control : A Linear Quadratic Approach.** MIT S.M. Thesis, March 1980.

[13] Stein, G. **LQG-Based Multivariable Design - Frequency Domain Interpretation.** AGARD, NATO, 1981.

[14] Groom., N.J. **Mgnetic Suspension System for a Laboratory Model Annular Momentum Control Device.** AAAII Guidance and Control Conference, Boulder, Colorado 1979

[15] Earnshaw, S. **On the Nature of the Molecular Forces which regulate the Constitution of the Luminiferous Ether.** Trandsactions of the Cambridge Philosophical Society. 7 (1842)

[16] Geary, P.J. **Magnetic and Electric Suspensions.** SIRA Survey of Instrument Parts, n 6. South Hill, Chislehurst, Kent : British Scientific Instrument Reasearch Association, 1964.

[17] Ulbrich H. and E. Anton. **Theory and Application of Mangetic Bearings with Integrated Displacement and Velocity Sensors.** Proceedings of the Third International Conference on Vibration in Rotating Machinery, University of York, England : September 11-13, 1984.

[18] Hendrickson, T.A., J.S. Leonard and D.A. Weise. **Application of Magnetic Bearing Technonlogy for Vibration Free Machinery.** Naval Engineers Journal, May 1987.

[19] Schweitzer, G. and R. Lange. **Characteristics of a Magnetic Rotor Bearing for Active Rotor Control.** Proceedings of the Intrernational Conference on Vibration in Rotational Machinery, Cambridge, England, 1976.

[20] Zmood, R.B., D. K. Anand and J.A. Kirk. **The Design of a Magnetic Bearing for High Speed Shaft Driven Applications.** AIAA , 1987.

Appendix A

Appendix A.1 : Nonlinear Bearing Equations

This Appendix contains the expressions for magnetic bearing parameters as discussed in Chapter 2. It also contains the nonlinear magnetic bearing equations for use in nonlinear simulations.

Recall equation (2.1) : $F = K_s x + K_i i$. Here, we seek to define K_s and K_i . From McCallum [6] :

$$K_i = \frac{2 A_g \mu_0 M_0 N}{g_0^2}$$

$$K_s = \frac{2 A_g \mu_0 \left(M_0^2 + \left(N i_0 \right)^2 \right)}{g_0^3}$$

where M_0 is the magneto motive force provided by the permanent magnets, μ_0 is the permeability of free space, g_0 i s the initial gap size at null, A_g is the area of the pole face, N is the number of wire turns on each coil, and i_0 is the equilibrium current level in each coil. Specific values for these parameters are given in Appendix B.

Next, the nonlinear bearing equations will be given, with reference again to McCallum [6] or Schweitzer [19] for the derivations. The complete nonlinear bearing force equation for the complete system are

$$F_{x_a} = \frac{A_g \mu_0}{2}\left[\frac{\left(M_0 + N i x_a\right)^2}{\left(g_0 - x_a\right)^2} - \frac{\left(M_0 - N i x_a\right)^2}{\left(g_0 + x_a\right)^2}\right]$$

$$F_{x_b} = \frac{A_g \mu_0}{2}\left[\frac{\left(M_0 + N i x_b\right)^2}{\left(g_0 - x_b\right)^2} - \frac{\left(M_0 - N i x_b\right)^2}{\left(g_0 + x_b\right)^2}\right]$$

$$F_{y_a} = \frac{A_g \mu_0}{2}\left[\frac{\left(M_0 + N i y_a\right)^2}{\left(g_0 - y_a\right)^2} - \frac{\left(M_0 - N i y_a\right)^2}{\left(g_0 + y_a\right)^2}\right]$$

$$F_{y_b} = \frac{A_g \mu_0}{2}\left[\frac{\left(M_0 + N i y_b\right)^2}{\left(g_0 - y_b\right)^2} - \frac{\left(M_0 - N i y_b\right)^2}{\left(g_0 + y_b\right)^2}\right]$$

Appendix A.2 : Flexible Shaft / Rotor Model

This Appendix contains the state equations for a flexible shaft / rotor. The shaft / rotor is depicted in Figure 2.2, but that figure also contains magnetic bearings. The first set of system state equations are for the shaft / rotor alone, with unspecified force inputs. The second set of system state equations are for the shaft / rotor with the linearized magnetic bearings. These sets of equations were derived by McCallum [6, and are in his notation. A difference in notation is noted primarily in the axis definitions. In this thesis, the axis of rotation is the z-axis, while in McCallum, x it the axis of rotation. The system states therefore are defined in the Y-Z coordinate plane. The additional system parameters are given in Appendix B because this system is used in the development of modelling errors and in simulation testing.

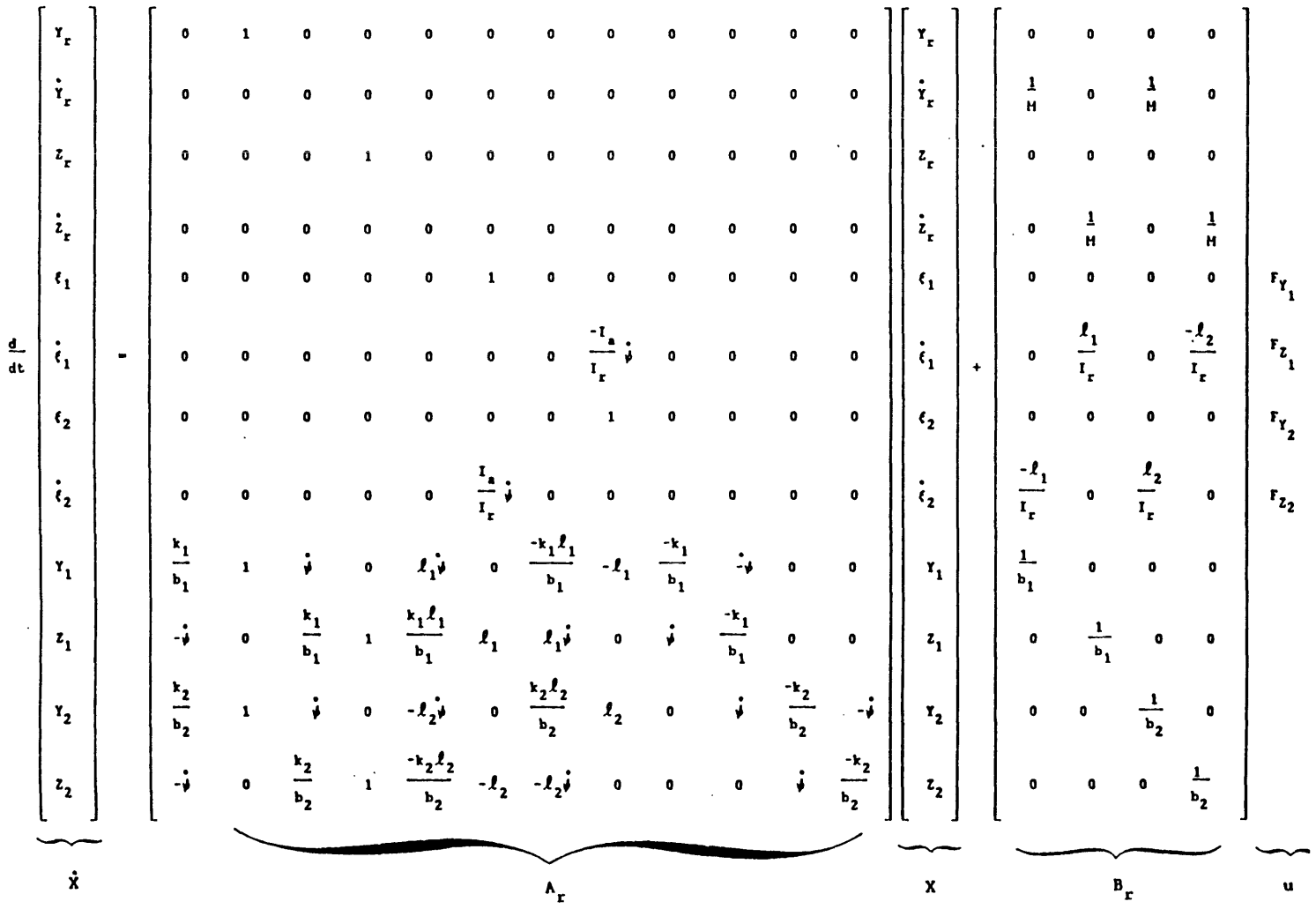

Figure A2.1 State Equations for Flexible Shaft / Rotor

$$\frac{d}{dt}\begin{bmatrix} Y_r \\ \dot{Y}_r \\ Z_r \\ \dot{Z}_r \\ \xi_1 \\ \dot{\xi}_1 \\ \xi_2 \\ \dot{\xi}_2 \\ Y_1 \\ Z_1 \\ Y_2 \\ Z_2 \end{bmatrix} = \begin{bmatrix} 0 & 1 & 0 & 0 & 0 & 0 & 0 & 0 & 0 & 0 & 0 & 0 \\ 0 & 0 & 0 & 0 & 0 & 0 & 0 & 0 & \frac{k_{Y_1}}{m} & 0 & \frac{k_{Y_2}}{m} & 0 \\ 0 & 0 & 0 & 1 & 0 & 0 & 0 & 0 & 0 & 0 & 0 & 0 \\ 0 & 0 & 0 & 0 & 0 & 0 & 0 & 0 & 0 & \frac{k_{Z_1}}{m} & 0 & \frac{k_{Z_2}}{m} \\ 0 & 0 & 0 & 0 & 0 & 1 & 0 & 0 & 0 & 0 & 0 & 0 \\ 0 & 0 & 0 & 0 & 0 & 0 & 0 & \frac{-I_a\omega}{I_r} & 0 & \frac{k_{Z_1}\ell_1}{I_r} & 0 & \frac{-k_{Z_2}\ell_2}{I_r} \\ 0 & 0 & 0 & 0 & 0 & 0 & 0 & 1 & 0 & 0 & 0 & 0 \\ 0 & 0 & 0 & 0 & 0 & \frac{I_a\omega}{I_r} & 0 & 0 & \frac{-\ell_1 k_{Y_1}}{I_r} & 0 & \frac{\ell_2 k_{Y_2}}{I_r} & 0 \\ \frac{k_1}{b_1} & 1 & \omega & 0 & \ell_1\omega & 0 & \frac{-k_1\ell_1}{b_1} & -\ell_1 & \frac{(k_{Y_1}-k_1)}{b_1} & -\omega & 0 & 0 \\ -\omega & 0 & \frac{k_1}{b_1} & 1 & \frac{k_1\ell_1}{b_1} & \ell_1 & \ell_1\omega & 0 & \omega & \frac{(k_{Z_1}-k_1)}{b_1} & 0 & 0 \\ \frac{k_2}{b_2} & 1 & \omega & 0 & -\ell_2\omega & 0 & \frac{k_2\ell_2}{b_2} & \ell_2 & 0 & 0 & \frac{(k_{Y_2}-k_2)}{b_2} & -\omega \\ -\omega & 0 & \frac{k_2}{b_2} & 1 & \frac{-k_2\ell_2}{b_2} & -\ell_2 & -\ell_2\omega & 0 & 0 & 0 & \omega & \frac{(k_{Z_2}-k_2)}{b_2} \end{bmatrix} \begin{bmatrix} Y_r \\ \dot{Y}_r \\ Z_r \\ \dot{Z}_r \\ \xi_1 \\ \dot{\xi}_1 \\ \xi_2 \\ \dot{\xi}_2 \\ Y_1 \\ Z_1 \\ Y_2 \\ Z_2 \end{bmatrix} + \begin{bmatrix} 0 & 0 & 0 & 0 \\ \frac{k_1}{m} & 0 & \frac{k_1}{m} & 0 \\ 0 & 0 & 0 & 0 \\ 0 & \frac{k_1}{m} & 0 & \frac{k_1}{m} \\ 0 & 0 & 0 & 0 \\ 0 & \frac{k_1\ell_1}{I_r} & 0 & \frac{-k_1\ell_2}{I_r} \\ 0 & 0 & 0 & 0 \\ \frac{-k_1\ell_1}{I_r} & 0 & \frac{k_1\ell_2}{I_r} & 0 \\ \frac{k_1}{b_1} & 0 & 0 & 0 \\ 0 & \frac{k_1}{b_1} & 0 & 0 \\ 0 & 0 & \frac{k_1}{b_2} & 0 \\ 0 & 0 & 0 & \frac{k_1}{b_2} \end{bmatrix} \begin{bmatrix} \\ \\ \\ \\ \\ \\ \\ \\ \\ \\ \\ \end{bmatrix} \begin{matrix} \\ \\ \\ \\ \\ i_{Y_1} \\ \\ i_{Z_1} \\ \\ i_{Y_2} \\ \\ i_{Z_2} \end{matrix}$$

Figure A2.2 State Equations for Flexible Shaft / Rotor with Linearized Magnetic Bearing

Appendix B : System Parameters

$L_1 = a$	= 0.3937	meters	
$L_2 = b$	= 0.4953	meters	
r	= 0.3536	meters	radius of gyration
K_s	= 3.4766 e 6	Newtons/meter	negative spring constant of linearized mag actuator
K_v	= 59.23	Newtons/Volts	Gain of linearized mag actuator
K_i	= 266.6660	Newtons/Amp	Gain of linearized mag actuator
M	= 136.3600	K_g	
$I_z = I_r$	= 17.0	$K_g\ m^2$	
$I_x = I_a$	= 1.6	$K_g\ m^2$	
K_{sensor}	= 1/2.54e-5	Volts/Meter	(1 V = 1 mil)

Additional parameters for the fully flexible rotor and non linear actuator

K_{s1}	= 6.57e7	N/m	Finite shaft stiffness
K_{s2}	= 5.63e7	N/m	Finite shaft stiffness
B_1	= 2600	N/m/s	Shaft damping
B_2	= 2200	N/m/s	Shaft damping
μ_0	= 4e-7 * pi	Permeability of free space	
A_g	= 1.1097e-3	Area of pole face	
g_0	= 5.08e-4	meters	initial gap size
N	= 61	turns	
M_0	= 404.25	magneto motive force provided by perm. magnet bias	
i_0	= 0	for this system	

Appendix C : DPM Matrices

The design plant model A (8 X 8) matrix :

Starting at row 1 columns 1 thru 6

0.0000D+00	0.0000D+00	0.0000D+00	0.0000D+00	1.0000D+00	0.0000D+00
0.0000D+00	0.0000D+00	0.0000D+00	0.0000D+00	0.0000D+00	1.0000D+00
0.0000D+00	0.0000D+00	0.0000D+00	0.0000D+00	0.0000D+00	0.0000D+00
0.0000D+00	0.0000D+00	0.0000D+00	0.0000D+00	0.0000D+00	0.0000D+00
5.7110D+04	-1.4278D+04	0.0000D+00	0.0000D+00	0.0000D+00	0.0000D+00
-1.4278D+04	7.5533D+04	0.0000D+00	0.0000D+00	0.0000D+00	0.0000D+00
0.0000D+00	0.0000D+00	5.7110D+04	-1.4278D+04	1.5714D+01	-1.5714D+01
0.0000D+00	0.0000D+00	-1.4278D+04	7.5533D+04	-1.9769D+01	1.9769D+01

Starting at row 1 columns 7 thru 8

0.0000D+00	0.0000D+00
0.0000D+00	0.0000D+00
1.0000D+00	0.0000D+00
0.0000D+00	1.0000D+00
-1.5714D+01	1.5714D+01
1.9769D+01	-1.9769D+01
0.0000D+00	0.0000D+00
0.0000D+00	0.0000D+00

The design plant model B (8 X 4) matrix :

0.0000D+00	0.0000D+00	0.0000D+00	0.0000D+00
0.0000D+00	0.0000D+00	0.0000D+00	0.0000D+00
0.0000D+00	0.0000D+00	0.0000D+00	0.0000D+00
0.0000D+00	0.0000D+00	0.0000D+00	0.0000D+00
9.7345D-01	-2.4336D-01	0.0000D+00	0.0000D+00
-2.4336D-01	1.2875D+00	0.0000D+00	0.0000D+00
0.0000D+00	0.0000D+00	9.7345D-01	-2.4336D-01
0.0000D+00	0.0000D+00	-2.4336D-01	1.2875D+00

The design plant model C (4 X 8) matrix :

Starting at row 1 columns 1 thru 6

3.9370D+04	0.0000D+00	0.0000D+00	0.0000D+00	0.0000D+00	0.0000D+00
0.0000D+00	3.9370D+04	0.0000D+00	0.0000D+00	0.0000D+00	0.0000D+00
0.0000D+00	0.0000D+00	3.9370D+04	0.0000D+00	0.0000D+00	0.0000D+00
0.0000D+00	0.0000D+00	0.0000D+00	3.9370D+04	0.0000D+00	0.0000D+00

Starting at row 1 columns 7 thru 8

0.0000D+00	0.0000D+00
0.0000D+00	0.0000D+00
0.0000D+00	0.0000D+00
0.0000D+00	0.0000D+00

The design plant model eigenvectors as graphed in Figs 3.2, 3.3 :

Eigenvector 1	Eigenvector 2	Eigenvector 3
-4.4986D-03 -1.6792D-05i	-4.4986D-03 +1.6792D-05i	4.4986D-03 -1.6792D-05i
-2.5159D-03 +3.6013D-04i	-2.5159D-03 -3.6013D-04i	2.5159D-03 +3.6013D-04i
-1.6792D-05 +4.4986D-03i	-1.6792D-05 -4.4986D-03i	-1.6792D-05 -4.4986D-03i
3.6013D-04 +2.5159D-03i	3.6013D-04 -2.5159D-03i	3.6013D-04 -2.5159D-03i
1.0000D+00 +0.0000D+00i	1.0000D+00 +0.0000D+00i	1.0000D+00 +0.0000D+00i
5.5895D-01 -8.2139D-02i	5.5895D-01 +8.2139D-02i	5.5895D-01 +8.2139D-02i
-3.0760D-11 -1.0000D+00i	-3.0825D-11 +1.0000D+00i	3.4798D-11 -1.0000D+00i
-8.2139D-02 -5.5895D-01i	-8.2139D-02 +5.5895D-01i	8.2139D-02 -5.5895D-01i

Eigenvector 4	Eigenvector 5	Eigenvector 6
4.4986D-03 +1.6792D-05i	-1.9398D-03 -1.0470D-04i	-1.9398D-03 +1.0470D-04i
2.5159D-03 -3.6013D-04i	3.4614D-03 -2.0332D-04i	3.4614D-03 +2.0332D-04i
-1.6792D-05 +4.4986D-03i	-1.0470D-04 +1.9398D-03i	-1.0470D-04 -1.9398D-03i
3.6013D-04 +2.5159D-03i	-2.0332D-04 -3.4614D-03i	-2.0332D-04 +3.4614D-03i
1.0000D+00 +0.0000D+00i	-5.5671D-01 -6.2949D-02i	-5.5671D-01 +6.2949D-02i
5.5895D-01 -8.2139D-02i	1.0000D+00 +0.0000D+00i	1.0000D+00 +0.0000D+00i
3.4818D-11 +1.0000D+00i	-6.2949D-02 +5.5671D-01i	-6.2949D-02 -5.5671D-01i
8.2139D-02 +5.5895D-01i	-1.7017D-12 -1.0000D+00i	-1.7090D-12 +1.0000D+00i

Eigenvector 7	Eigenvector 8
1.0470D-04 +1.9398D-03i	1.0470D-04 -1.9398D-03i
2.0332D-04 -3.4614D-03i	2.0332D-04 +3.4614D-03i
1.9398D-03 -1.0470D-04i	1.9398D-03 +1.0470D-04i
-3.4614D-03 -2.0332D-04i	-3.4614D-03 +2.0332D-04i
-6.2949D-02 -5.5671D-01i	-6.2949D-02 +5.5671D-01i
1.8933D-12 +1.0000D+00i	1.8954D-12 -1.0000D+00i
-5.5671D-01 +6.2949D-02i	-5.5671D-01 -6.2949D-02i
1.0000D+00 +0.0000D+00i	1.0000D+00 +0.0000D+00i

Appendix C.2 : SDPM Matrices

The scaled system matrices :

As =

Starting at row 1 columns 1 thru 6

0.0000D+00	0.0000D+00	0.0000D+00	0.0000D+00	2.2222D+02	0.0000D+00
0.0000D+00	0.0000D+00	0.0000D+00	0.0000D+00	0.0000D+00	2.2222D+02
0.0000D+00	0.0000D+00	0.0000D+00	0.0000D+00	0.0000D+00	0.0000D+00
0.0000D+00	0.0000D+00	0.0000D+00	0.0000D+00	0.0000D+00	0.0000D+00
2.5700D+02	-6.4249D+01	0.0000D+00	0.0000D+00	0.0000D+00	0.0000D+00
-6.4249D+01	3.3990D+02	0.0000D+00	0.0000D+00	0.0000D+00	0.0000D+00
0.0000D+00	0.0000D+00	2.5700D+02	-6.4249D+01	1.5714D+01	-1.5714D+01
0.0000D+00	0.0000D+00	-6.4249D+01	3.3990D+02	-1.9769D+01	1.9769D+01

Starting at row 1 columns 7 thru 8

0.0000D+00	0.0000D+00
0.0000D+00	0.0000D+00
2.2222D+02	0.0000D+00
0.0000D+00	2.2222D+02
-1.5714D+01	1.5714D+01
1.9769D+01	-1.9769D+01
0.0000D+00	0.0000D+00
0.0000D+00	0.0000D+00

Bs =

0.0000D+00	0.0000D+00	0.0000D+00	0.0000D+00
0.0000D+00	0.0000D+00	0.0000D+00	0.0000D+00
0.0000D+00	0.0000D+00	0.0000D+00	0.0000D+00
0.0000D+00	0.0000D+00	0.0000D+00	0.0000D+00
2.9204D+01	-7.3009D+00	0.0000D+00	0.0000D+00
-7.3009D+00	3.8624D+01	0.0000D+00	0.0000D+00
0.0000D+00	0.0000D+00	2.9204D+01	-7.3009D+00
0.0000D+00	0.0000D+00	-7.3009D+00	3.8624D+01

Cs =

Starting at row 1 columns 1 thru 6

1.7717D+01	0.0000D+00	0.0000D+00	0.0000D+00	0.0000D+00	0.0000D+00
0.0000D+00	1.7717D+01	0.0000D+00	0.0000D+00	0.0000D+00	0.0000D+00
0.0000D+00	0.0000D+00	1.7717D+01	0.0000D+00	0.0000D+00	0.0000D+00
0.0000D+00	0.0000D+00	0.0000D+00	1.7717D+01	0.0000D+00	0.0000D+00

Starting at row 1 columns 7 thru 8

0.0000D+00	0.0000D+00
0.0000D+00	0.0000D+00
0.0000D+00	0.0000D+00
0.0000D+00	0.0000D+00

The scaled system eigenvectors :

```
 3.7315D-03 -9.9969D-01i   3.7315D-03 +9.9969D-01i   3.7315D-03 +9.9969D-01i
-8.0028D-02 -5.5909D-01i  -8.0028D-02 +5.5909D-01i  -8.0028D-02 +5.5909D-01i
-9.9969D-01 -3.7315D-03i  -9.9969D-01 +3.7315D-03i   9.9969D-01 -3.7315D-03i
-5.5909D-01 +8.0028D-02i  -5.5909D-01 -8.0028D-02i   5.5909D-01 +8.0028D-02i
-2.3425D-15 +1.0000D+00i  -2.5960D-15 -1.0000D+00i  -9.2697D-15 +1.0000D+00i
 8.2139D-02 +5.5895D-01i   8.2139D-02 -5.5895D-01i  -8.2139D-02 +5.5895D-01i
 1.0000D+00 +0.0000D+00i   1.0000D+00 +0.0000D+00i   1.0000D+00 +0.0000D+00i
 5.5895D-01 -8.2139D-02i   5.5895D-01 +8.2139D-02i   5.5895D-01 +8.2139D-02i


 3.7315D-03 -9.9969D-01i   2.3267D-02 +4.3107D-01i   2.3267D-02 -4.3107D-01i
-8.0028D-02 -5.5909D-01i   4.5183D-02 -7.6921D-01i   4.5183D-02 +7.6921D-01i
 9.9969D-01 +3.7315D-03i   4.3107D-01 -2.3267D-02i   4.3107D-01 +2.3267D-02i
 5.5909D-01 -8.0028D-02i  -7.6921D-01 -4.5183D-02i  -7.6921D-01 +4.5183D-02i
-9.2738D-15 -1.0000D+00i  -6.2949D-02 -5.5671D-01i  -6.2949D-02 +5.5671D-01i
-8.2139D-02 -5.5895D-01i  -1.6595D-15 +1.0000D+00i  -1.7439D-15 -1.0000D+00i
 1.0000D+00 +0.0000D+00i  -5.5671D-01 +6.2949D-02i  -5.5671D-01 -6.2949D-02i
 5.5895D-01 -8.2139D-02i   1.0000D+00 +0.0000D+00i   1.0000D+00 +0.0000D+00i

-4.3107D-01 -2.3267D-02i   2.3267D-02 +4.3107D-01i
 7.6921D-01 -4.5183D-02i   4.5183D-02 -7.6921D-01i
-2.3267D-02 +4.3107D-01i  -4.3107D-01 +2.3267D-02i
-4.5183D-02 -7.6921D-01i   7.6921D-01 +4.5183D-02i
-5.5671D-01 -6.2949D-02i   6.2949D-02 +5.5671D-01i
 1.0000D+00 +0.0000D+00i  -7.9503D-16 -1.0000D+00i
-6.2949D-02 +5.5671D-01i  -5.5671D-01 +6.2949D-02i
-8.1032D-16 -1.0000D+00i   1.0000D+00 +0.0000D+00i
```

Appendix D : Controller Design Parameters and

Singular Value matching done with SDPM matrices.

ll = - 1500*inv(cn*inv(an)*bn) =

-7.4508D+02	0.0000D+00	0.0000D+00	0.0000D+00
2.5681D-15	-7.4508D+02	0.0000D+00	0.0000D+00
0.0000D+00	0.0000D+00	-7.4508D+02	0.0000D+00
0.0000D+00	0.0000D+00	2.5681D-15	-7.4508D+02

lh = 6000*cn'*inv(cn*cn') =

3.3867D+02	0.0000D+00	0.0000D+00	0.0000D+00
0.0000D+00	3.3867D+02	0.0000D+00	0.0000D+00
0.0000D+00	0.0000D+00	3.3867D+02	0.0000D+00
0.0000D+00	0.0000D+00	0.0000D+00	3.3867D+02
0.0000D+00	0.0000D+00	0.0000D+00	0.0000D+00
0.0000D+00	0.0000D+00	0.0000D+00	0.0000D+00
0.0000D+00	0.0000D+00	0.0000D+00	0.0000D+00
0.0000D+00	0.0000D+00	0.0000D+00	0.0000D+00

```
wcmax=2*pi*1500;
mu=(1/wcmax)**2;
l=[ll;lh];
l2=l*l';
```

```
 MU            =       1.1258D-08
```

```
theta=1/mu*eye(4);
Q=EYE(12);
```

The CTRL-C command for the FARE, using augmented SDPM matrices :

```
        H=LQE(AAN,L2,CAN,Q,THETA)
```

```
 H             =
```

6.3956D+01	8.3582D-01	6.6975D+00	-7.0990D+00
7.4903D-01	6.3860D+01	-7.1087D+00	7.5603D+00
-6.6975D+00	7.0990D+00	6.3956D+01	8.3582D-01
7.1087D+00	-7.5603D+00	7.4903D-01	6.3860D+01
4.6788D+01	-2.4233D+00	2.0060D-14	2.5200D-04
-2.4233D+00	4.9963D+01	-2.5200D-04	1.0738D-13
-4.3327D-15	-2.5200D-04	4.6788D+01	-2.4233D+00
2.5200D-04	-1.4127D-15	-2.4233D+00	4.9963D+01
5.3019D+01	-9.3507D+00	-8.3125D-01	1.0107D+00
-9.3412D+00	6.5264D+01	1.0088D+00	-1.2290D+00
8.3125D-01	-1.0107D+00	5.3019D+01	-9.3507D+00
-1.0088D+00	1.2290D+00	-9.3412D+00	6.5264D+01

The CTRL-C command for the CARE, using augmented SDPM matrices, and qg=can'*can, rho= 1e-11 * eye(4).

```
g=lqr(aan,ban,qg,rho)

 G           =

    Starting at row   1 columns   1 thru   6
  6.5972D+03  -5.0782D+02  -1.7626D-13  -8.3556D-06   5.6605D+06  -4.4172D+03
 -5.0782D+02   7.2525D+03   8.3556D-06   2.0714D-14  -4.4083D+03   5.6662D+06
 -1.8783D-11   8.3556D-06   6.5972D+03  -5.0782D+02  -1.6166D+04   1.7686D+04
 -8.3556D-06   1.0144D-11  -5.0782D+02   7.2525D+03   1.7686D+04  -1.9435D+04

    Starting at row   1 columns   7 thru  12
  1.6166D+04  -1.7686D+04   7.6286D+05   5.3152D+04  -1.0305D+03   9.3340D+02
 -1.7686D+04   1.9435D+04   5.3154D+04   6.9428D+05   1.2155D+03  -1.1066D+03
  5.6605D+06  -4.4172D+03   1.0305D+03  -9.3340D+02   7.6286D+05   5.3152D+04
 -4.4083D+03   5.6662D+06  -1.2155D+03   1.1066D+03   5.3154D+04   6.9428D+05
```

Appendix E.1 : Augmented Compensator Matrices

The SCALED, AUGMENTED Model Based Compensator system matrices :

ACOMPA (16 X 16) =

Starting at row 1 columns 1 thru 6

-6.5972D+03	5.0782D+02	1.7626D-13	8.3556D-06	-5.6616D+06	4.4023D+03
5.0782D+02	-7.2525D+03	-8.3556D-06	-2.0714D-14	4.3950D+03	-5.6674D+06
1.8783D-11	-8.3556D-06	-6.5972D+03	5.0782D+02	1.6285D+04	-1.7812D+04
8.3556D-06	-1.0144D-11	5.0782D+02	-7.2525D+03	-1.7812D+04	1.9569D+04
0.0000D+00	0.0000D+00	0.0000D+00	0.0000D+00	-8.2892D+02	4.2933D+01
0.0000D+00	0.0000D+00	0.0000D+00	0.0000D+00	4.2933D+01	-8.8517D+02
0.0000D+00	0.0000D+00	0.0000D+00	0.0000D+00	7.6760D-14	4.4646D-03
0.0000D+00	0.0000D+00	0.0000D+00	0.0000D+00	-4.4646D-03	2.5028D-14
2.9204D+01	-7.3009D+00	0.0000D+00	0.0000D+00	-6.8231D+02	1.0141D+02
-7.3009D+00	3.8624D+01	0.0000D+00	0.0000D+00	1.0124D+02	-8.1635D+02
0.0000D+00	0.0000D+00	2.9204D+01	-7.3009D+00	-1.4727D+01	1.7906D+01
0.0000D+00	0.0000D+00	-7.3009D+00	3.8624D+01	1.7872D+01	-2.1773D+01
6.5972D+03	-5.0782D+02	-1.7626D-13	-8.3556D-06	5.6605D+06	-4.4172D+03
-5.0782D+02	7.2525D+03	8.3556D-06	2.0714D-14	-4.4083D+03	5.6662D+06
-1.8783D-11	8.3556D-06	6.5972D+03	-5.0782D+02	-1.6166D+04	1.7686D+04
-8.3556D-06	1.0144D-11	-5.0782D+02	7.2525D+03	1.7686D+04	-1.9435D+04

Starting at row 1 columns 7 thru 12

-1.6285D+04	1.7812D+04	-7.6286D+05	-5.3152D+04	1.0305D+03	-9.3340D+02
1.7812D+04	-1.9569D+04	-5.3154D+04	-6.9428D+05	-1.2155D+03	1.1066D+03
-5.6616D+06	4.4023D+03	-1.0305D+03	9.3340D+02	-7.6286D+05	-5.3152D+04
4.3950D+03	-5.6674D+06	1.2155D+03	-1.1066D+03	-5.3154D+04	-6.9428D+05
-3.5539D-13	-4.4646D-03	2.2222D+02	0.0000D+00	0.0000D+00	0.0000D+00
4.4646D-03	-1.9025D-12	0.0000D+00	2.2222D+02	0.0000D+00	0.0000D+00
-8.2892D+02	4.2933D+01	0.0000D+00	0.0000D+00	2.2222D+02	0.0000D+00
4.2933D+01	-8.8517D+02	0.0000D+00	0.0000D+00	0.0000D+00	2.2222D+02
1.4727D+01	-1.7906D+01	0.0000D+00	0.0000D+00	-1.5714D+01	1.5714D+01
-1.7872D+01	2.1773D+01	0.0000D+00	0.0000D+00	1.9769D+01	-1.9769D+01
-6.8231D+02	1.0141D+02	1.5714D+01	-1.5714D+01	0.0000D+00	0.0000D+00
1.0124D+02	-8.1635D+02	-1.9769D+01	1.9769D+01	0.0000D+00	0.0000D+00
1.6166D+04	-1.7686D+04	7.6286D+05	5.3152D+04	-1.0305D+03	9.3340D+02
-1.7686D+04	1.9435D+04	5.3154D+04	6.9428D+05	1.2155D+03	-1.1066D+03
5.6605D+06	-4.4172D+03	1.0305D+03	-9.3340D+02	7.6286D+05	5.3152D+04
-4.4083D+03	5.6662D+06	-1.2155D+03	1.1066D+03	5.3154D+04	6.9428D+05

Starting at row 1 columns 13 thru 16

0.0000D+00	0.0000D+00	0.0000D+00	0.0000D+00
0.0000D+00	0.0000D+00	0.0000D+00	0.0000D+00
0.0000D+00	0.0000D+00	0.0000D+00	0.0000D+00
0.0000D+00	0.0000D+00	0.0000D+00	0.0000D+00
0.0000D+00	0.0000D+00	0.0000D+00	0.0000D+00
0.0000D+00	0.0000D+00	0.0000D+00	0.0000D+00
0.0000D+00	0.0000D+00	0.0000D+00	0.0000D+00
0.0000D+00	0.0000D+00	0.0000D+00	0.0000D+00
0.0000D+00	0.0000D+00	0.0000D+00	0.0000D+00
0.0000D+00	0.0000D+00	0.0000D+00	0.0000D+00
0.0000D+00	0.0000D+00	0.0000D+00	0.0000D+00
0.0000D+00	0.0000D+00	0.0000D+00	0.0000D+00
0.0000D+00	0.0000D+00	0.0000D+00	0.0000D+00
0.0000D+00	0.0000D+00	0.0000D+00	0.0000D+00
0.0000D+00	0.0000D+00	0.0000D+00	0.0000D+00
0.0000D+00	0.0000D+00	0.0000D+00	0.0000D+00

BCOMPAS (16 X 4) =

6.3956D+00	8.3582D-02	6.6975D-01	-7.0990D-01
7.4903D-02	6.3860D+00	-7.1087D-01	7.5603D-01
-6.6975D-01	7.0990D-01	6.3956D+00	8.3582D-02
7.1087D-01	-7.5603D-01	7.4903D-02	6.3860D+00
4.6788D+00	-2.4233D-01	2.0060D-15	2.5200D-05
-2.4233D-01	4.9963D+00	-2.5200D-05	1.0738D-14
-4.3327D-16	-2.5200D-05	4.6788D+00	-2.4233D-01
2.5200D-05	-1.4127D-16	-2.4233D-01	4.9963D+00
5.3019D+00	-9.3507D-01	-8.3125D-02	1.0107D-01
-9.3412D-01	6.5264D+00	1.0088D-01	-1.2290D-01
8.3125D-02	-1.0107D-01	5.3019D+00	-9.3507D-01
-1.0088D-01	1.2290D-01	-9.3412D-01	6.5264D+00
0.0000D+00	0.0000D+00	0.0000D+00	0.0000D+00
0.0000D+00	0.0000D+00	0.0000D+00	0.0000D+00
0.0000D+00	0.0000D+00	0.0000D+00	0.0000D+00
0.0000D+00	0.0000D+00	0.0000D+00	0.0000D+00

CCOMPAS (4 X 16) =

Starting at row 1 columns 1 thru 12

0.	0.	0.	0.	0.	0.	0.	0.	0.	0.	0.	0.
0.	0.	0.	0.	0.	0.	0.	0.	0.	0.	0.	0.
0.	0.	0.	0.	0.	0.	0.	0.	0.	0.	0.	0.
0.	0.	0.	0.	0.	0.	0.	0.	0.	0.	0.	0.

Starting at row 1 columns 13 thru 16

30.	0.	0.	0.
0.	30.	0.	0.
0.	0.	30.	0.
0.	0.	0.	30.

Appendix E.2 : Compensator Poles and Zeroes

Augmented compensator poles and zeroes

```
 -2.6499D-13 +0.0000D+00i          (poles)
 -7.9575D-12 +0.0000D+00i
  1.2891D-11 +0.0000D+00i
 -3.6004D-11 +0.0000D+00i
 -1.6308D+03 -3.1525D+03i
 -1.6308D+03 +3.1525D+03i
 -1.6308D+03 +3.1536D+03i
 -1.6308D+03 -3.1536D+03i
 -3.8646D+03 +6.0840D-01i
 -3.8646D+03 -6.0840D-01i
 -1.9346D+03 +3.7253D+03i
 -1.9346D+03 -3.7253D+03i
 -1.9338D+03 +3.7475D+03i
 -1.9338D+03 -3.7475D+03i
 -4.5690D+03 +1.1559D+01i
 -4.5690D+03 -1.1559D+01i


 -2.6750D+02 +1.8514D+01i     (zeroes)
 -2.6750D+02 -1.8514D+01i
 -2.0149D+02 +9.1692D-01i
 -2.0149D+02 -9.1692D-01i
 -3.7240D+01 +5.6535D+00i
 -3.7240D+01 -5.6535D+00i
 -3.4294D+01 +1.0443D-01i
 -3.4294D+01 -1.0443D-01i
```